Bose-Einstein Condensation of Sodium Atoms

by

Marc-Oliver Mewes

Physik-Vordiplom, Technische Universität Berlin (1991)

Submitted to the Department of Physics in

partial fulfillment of the requirements

for the degree of

DOCTOR OF PHILOSOPHY

at the

MASSACHUSETTS INSTITUTE OF TECHNOLOGY

February, 1997

Signature of the Author _____

Department of Physics
January 9, 1997

Certified by _____

Wolfgang Ketterle
Assistant Professor of Physics
Thesis Supervisor

Accepted by _____

George F. Koster
Chairman, Department Committee
on Graduate Studies

Bose-Einstein Condensation of Sodium Atoms

by

Marc-Oliver Mewes

submitted to the Department of Physics
on January 9th 1997, in partial fulfillment of the
requirements for the degree of Doctor of Philosophy

Abstract

Bose-Einstein Condensation in an ultracold gas of neutral sodium atoms has been observed and studied. This was achieved utilizing a combination of laser cooling techniques, magnetic trapping and evaporative cooling.

A novel tightly confining dc magnetic trap was developed and demonstrated. This trap combines tight confinement with excellent optical access. Evaporative cooling in this trap produced Bose condensates of 5×10^6 atoms, a tenfold improvement over previous results.

The Bose-Einstein phase transition was studied and characterized by mapping out the condensed fraction as a function of temperature across the transition point. The characteristic mean-field interaction of particles in the condensate was investigated.

Collective excitations of a dilute Bose condensate have been observed. These excitations are analogous to phonons in superfluid helium. The frequencies of the lowest modes were studied for a temperature close to 0 K and compared with theoretical predictions based on mean-field theory. The characteristic damping of one of the modes was measured and compared to damping of "sound waves" in an ultra-cold gas above the Bose-Einstein transition.

We have also demonstrated an output coupler for Bose condensed atoms in a magnetic trap. With short rf pulses Bose condensates were put into a superposition of trapped and untrapped hyperfine states. By varying the rf amplitude we could adjust the fraction of outcoupled atoms between 0 and 100%. This source produces pulses of coherent atoms and can be regarded as a pulsed "atom laser".

Thesis Supervisor: Dr. Wolfgang Ketterle
Title: Assistant Professor of Physics

To my parents,
Hannelore and Dieter.

Here is Edward Bear, coming downstairs now, bump, bump, bump, on the back of his head, behind Christopher Robin. It is, as far as he knows, the only way of coming downstairs, but sometimes he feels there really is another way, if only he could stop bumping for a moment and think of it. And then he feels that perhaps there isn't. Anyhow here he is at the bottom, and ready to be introduced to you. Winnie-the-Pooh.

A.A. Milne, Winnie the Pooh

TABLE OF CONTENTS

LIST OF FIGURES

LIST OF TABLES

1. INTRODUCTION

The introduction first briefly outlines the history of Bose-Einstein condensation in dilute atomic gases up to the realization of the phenomenon in 1995. It is followed by a coarse outline of this thesis. The chapter is supplemented by a derivation of Bose -Einstein condensation is in the appendix.

1.1 Historical Background

In 1924 Albert Einstein calculated that an ideal quantum gas will undergo a phase transition when the average distance between the particles is comparable to the thermal de Broglie wavelength [1]. This transition occurs when

$$n\,\Lambda^3 = 2.612, \tag{1.1}$$

where n is the peak number density of the sample. The thermal de Broglie wavelength Λ is given by

$$\Lambda = (2\pi\hbar^2/mk_BT)^{1/2}, \tag{1.2}$$

where m is the mass of the particle and T the temperature of the gas.

Below the transition temperature a macroscopic number of particles occupies the ground state of the system, i.e. the state with lowest energy. The remaining *uncondensed* atoms, the so called *normal* fraction, behave like a saturated gas with the saturated peak density given in Eq. (1.1). The quantity $n\Lambda^3$ is used as a measure of the proximity to this transition. (For high temperatures it is the occupation of the ground state and usually called the *phase space density*). A short derivation of the Bose-Einstein condensation (BEC) phenomenon based on quantum-statistical mechanics will be given in the appendix of this introduction.

It is remarkable that Einstein made this prediction before quantum theory had been fully developed, and before differences between bosons and fermions had been revealed. The Bose-Einstein phase transition only occurs in bosonic systems: systems with completely symmetrized many-particle wave functions.

After Einstein's seminal work, important contributions were made by, most notably, London, Landau, Bogoliubov, Penrose and Onsager, Feynman, Lee, Yang and Huang, Goldstone and Anderson (See Ref. in [2-4]). The relationship between Bose-Einstein condensation and superfluidity in liquid helium has always been an important issue. The history of this subject is extremely interesting by itself. The references to the historically relevant publications can be found in [2], but a comprehensive review from a science historical perspective does not exist (yet).

What makes this phenomenon of BEC remarkable is the fact that it occurs even in the complete absence of interactions among the particles. Einstein called it "condensation without interaction" [1]. It is a purely quantum-statistical phase transition and hence an important paradigm for statistical mechanics. However, in "real life" there will always be some interaction among particles in the system and an interacting Bose-gas will behave qualitatively differently than the ideal case (see e.g. Ref.[2]).

Another remarkable fact is that, even though Bose-Einstein condensation has been invoked as an important process in condensed matter physics, nuclear physics, elementary particle physics and astrophysics, until recently there have only been two experimental systems which actually exhibit BEC: liquid helium and exciton systems [4, 5]. However, strong interactions in the liquid state significantly modify the nature of the BEC phenomenon. It is therefore understandable that the realization of Bose-Condensation in weakly-interacting gases was a long standing goal in atomic physics.

Already in 1959 Hecht [6] realized that a magnetic field can polarize the electron-spin of gaseous hydrogen atoms and prevent them from recombining to molecules. He reasoned that this fact might allow the atoms to stay a gas all the way down to zero temperature, making it an ideal candidate for Bose condensation. Later on, in 1976,

Stwalley and Nosanow [7] brought up this idea again and also who pointed out that due to weak interactions the Bose condensate of the polarized hydrogen could exhibit superfluid properties. They also realized that the weakness of the interactions and the ability to change the density make it an ideally suited "quantum" gas for a detailed comparison to theory. In 1980 Silvera and Walraven first stabilized spin polarized hydrogen in the laboratory [8]. An exciting discovery made soon thereafter was that the stabilized sample also develops nuclear polarization [9, 10]. Between 1980 and 1987 several groups tried to reach BEC by compressing a cryogenically cooled and doubly spin-polarized hydrogen gas [11-13]. They soon had to realize that a novel molecular recombination effect, three-body recombination, limited the density of the sample to about 1/50 of the density needed to reach the phase transition and blocked the route to quantum degeneracy.

In 1986, soon after the first observation of magnetically trapped atoms in 1985 [14], Harald Hess realized that it was possible to trap the "low field"- seeking spin state of hydrogen in an inhomogeneous magnetic field and, hence, to thermally isolate the atoms from the dewar walls. Hess proposed to avoid the three-body-recombination "roadblock" by choosing a lower density and low temperature route to BEC, namely to cool magnetically trapped spin-polarized hydrogen through evaporation [15]. This is the same process that also cools water in a bathtub or a cup of coffee. Evaporative cooling is discussed in chapter 2 of this thesis. Briefly, evaporative cooling works by continuously removing the most energetic atoms from the distribution while the remaining sample equilibrates at a lower temperature through elastic collisions. The driving force for this process is elastic collisions. Evaporative cooling of magnetically trapped hydrogen was first achieved at MIT in 1987 [16] and resulted in the closest approach to BEC with doubly polarized Hydrogen so far [17]. This cooling technique reached a temperature of 100 μK and a density of 8×10^{13} atoms/cm^3, a factor of three in temperature short of BEC.

The development of laser cooling and trapping during the 1980's had a profound impact on atomic physics and opened up a novel route to low temperatures which does not impose the constraints of cryogenic techniques. These methods made sub-mK atoms routinely available to a variety of experiments. The most commonly used techniques are Doppler cooling[18, 19], polarization gradient cooling [19-21] and the magneto optical trap (MOT) [22]. Attempts to achieve BEC solely with laser cooling methods had to maneuver around serious obstacles such as heating due spontaneous emission and density limitations due to radiation trapping [23]. The closest approach to BEC with conventional laser cooling techniques stopped five orders of magnitude short in phase space density (see e.g. Ref.[24]). More refined optical techniques which overcame some of the above limitations came as close to BEC as a factor of 400 in phase space density [25].

The only successful approach to BEC so far has been a "joint venture" of the spin-polarized hydrogen community and the laser cooling community: Ultracold alkali atoms which were predominantly used for laser cooling have approximately a 1000 times larger elastic collision cross section than hydrogen while the cross section for the inelastic processes (dipolar relaxation) is about the same. Since elastic collisions are the driving force of evaporative cooling (see chapter 2), this permits evaporative cooling at densities much lower than those necessary for hydrogen. The inelastic loss processes and the implied limitations to evaporative cooling become insignificant. The key idea was to laser-precool a sample of alkali atoms in order to achieve the condition at which evaporation can start. The sample would then be transferred into a magnetic trap for further evaporative cooling. The challenge was to reach densities and temperatures sufficient for the onset of evaporative cooling in a magnetic trap and then successfully join both techniques. Work focused towards this goal in our group at MIT in 1991. Similar techniques were developed by Eric Cornell and Carl Wieman in parallel at JILA, Colorado[26]. Related work was also done at Rice [27] and Stanford [28].

Very recently Bose-Einstein Condensation has been realized in dilute atomic alkali vapors: Eric Cornell's group at JILA, Colorado observed BEC in a Rubidium (Rb^{87}) vapor in June 1995 [26], while our group at MIT reached the transition with Sodium (Na^{23}) in September 1995 [29] (Chapter 3 of this thesis). A few month later, in March 1996, our group achieved BEC in a novel "cloverleaf" magnetic trap with up to 10^7 condensed sodium atoms [30] (Chapter 4 of this thesis). Subsequently there have been further reports on the successful realization of Bose-Einstein Condensation with Rubidium in Carl Wieman's group at JILA, Colorado [31] and also in Lithium by Randy Hulet's group at Rice University, Houston [32]. Fig. 1.1 illustrates the routes towards large phase space densities taken by the different BEC experiments. Fig 1.2 shows the progress made over the last two years by the evaporative cooling experiments working with alkalis.

These experiments received a lot of attention inside and outside the physics community (see e.g. Ref.[33]) and they have raised hopes and expectations for a very fruitful experimental future. As of December 1996, there are more than 35 experimental groups who are pursuing BEC in atomic gases, and there has been an equally impressive amount of theoretical work related to BEC. An excellent discussion on why BEC in atomic gases created so much excitement can be found in Daniel Kleppner's PHYSICS TODAY-article *"The Fuss About Bose-Einstein Condensation"*[34]. This essay also includes a short historical background on BEC.

The realization of BEC by itself is not new physics. The recent BEC experiments just showed that it is experimentally possible to cool and compress atomic gases into the quantum degenerate regime before molecule formation or other inelastic processes set in. In that sense, the more than 15 year long quest for BEC in atomic gases was more a search for adequate cooling and storage mechanisms.

The study of BEC in weakly-interacting systems promises to reveal new macroscopic quantum phenomena that can be understood from first principles. It also may advance our understanding of superconductivity and superfluidity in more complex systems. During the last year the experiments at JILA and (here) at MIT have explored

the properties of the Bose-Einstein phase transition and this new form of "quantum" matter. A summary of results can be found in the proceedings of ICAP 1996 [35, 36]. Some of the most recent progress is only available in the from of preprints (as of November 1996). This includes studies of a pulsed source of Bose condensed atoms (Chapter 6 of this thesis) [37], the production of condensates of Rubidium atoms in two different hyperfine states simultaneously trapped in the same magnetic trap [31] and studies of collective condensate excitations at finite temperatures [38].

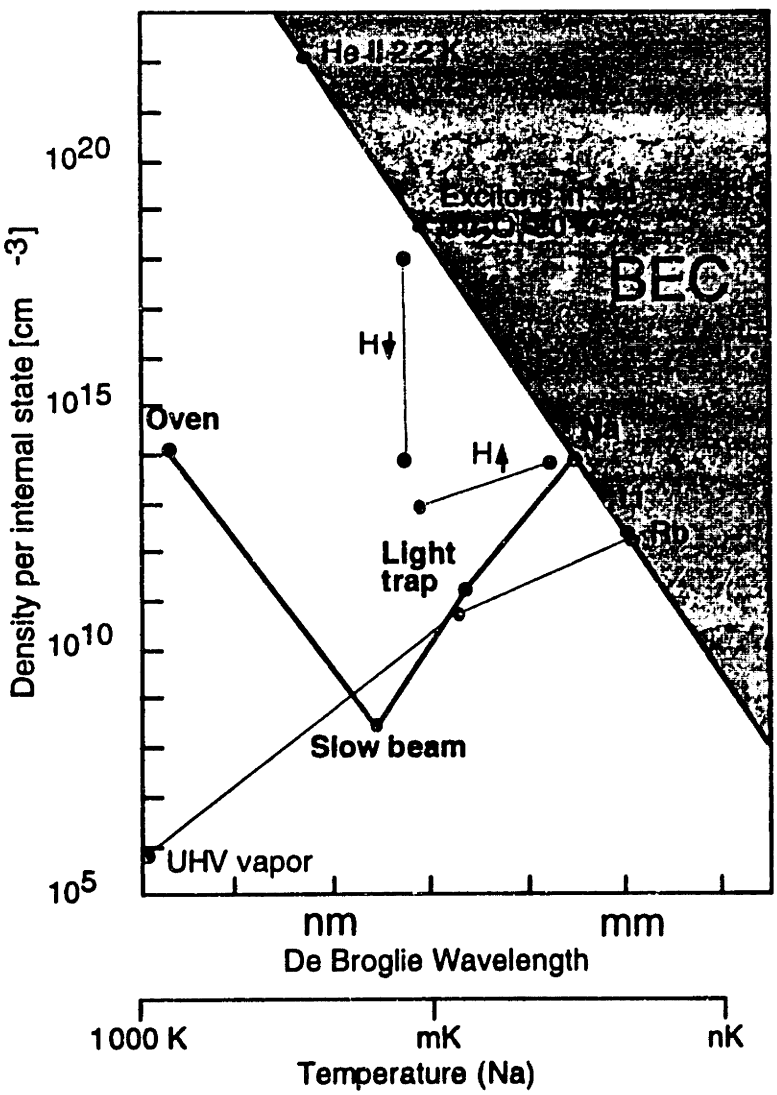

Fig.1.1 Approaches to BEC taken by the different cooling experiments. The trajectories are plotted in a space defined by the relevant cooling parameters, the density n and the de Broglie wavelength Λ, with the phase space density given as $n\Lambda^3$. The diagonal line marks the BEC phase transition. Points on the BEC line mark the different density regimes at which BEC was observed.

Trajectories and Points
H↓: compressed atomic hydrogen (MIT
H↑: evaporatively cooled atomic hydrogen (MIT).
Na, Rb, Li: evaporatively cooled sodium (MIT), Rubidium (JILA) and Lithium (Rice) respectively.
He II: Bose condensed Helium II.
Excitons: Bose condensed exciton system (Urbana)

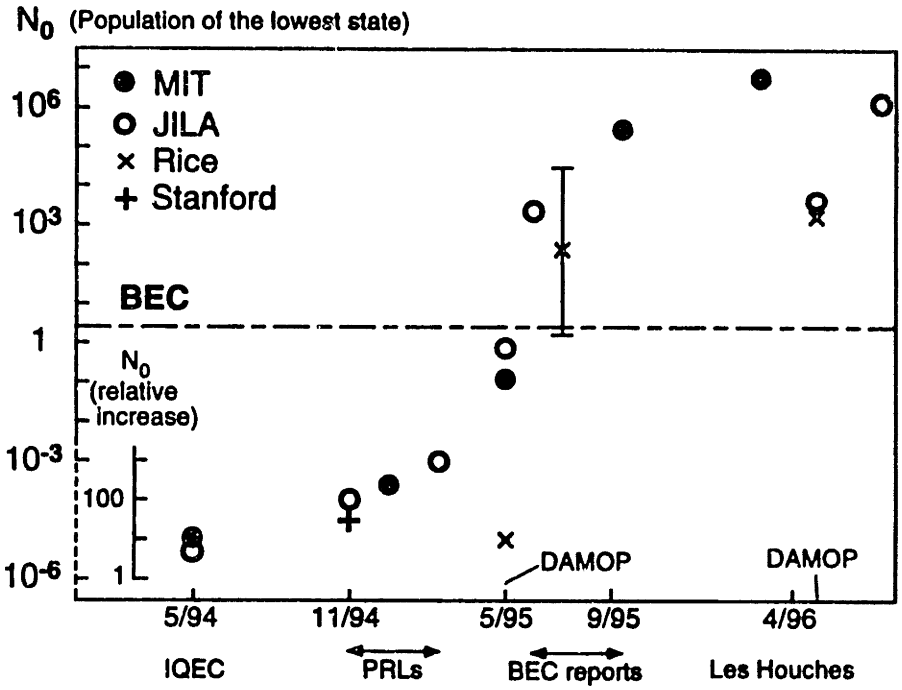

Fig.1.2 Progress in evaporative cooling of alkali atoms. It incorporates all experiments reported thus far. Plotted is the number of atoms in the lowest quantum state of the system. It is proportional to the phase space density and has to exceed 2.612 in order to achieve Bose condensation. For $N_0<10^{-3}$ the increase in phase space density is plotted. *IQEC, DAMOP* and *Les Houches* are conferences during which results were reported. MIT and Stanford cool sodium, Rice cools lithium and JILA rubidium.

1.2 A Coarse Outline of this Thesis

The "backbone" of this thesis consists of three papers which have been published in *Physical Review Letters* [29, 30, 39] and of one manuscript which has been submitted to the same journal [37]. The chapters in this thesis are only supplementing these publications.

Chapter 1 gives a brief historically motivated introduction to Bose-Einstein condensation in atomic gases. It is supplemented by a section in which Bose-Einstein

condensation of an ideal gas is derived in order to point out the quantum-statistical nature of the transition.

Chapter 2 is a brief overview of the experimental techniques used to obtain BEC in a dilute gas of atomic sodium. This includes evaporative cooling in a magnetic trap, a short outline of the preparation of the sample for evaporation with laser cooling, as well as rf induced evaporation. The transfer of cold atoms into the magnetic potential is covered in more detail since it has not (yet) been extensively discussed in the literature. The chapter concludes with a short explanation of absorption imaging, the method used to observe the ultra-cold atomic gas.

Chapter 3 presents the realization of BEC in a gas of atomic sodium. It first explains Majorana Flops, the trap loss mechanism encountered in linear magnetic trapping potentials and introduces a "hybrid" atom trap which avoids this trap loss phenomenon: the optically-plugged (OP) trap. The chapter concludes with the realization of BEC in the optically plugged trap and the reprint of the publication on this subject.

Chapter 4 introduces a novel, tightly-confining magnetostatic trap, the "clover-leaf" trap. This trap combines tight confinement with excellent optical access. Evaporative cooling in this trap produced Bose condensates of up to 10^7 atoms, a tenfold improvement over the results presented in Chapter 3. The Bose-Einstein phase transition was studied and characterized by mapping out the condensed fraction as a function of temperature. The characteristic mean-field interaction of particles in the condensate was investigated. A brief comparison of the different experiments producing Bose condensates supplements the chapter.

Chapter 5 is devoted to low-lying collective excitations of a condensate. These excitations are similar to phonons in superfluid helium. In the experiment the frequencies of the lowest modes were studied and compared with theoretical predictions. The characteristic damping of one of the modes was measured and compared to damping of "sound waves" in an ultra-cold gas above the Bose-Einstein transition.

Chapter 6 discusses the recent demonstration of an output coupler for Bose condensed atoms in a magnetic trap. With short rf pulses Bose condensates were put into a superposition of trapped and untrapped hyperfine states. By varying the rf amplitude we could adjust the fraction of outcoupled atoms between 0 and 100%. This source produces pulses of coherent atoms and can be regarded as a pulsed "atom laser".

Chapter 7 concludes this thesis with a brief overview of very recent experiments not presented in this thesis, such as the non-destructive, "real" time observation of Bose-Einstein condensation and interference of two independent condensates. It also discusses possible directions for future experiments

Note: This thesis does not aspire to describe the experiment in technical detail. It was written with the intention of putting the results of my thesis research which have been published into a more general physics context. The depth of the presentation varies throughout the thesis. Topics that have not been discussed extensively in the literature, such as the transfer of laser cooled atoms into a magnetic trap, are covered in more detail, but are not necessarily the most important issues.

Appendix to Chapter 1: Bose-Einstein Condensation of an Ideal Gas

In this supplement I derive Bose-Einstein condensation of an ideal gas in order to point out the quantum-statistical nature of the transition.

We consider the grand partition function $\Im$ for ideal Bosons as a function of the fugacity z and the Boltzmann factor $\beta=1/k_BT$:

$$\Im(z,\beta)=\sum_{N=0}^{\infty}\sum_{\{n_\varepsilon\},\ \sum n_\varepsilon=N} z^N e^{-\beta\sum E_\varepsilon n_\varepsilon}=\sum_{N=0}^{\infty}\sum_{\{n_\varepsilon\},\ \sum n_\varepsilon=N}\prod_\varepsilon (ze^{-\beta E_\varepsilon})^{n_\varepsilon} \tag{1.3}$$

$$=\prod_\varepsilon\left[\sum_{n=0}^{\infty}(ze^{-\beta E_\varepsilon})^n\right]=\prod_\varepsilon\frac{1}{1-ze^{-\beta E_\varepsilon}}$$

N is the total number of Bosons in the sample, while n_ε is the occupation number of the energy level ε with energy E_ε . The products in Eq.1.3 extend over all possible energy levels ε of the system, while the sums include all possible level occupation numbers which add up to N. This grand partition function leads to the equation of state for an ideal Bose gas

$$\frac{pV}{k_B T} = \log \Im(z, V, T) = -\sum_{\varepsilon} \log(1 - z e^{-\beta E_\varepsilon}) \tag{1.4}$$

where p is the pressure exerted by the gas which occupies a volume V. The sum extends again over all existing energy levels ε. From Eq.(1.3) we deduce the expected number of particles occupying an energy level ε as

$$\langle n_\varepsilon \rangle = -\frac{1}{\beta}\frac{\partial}{\partial E_\varepsilon}\log \Im = \left(\frac{e^{\beta E_\varepsilon}}{z} - 1\right)^{-1}. \tag{1.5}$$

Since occupation numbers $\langle n_\varepsilon \rangle$ for all possible energy levels have to add up to the total number N, we obtain an implicit expression for the fugacity z:

$$\sum_{\varepsilon}\left(\frac{e^{\beta E_\varepsilon}}{z} - 1\right)^{-1} = N. \tag{1.6}$$

So far we have discussed a general system of ideal bosonic particles. We did not specify the energy level structure, i.e. the density of states. It is this structure which determines whether the system Bose condenses.

Let's examine a non-relativistic gas in a three dimensional box at a given density N/V. In this case the dispersion relation is

$$E_p = \frac{p^2}{2m} \tag{1.7}$$

where E_p is the energy of a particle of mass m with the quantized momentum p. The quantization of the momentum states in a volume V allows us to transform the sum in Eq.(1.6) into an integral for $V\to\infty$:

$$\frac{N}{V}=\frac{4\pi}{h^3}\int_0^\infty dp\cdot p^2\,\frac{1}{z^{-1}e^{\beta p^2/2m}-1}+\frac{1}{V}\frac{z}{1-z} \tag{1.8}$$

As $z\to 1$ the single term corresponding to p=0 diverges. This term may therefore be as important as the entire integral. The integral in Eq.(1.8) can be expressed by the infinite sum $g_{3/2}(z)$ [3] as

$$\frac{N}{V}=\frac{1}{\Lambda^3}g_{3/2}(z)+\frac{1}{V}\frac{z}{1-z}, \tag{1.9}$$

$$g_{3/2}(z)=\sum_{l=1}^{\infty}\frac{z^l}{l^{3/2}}$$

where $\Lambda = (2\pi\hbar^2/mk_BT)^{1/2}$ is the thermal de Broglie wavelength of the particles. Eq.(1.6) requires z to assume values between 0 and 1. $g_{3/2}(z)$ then is a monotonically increasing function of z which vanishes for z=0 and is bounded by 1 for $z\to 1$.

We rewrite Eq.1.9 in the form

$$\frac{\langle n_0\rangle}{V}=\frac{N}{V}-g_{3/2}(z)/\Lambda^3 \tag{1.10}$$

where

$$\langle n_0\rangle=\frac{z}{1-z} \tag{1.11}$$

is the number of particles in the ground state of the system. This implies that if we increase the density of particles in the system such that

$$\frac{N}{V} \geq g_{3/2}(1)/\Lambda^3, \tag{1.12}$$

a finite fraction of particles will occupy the ground state. This phenomenon is called *Bose-Einstein condensation*. The condition above also defines the critical temperature T_c at which the transition occurs

$$kT_c = \frac{2\pi\hbar^2/m}{[2.612...\cdot V/N]^{3/2}} \tag{1.13}$$

The condensate fraction $\langle n_0 \rangle / N$ vanishes for temperatures above T_c. For temperatures below T_c it varies as

$$\langle n_0 \rangle / N = 1 - (T/T_c)^{3/2} \tag{1.14}$$

The nature of the phase transition is purely quantum statistical. I want to give a "hand waving" argument for this: Consider a system with N bosons. The total energy E in the system is fixed and a number of accessible states per particle increases with the energy ε per particle as ε^d (d=2 for the free three dimensional gas considered above). In thermal equilibrium all possible realizations of the ensemble which conserve the total energy are equally likely to occur. The expected ground state occupation is obtained as the average over all members of the ensemble. To find out what makes indistinguishable particles accumulate in the ground state of the system (under certain conditions), we have to understand the structure of possible realizations of the ensemble. There are two extreme cases:

(a) The available energy can be distributed over as many particles as possible. For a total energy E which is large enough, that there are far more than N states accessible to each particle, even if the energy is evenly spread over all N particles, the number of possible realizations of type (a) scales as $(E/N)^{dN}$. In this case there are hardly any particles populating the ground sate.

(b) In the other extreme, the total energy is distributed only over a small number of particles fN ($f<<1$), such that each particle can access a very large number of states, the number of possible realizations of type (b) scales as $(E / fN)^{dNf}$. Is this case the majority of the particles populates the ground state.

As long as the total energy E is large and the indistinguishability of the particles is *not* relevant, i.e. the range of accessible states is so large, that it is extremely unlikely for particles to occupy the same state, most realizations in the ensemble are of type (a). For decreasing energies however, fewer states are accessible to each particle in (a) and realizations with levels occupied by more than one particle occur. This reduces the number of "type (a)"-realizations *due to the indistinguishability of the particles.* The number of "type (b)"-realizations is not affected significantly by the indistinguishability of particles as only a few particles are distributed over many states and are not very likely to occupy the same state. The entropy of case (a) might fall below the entropy of case (b) and the system Bose condenses. Whether this is the case depends on the energy level structure of the system: In the thermodynamic limit, a system is able to undergo Bose condensation, if the number of states accessible to a particle as a function of its energy ε increases more rapidly than $\varepsilon^{1/2}$.

So far we only discussed a gas of bosons in a three dimensional box in the thermodynamic limit ($N\to\infty$, $V\to\infty$) quantitatively. In all BEC experiments a finite number of particles is condensed in a anisotropic harmonic potential U which has approximately cylindrical symmetry:

$$U(r,z) = \tfrac{1}{2}m\omega_z^2 z^2 + \tfrac{1}{2}m\omega_r^2 r^2. \qquad (1.15)$$

z is the position along the symmetry axis of the potential, r is the radial coordinate and ω_z, ω_r are the respective trapping frequencies. This case is very similar to the "3D-box" and was discussed by Bagnato *et. al.* [40] as well as by de Groot[41] for the thermodynamic limit. The critical temperature is given as

$$T_c = \frac{\hbar\varpi}{k_B}\left(\frac{N}{1.202}\right)^{1/3}. \tag{1.16}$$

where $\varpi = \left(\omega_z\omega_r^2\right)^{1/3}$ is the geometric mean of the trapping frequencies. The condensate fraction is given as

$$\langle n_0\rangle / N = 1-(T/T_c)^3. \tag{1.17}$$

Intuitively one expects Bose condensation in three dimensions to begin when the density of particles is approximately Λ^{-3}, i.e. one particle per cubic de Broglie wavelength. In fact, as was shown in [40], the onset of BEC is given by Eq.(1.12) irrespective of nature of the trapping potential (N/V in this equation denotes the *peak* density of the sample).

Strictly speaking, a phase transition only occurs in the thermodynamic limit. However, as was shown e.g. by Ketterle and van Druten [42], the behavior of the finite N system is very similar to the thermodynamic limit. Phase transitions are usually defined by singularities or critical behavior. However, there are no singularities in a finite system. For finite N-systems we take the macroscopic occupation of the ground state as the defining characteristics of the phase transition. As a consequence systems which Bose condense in the thermodynamic limit also condense in the finite-N case.

References in Chapter 1

1 A. Einstein, Sitzungsberichte der preussischen Akademie der Wissenschaften, 18-25 (1925).

2 K. Huang, in *Bose-Einstein Condensation*, edited by A. Griffin, D. W. Snoke and S. Stringari (Cambridge University Press, Cambridge, 1995), p. 31-50.

3 K. Huang, *Statistical Mechanics* (Wiley, New York, 1987).

4 A. Griffin, D. W. Snoke, and S. Stringari, *Bose-Einstein Condensation* (Cambridge University Press, Cambridge, 1995).

5 J. L. Lin and J. P. Wolfe, Physical Review Letters **71**, 1222 (1993).

6 C. E. Hecht, Physica **25**, 1159 (1959).

7 W. C. Stwalley and L. H. Nosanow, Physical Review Letters **36**, 910 (1976).

8 I. F. Silvera and J. T. M. Walraven, Physical Review Letters **44**, 164-168 (1980).

9 R. W. Cline, T. J. Greytak, and D. Kleppner, Physical Review Letters **47**, 1195 (1981).

10 A. J. Berlinsky and B. W. Statt, Physical Review Letters **45**, 2105 (1980).

11 R. Sprik, J. T. M. Walraven, and I. F. Silvera, Physical Review B **32**, 5668 (1985).

12 D. A. Bell, H. F. Hess, G. P. Kochanski, *et al.*, Physical Review B **34**, 7670 (1986).

13 T. Tommila, E. Tjukonov, M. Krusius, *et al.*, Physical Review B **36**, 6837 (1987).

14 A. L. Migdall, J. V. Prodan, W. D. Phillips, *et al.*, Physical Review Letters **54**, 2596 (1985).

15 H. F. Hess, Physical Review B **34**, 3476 (1986).

16 N. Masuhara, J. M. Doyle, J. C. Sandberg, *et al.*, Physical Review Letters **61**, 935 (1988).

17 J. M. Doyle, J. C. Sandberg, I. A. Yu, *et al.*, Physical Review Letters **67**, 603 (1991).

18 S. Chu, L. Hollberg, J. E. Bjorkholm, *et al.*, Physical Review Letters **55**, 48 (1985).

19 P. D. Lett, R. N. Watts, C. I. Westbrook, *et al.*, Physical Review Letters **61**, 169 (1988).

20 P. Ungar, D. Weiss, E. Riis, *et al.*, Journal of the Optical Society of America B , 2058 (1989).

21 J. Dalibard and C. Cohen-Tannoudji, Journal of the Optical Society of America B , 2023 (1989).

22 E. L. Raab, M. Prentiss, A. Cable, *et al.*, Physical Review Letters **59**, 2631 - 2634 (1987).

23 E. Arimondo, W. D. Phillips, and F. Strumia, *Laser Manipulation of Atoms and Ions* (North-Holland, Amsterdam, 1992).

24 C. G. Townsend, N. H. Edwards, C. J. Cooper, *et al.*, Physical Review A **52**, 1423-1440 (1995).

25 H. J. Lee, C. S. Adams, M. Kasevich, *et al.*, Physical Review Letters **76**, 2658 (1996).

26 M. H. Anderson, J. R. Ensher, M. R. Matthews, *et al.*, Science **269**, 198-210 (1995).

27 C. C. Bradley, C. A. Sackett, J. J. Tollet, *et al.*, Physical Review Letters **75**, 1687 (1995).

28 C. S. Adams, H. J. Lee, N. Davidson, *et al.*, Physical Review Letters **74**, 3577 (1995).

29 K. B. Davis, M.-O. Mewes, M. R. Andrews, *et al.*, Physical Review Letters **75**, 3969 (1995).

30 M.-O. Mewes, M. R. Andrews, N. J. van Druten, *et al.*, Physical Review Letters **77**, 416-419 (1996).

31 C. J. Myatt, E. A. Burt, R. W. Ghrist, *et al.*, preprint (1996).

32 C. C. Bradley, C. A. Sackett, and R. G. Hulet, preprint (1996).

33 E. Culotta, in *Science*, 1995, Vol. 270, p. 1902-1903.

34 D. Kleppner, in *Physics Today*, August 1996, p.11-13.

35 C. E. Wieman, E. A. Cornell, D. Jin, *et al.*, in *ICAP 15* (to be published, Amsterdam, 1996).

36 C. G. Townsend, N. J. van Druten, M. R. Andrews, *et al.*, in *ICAP 15* (to be published, Amsterdam, 1996).

37 M.-O. Mewes, M. R. Andrews, D. M. Kurn, *et al.*, Physical Review Letters, in press (1996).

38 D. S. Jin, J. R. Ensher, M. R. Matthews, *et al.*, preprint (1996).

39 M.-O. Mewes, M. R. Andrews, N. J. van Druten, *et al.*, Physical Review Letters **77**, 416 (1996).

40 V. Bagnato, D. E. Pritchard, and D. Kleppner, Physical Review A **35**, 4354 (1987).

41 S. R. de Groot, G. J. Hooyman, and C. A. ten Seldam, Proc. Roy. Soc. London **Ser. A 203**, 266 (1950).

42 W. Ketterle and N. J. v. Druten, Physical Review A **54**, 656-660 (1996).

2. EXPERIMENTAL TECHNIQUES

This chapter presents the techniques used to achieve and observe Bose-Einstein condensation in a dilute atomic vapor of sodium. Some experimental methods are discussed in more detail in the theses of Michael Joffe [1] and Kendall Davis [2].

In order to reach Bose-Einstein condensation starting out with a 600 K hot saturated vapor of atomic sodium we have to increase the phase space density by *twelve* orders of magnitude. So far, there is no *single* technique that accomplishes such an enormous increase. Several different schemes have to be applied consecutively. The first part of this chapter (sections 2.1-2.3) explains magnetic trapping and evaporative cooling, the techniques used to cool a sample of ultracold atoms into the quantum degenerate regime. The second part of the chapter (sections 2.4-2.5) deals with the preparation of such an ultra-cold sample and the transfer into a magnetic trap.

2.1 Magnetic Trapping of Neutral Atoms

According to Eq.(1.13) sodium atoms Bose condense at the critical temperature[1]

$$T_c = \frac{h^2}{2\pi k_B m}\left(\frac{1}{2.612}n_c\right)^{2/3} = \left(\frac{n_c}{5.4\cdot 10^{13} cm^{-3}}\right)^{2/3} \mu K \qquad (2.1)$$

where n_c denotes the peak density of the sample. Above densities of 10^{15} atoms/cm^3 a sample of sodium atoms is estimated to decay within less than a second into molecules through three-body collisions [4]. We have to observe BEC at a density below 10^{15} atoms/cm^3. This requires a transition temperature T_c smaller than 7μK. This temperature is close to the single-photon recoil limit T_{recoil}=2.4μK. $k_B T_{recoil}/2$ equals the kinetic energy transferred to a sodium atom at rest due to the emission or absorption of a photon resonant with the dominant optical transition (589 nm). In order to achieve Bose

[1] Eq.(2.1) is valid for a non-interacting gas. Weak interactions can increase the transition temperature in a harmonic oscillator potential [3]. For a samples of sodium with a critical peak density around 10^{14} cm^{-3} the shift is predicted to be less than 10%.

condensation the temperature has to be controlled with a precision better than the recoil limit. The atoms need to be confined in a trap which has a intrinsic heating rate that is much smaller than the cooling rate down to T_c. Consequently the atoms also have to be isolated from the "hot" environment such as the walls of a vacuum chamber or the background gas in the chamber. Collisions with the background gas can be avoided by storing the sample in ultra-high vacuum. Confinement principles for neutral atoms, which satisfy the above conditions, are: trapping with the far-off resonant dipole (light) force and magnetic trapping. We confine sodium atoms magnetically.

An atom with a magnetic dipole moment $\vec{\mu}$ in a magnetic field $\vec{B}(\vec{r})$ experiences the potential

$$U(\vec{r}) = -\vec{\mu}\vec{B}(\vec{r}) \tag{2.2}$$

provided it moves slowly enough for $\vec{\mu}$ to follow the changes in the orientation of $\vec{B}(\vec{r})$ adiabatically[2]. The absolute value B of an inhomogeneous magnetic field can possess a local minimum, Maxwell's equation however exclude a magnetic field configuration with a local maximum. Atoms with a magnetic moment oriented anti-parallel to $\vec{B}(\vec{r})$ can be trapped in a magnetic field minimum and are called "weak-field seekers", while it is impossible to magneto-statically confine the "strong-field seekers", atoms with a magnetic moment parallel to $\vec{B}(\vec{r})$.

We magnetically trap sodium atoms in the F=1, m_F= -1 hyperfine ground state. F is the quantum number of the total angular momentum and m_F denotes the quantum number of its projection onto the local magnetic field. These weak-field seeking atoms are moving in a magnetic potential

$$U(\vec{r}) = \tfrac{1}{2}\mu_{Bohr}B(\vec{r}) = h \cdot \frac{0.70MHz}{Gauss}B(\vec{r}) \tag{2.3}$$

[2] This is the case if the Lamor precession of the atom is much faster than the rotation of the magnetic field in the reference frame of the atom. A detailed dicussion of this subject is included in chapter 3.1.

So far we have not specified the geometry of the magnetic trapping field. There are two classes of static magnetic traps: Traps with a vanishing magnetic field in the center, which leads to a linear trapping potential in the vicinity of the origin, and traps with finite magnetic field at the origin. The latter trap type produces a magnetic trapping potential which is quadratic.

Which of the two classes is better suited for cooling atoms ? "Real" cooling is synonymous with the increase of the sample's phase space density $\mathcal{D}$, which scales as $n_0 T^{-3/2}$ according to Eq.(1.1) and Eq.(1.2). n_0 is the peak density and T the temperature of the sample. Our objective is to achieve a *high* densities and a *low* temperatures in the trap. In order to maximize the density of a trapped sample we have to provide confinement, i.e. a restoring force, which is as strong as possible for a given magnet current. In this respect a linear trap is clearly superior. The trapping potential we initially chose to cool sodium atoms into the quantum degenerate regime was therefore linear [5]. It was constructed from two current carrying coils in "Anti-Helmholtz" configuration as shown in Fig.2.1 .

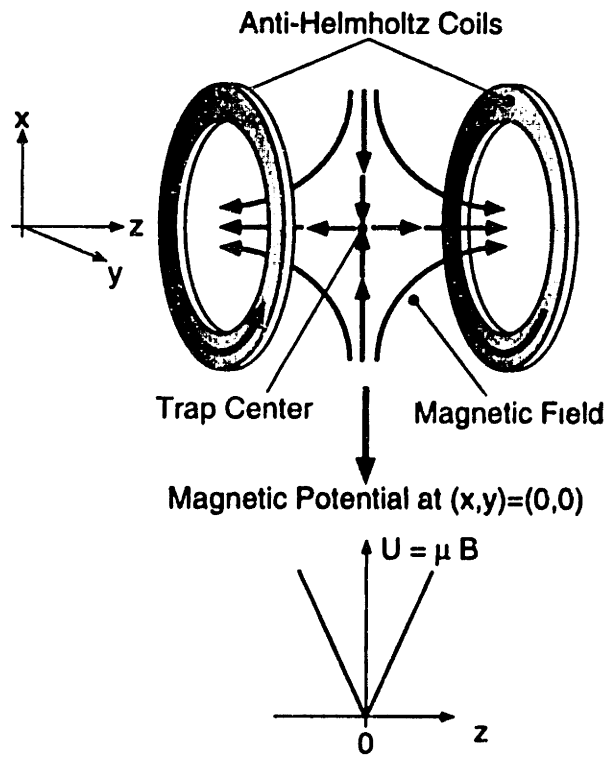

Fig. 2.1. A linear magnetic trapping potential can be realized with two identical coils , which have the same symmetry axis and are separated by approx. the coil diameter. The currents flowing through the coils are of equal magnitude but have opposite sign. The magnetic field geometry is that of a spherical quadrupole field. The field in the geometric center between both coils vanishes. From the center outwards along the z axis, as well as in the x-y plane the magnetic field increases linearly. The magnetic field gradient in the z direction is twice as large as the gradients in the x-y plane. This follows from Maxwell's equations and results in an anisotropic potential.

2.2 Evaporative Cooling

In addition to a storage mechanism, we also require a cooling technique which increases the phase space density of the confined atoms. In section 2.1 it was shown that in order to achieve BEC we have to cool to temperatures close to or even below the photon-recoil limit. Optical cooling methods which cool atoms below the recoil limit in three dimensions have been developed and demonstrated [6, 7], but the successful combination of optical sub-recoil cooling and high atomic densities has not yet been achieved. We decided not to cool the magnetically trapped atoms with photons. Instead, the temperature is lowered by evaporation: Atoms with more than average energy are continuously removed from the sample while the remainder thermally equilibrates through elastic collisions. These collisions replenish the "high-energy" tail of the distribution.

Evaporation is a universal phenomenon. It denotes the transition from a liquid to a gaseous state or, more accurately, it describes the process of energetic particles leaving a system of finite binding energy. Since the evaporating particles remove more than their average share in energy, the temperature of the remaining system is lowered. Hence, evaporation results in cooling. It is this phenomenon that efficiently cools a hot cup of coffee. Evaporative cooling occurs naturally since a thermalized system always has a population of high energetic particles. It persists as long as the system is able to thermalize and replenish the high-energy tail of the distribution. However, the efficiency of evaporation process can be greatly improved by forcing it i.e. by lowering the energy threshold above which particles evaporate as the temperature of the system decreases.

The idea to apply evaporation to an ultra-cold trapped atomic gas was first conceived by Hess [8] and implemented with spin polarized atomic hydrogen at MIT [9]. In order to simply model evaporative cooling analytically, it can be approximated as a series of discrete two-step processes [10]: A sample of atoms in thermal equilibrium is trapped in a conservative potential. In the *truncation step* the high energy tail of the distribution is removed from the system. It then reequilibrates at a lower temperature in the *equilibration step*. The atoms have to elastically collide to redistribute energy. The

speed of evaporation is therefore determined by the elastic collision rate in the sample. It is vital to the method that we prepare a sample of atoms with collision times much shorter than the trapping time.

The physics governing evaporative cooling of trapped atoms is discussed in detail in the theses of Kendall Davis [2] and Michael Joffe [1] as well as in the review by Ketterle and van Druten [11] and references therein. In the following I will summarize the issues and considerations relevant for the research reported in this thesis.

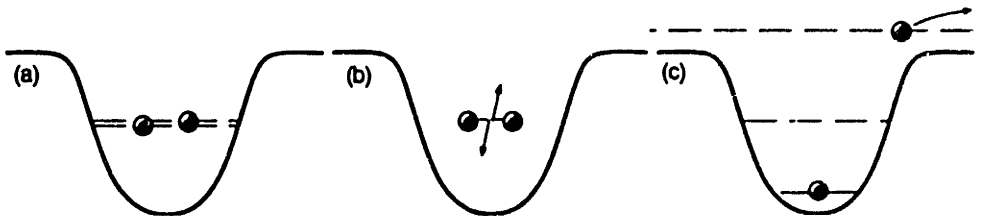

Fig.2.2 Evaporative cooling is driven by elastic collisions. Trapped atoms (a) redistribute energy through elastic collisions (b) and produce atoms in the high energetic tail of the distribution. These atoms escape the potential of finite depth (c). The remaining atoms will collide with less average energy and the temperature is lowered.

Evaporative cooling is driven by elastic collisions as illustrated in Fig.2.2. The peak elastic collision rate in a sample is

$$\Gamma_{el} = n_0 \sigma_{el} \sqrt{\frac{16 k_B T}{\pi m}} \tag{2.4}$$

where n_0 is the peak density and σ_{el} is the elastic scattering cross section at temperature T. A sodium atom at T=200μK and a density of 10^{11} atoms/cm^3 collides with a rate of 20Hz. After truncation about 5 collisions per atom are needed to approach thermal equilibrium [12]. A possible scenario is a continuous truncation at $6k_BT$ in a 3-dimensional harmonic potential, which leads to a 0.8% decrease in number per collision time and to a phase space density increase of 2.3% per collision time. Starting from a phase space density which is approximately by a factor 10^6 short of BEC, this typically

leads to the onset of the phase transition in 600 collisions per atom with 1% of the original number of atoms remaining [11].

We have to truncate in such a way that the collision rate increases as the evaporation process proceeds, i.e. the sample density has to increase faster than $T^{1/2}$ decreases. If this criterion is fulfilled the cooling process speeds up as it progresses and does not fade out. This regime is called *runaway* evaporation.

The role of inelastic collisions is discussed in [11]. For sodium inelastic collisions determine the lowest temperature practically achievable with evaporation, ~100pK [11]. This is much lower than typical transition temperatures of 2μK in our experiments [13, 14].

So far we have assumed that the evaporated atoms are selected based on their total energy. However, some truncation mechanisms only use the energy of the atoms in one or two of the three dimensions as a selection criterion [11]. This "washes" out the edge of evaporation and lowers the cooling efficiency (see also chapter 4.2).

2.3 Rf-Induced Evaporation

There are several ways to truncate the energy distribution of trapped atoms. For magnetically trapped atoms radio frequency (rf) induced evaporation is a very convenient method. This technique "flips" trapped atoms into the untrapped hyperfine state with a very narrow energy-selective rf transition. It was first proposed by David Pritchard [15].

Sodium atoms in the trapped $F=1,m_F=-1$ hyperfine level experience a linear Zeeman shift as they are oscillating in a relatively weak magnetic field of the trap (<100 Gauss). This energy shift is given by Eq.(2.3) and corresponds to the potential energy of the atom in the trap. The Zeeman shift of the untrapped $F=1,m_F=1$ state has the opposite sign. Atoms in the trapped state can be coupled to this untrapped state with radio frequency radiation through electron-spin resonance. Both states are coupled by a resonant two-photon transition through the intermediate $F=1,m_F=0$ state. Rf induced evaporation spin-flips atoms on a resonant shell where

$$\nu_{rf} = \frac{0.70MHz}{Gauss} B(\vec{r}). \tag{2.5}$$

ν_{rf} is the frequency of the rf field. By adjusting the radio frequency we can decrease the edge of truncation to force the evaporation. Rf-induced evaporation is a three-dimensional energy truncation as long as B=const is a equipotential surface. This is the case if gravity is negligible. Gravity pulls the cloud downwards in the potential. If the temperature decreases to a value such that potential due to gravity varies by more than kT over the B=const truncation surface, the energy-selection becomes lower-dimensional [11] (see also chapter 4.2).

Rf evaporation can be described in the dressed atom formalism which is illustrated in Fig.2.3 . One important feature of rf evaporation is that it does not modify the confinement due to the magnetic trapping field. It allows for independent control of trap parameters and the edge of evaporation.

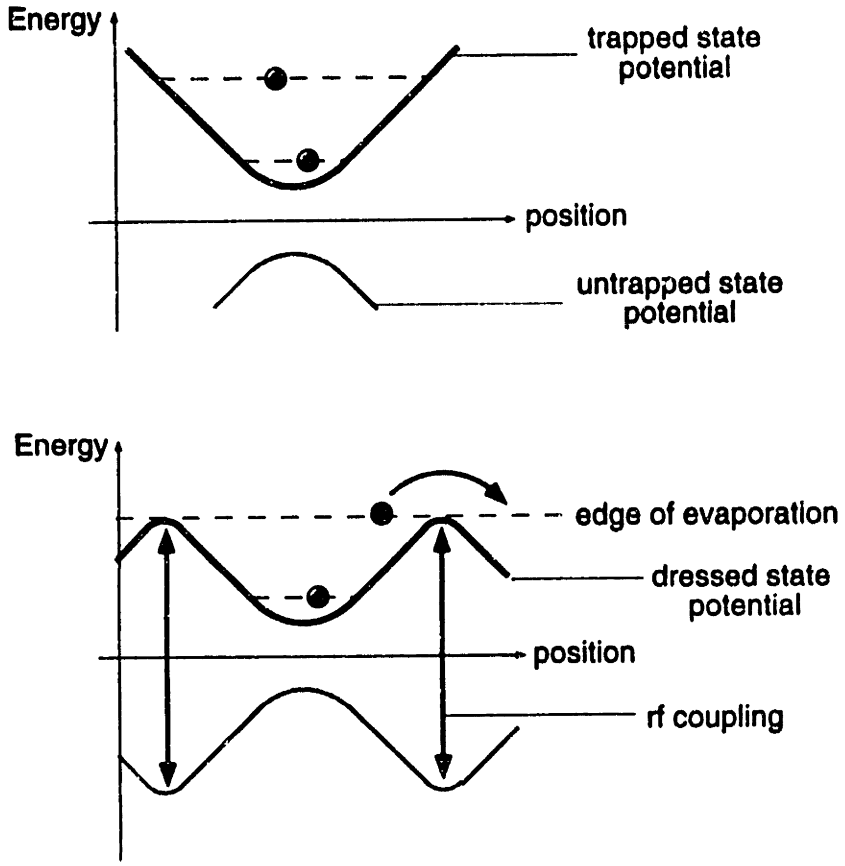

Fig. 2.3 Radio frequency induced evaporation of atoms trapped in a magnetic potential. Depicted (top) is the potential energy of the trapped and the untrapped hyperfine state. Rf radiation of an adjustable resonance frequency corresponding to a given potential energy shell couples the trapped with the untrapped state. In the dressed atom picture [16] the rf radiation introduces energy levels which are a mixture trapped and trapped states near resonance. An atom which slowly passes through the resonant region adiabatically follows the energy levels. The atom is adiabatically transferred from the trapped into the untrapped state and escapes (bottom). For fast atoms the adiabaticity condition is not valid and the probability for spin-flips is determined by Landau-Zener theory[17].

2.4 Preparing Atoms for Evaporative Cooling

The depth of magnetic traps based on conventional electro-magnets is in the mK range. In addition evaporative cooling requires atoms to be dense enough to collide elastically. We therefore need to prepare a sample of atoms with a temperature of less than one mK and a density around 10^{11} atoms/cm^3. In order to achieve this goal, we use laser cooling and trapping techniques developed during the 1980's [18] for the preparation of the sample:

In our experimental setup the source is a thermal beam of sodium atoms originating from an oven with an average velocity of 800 m/s. The phase space density of this beam is about 12 orders of magnitude short of BEC. A Zeeman slower first slows these atoms to a velocity of 30 m/s, a kinetic energy corresponding to 1K [19], sufficient for capturing by a Magneto Optical Trap (MOT) [20]. The Zeeman slower has an increasing magnetic field and produces a flux of up to 10^{12} atoms/cm^2 [21]. This allows us to load the MOT with about 10^{10} atom within 1s. The MOT compresses atoms into a volume of 2 mm diameter at an approximate density of $5x10^{11}$ atoms/cm^3. In the MOT atoms are cooled to 1mK. The MIT group had developed a "dark" version of the MOT in which the atoms are mainly confined in a hyperfine level which only hardly interacts with the trapping light. This *dark SPOT* (dark **S**pontaneous-force **O**ptical **T**rap) [22] reduces the reabsorption of spontaneously scattered photons and consequently removes the strong radiation pressure forces between atoms. This "trick" leads to an improvement in density by almost two orders of magnitude over "conventional" magneto-optical traps. This development provides the crucial link between laser cooling and evaporative cooling by providing sufficient density to start evaporation. After compression and cooling in the dark SPOT the magnetic fields of the dark SPOT are extinguished instantaneously and polarization gradient cooling [23] is applied for 3 ms. During this short time the ballistic expansion of the atoms is negligible and the temperature is reduced to 100 μK. This cold

cloud is then caught by quickly switching off the light and turning on the magnetic trap (chapter 2.5).

2.5 Loading Atoms into a Magnetic Trap

The last necessary step, which has not been discussed so far, is to join laser cooling and evaporative cooling by transferring the optically pre-cooled sample into the magnetic trap. I first describe the procedure qualitatively and then present a simplified quantitative analysis of the transfer conditions.

The atoms have been cooled and trapped in the dark SPOT trap. After polarization gradient cooling the density of $5x10^{11}$ atoms/cm^3 at the temperature of ~100μK allows for 40 elastic collisions per atom per second: A starting point for evaporative cooling in a magnetic trap. How do we transfer the atoms into a magnetic trap without loosing the initially gained phase space density and the already achieved collision rate ?

Since the magneto-static potential is conservative, it is impossible to "drop" the atoms into a magnetic potential without providing an additional damping mechanism. We suddenly switch on the magnetic potential around the atoms instead. Only the "weak-field seeking" $F=1,m_F=-1$ hyperfine state can be confined magnetically. After laser cooling the atoms are approx. equally distributed over all three m_F-states in the F=1 hyperfine manifold. This leads to a loss of ~2/3 of the atoms during the transfer. This loss can be avoided by optically pumping all atoms into the $m_F=-1$ state immediately before transfer (while providing a small magnetic guiding field). We have not implemented this technique because our initial collision rate in the magnetic trap is sufficient. (Note that this loss in number is not a loss in phase space density, since we reduce the number of internal states accessible to the trapped atoms by a factor of 3. Optical pumping would therefore increase the phase space density.) The magnetic trap is switched on in about 1 ms in order to avoid spreading of the pre-cooled and unconfined cloud. The strength of the magnetic potential has to be chosen appropriately: If it is too shallow, the trapped cloud

will spread out and density is lost. If it is too stiff, too much potential energy will be added to the cloud and causes unnecessary heating. After an optimized ("mode matched") transfer the confinement is increased adiabatically by ramping up the current flowing through the trap coils to its maximum value.

The peak phase space density during adiabatic compression is preserved if the power law of the potential remains unchanged [24]. During the compression the density and the temperature of the sample increase, which results in a gain in elastic collision rate. Fig. (2.4) illustrates the steps involved in the transfer into a linear potential.

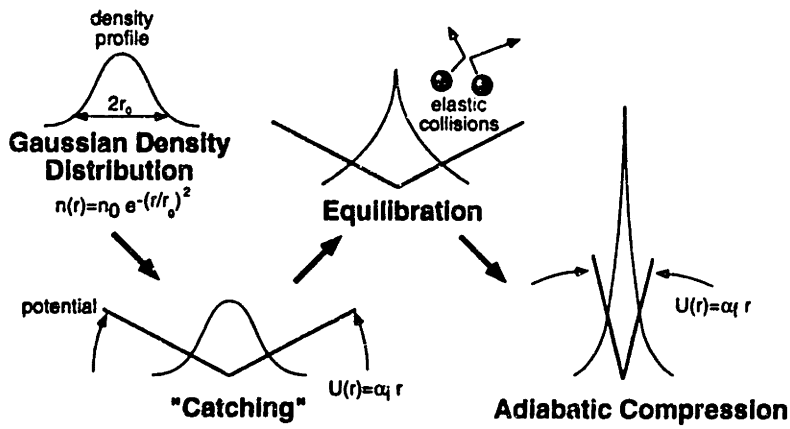

Fig.2.4 Transfer of laser-cooled atoms into a linear magnetic trap and subsequent adiabatic compression. Atoms with Gaussian density distribution are caught in a magnetic trap, which is switched on instantaneously ("catching"). The density distribution in the linear trap "relaxes" with a few collisions per atom. This "relaxation" can increase the samples phase space density (see section below). After "equilibration" the sample is compressed adiabatically, which increases the elastic collision rate.

In the following paragraphs the transfer and the adiabatic compression are discussed quantitatively. We only consider the transfer into isotropic linear and harmonic traps and the subsequent compression by increasing the confinement current. The "idealized" atoms have no internal degree of freedom and are transferred with a 100% efficiency. In reality the confining potentials are anisotropic (e.g. see Fig.2.1) and 2/3 of the atoms are in the "wrong" spin state and lost during the transfer. These discrepancies of the model do not affect the conclusions.

After polarization gradient cooling the density distribution of the N atoms in free space is approximately gaussian

$$n_{prep} = n_0 e^{-\pi\left(\frac{n_0}{N}\right)^{\frac{2}{3}} r^2} \tag{2.6}$$

n_0 is the peak density and the temperature of the sample is $T_{pol.grad.}$. N atoms, which thermalize at a temperature T in a linear trapping potential $U(r) = \alpha r$, have an exponential density distribution

$$n_{linear} = \frac{N\alpha^3}{8\pi(k_B T)^3} e^{-\frac{\alpha r}{k_B T}}. \tag{2.7}$$

In a harmonic trapping potential $U(r) = \alpha r^2$ the thermalized distribution is gaussian

$$n_{harmonic} = \frac{N\alpha^{3/2}}{\pi^{3/2}(k_B T)^{3/2}} e^{-\frac{\alpha r^2}{k_B T}}. \tag{2.8}$$

The strength of the confinement α is proportional to the current through the trap coils for both the linear and the harmonic traps. α can therefore be regarded as the normalized trapping current. According to the virial theorem the relation between the total energy of the trapped atoms E_{total} and the temperature T is

$$E_{total} = \left(\frac{3}{2} + \frac{3}{p}\right) N k_B T \tag{2.9}$$

where p=1 for the linear case and p=2 for a harmonic potential. During the instantaneous transfer atoms receive potential energy in addition to their thermal energy. After performing the integral of the density distribution this leads to a sample temperature

$$k_B T = \frac{4\alpha(N/n_0)^{\frac{1}{3}}}{9\pi} + \frac{k_B T_{pol.grad.}}{3} \tag{2.10}$$

in the linear trap after thermalization. In a harmonic trap the relation is

$$k_B T = \frac{\alpha (N/n_0)^{\frac{1}{3}}}{2\pi} + \frac{k_B T_{pol.grad.}}{2}. \tag{2.11}$$

We want to preserve (or even increase) the phase space density during the transfer. The peak phase space density of the sample scales as $n_{peak}T^{-3/2}$ according to Eq. 1.1 and Eq.1.2. n_{peak} is the peak density of the sample.

We can analytically show that the phase space density after the transfer is maximized if $T=T_{pol.grad.}$. This is the condition for "mode matched" transfer. We normalize the phase space density such that it is unity in the sample right before the transfer. α is normalized to $\tilde{\alpha}$ such that it is unity in the mode matched case. The normalized phase space density $\tilde{\mathcal{D}}=n_{peak}/n_0\,(T_{pol.grad}/T)^{3/2}$ after the transfer into the linear trap (and relaxation) is

$$\tilde{\mathcal{D}}_{linear} = \frac{3^7\sqrt{3}\pi^2\tilde{\alpha}^3}{2^6(1+2\tilde{\alpha})^{\frac{9}{2}}} \tag{2.12}$$

For harmonic trap it is given by

$$\tilde{\mathcal{D}}_{harmonic} = \frac{8\tilde{\alpha}^{3/2}}{(1+\tilde{\alpha})^3}. \tag{2.13}$$

The phase space density vs. trap current is displayed in Fig.2.5. The phase space density after the mode matched transfer into the linear trap has increased by approx. a factor of 4. This is a surprising result but does not violate Liouville's theorem since collisions are involved in the relaxation. Fig. 2.5 also indicates that the phase space density is not very sensitive to α. A deviation from the "mode matched" current by a factor of three barley halves the phase space density !

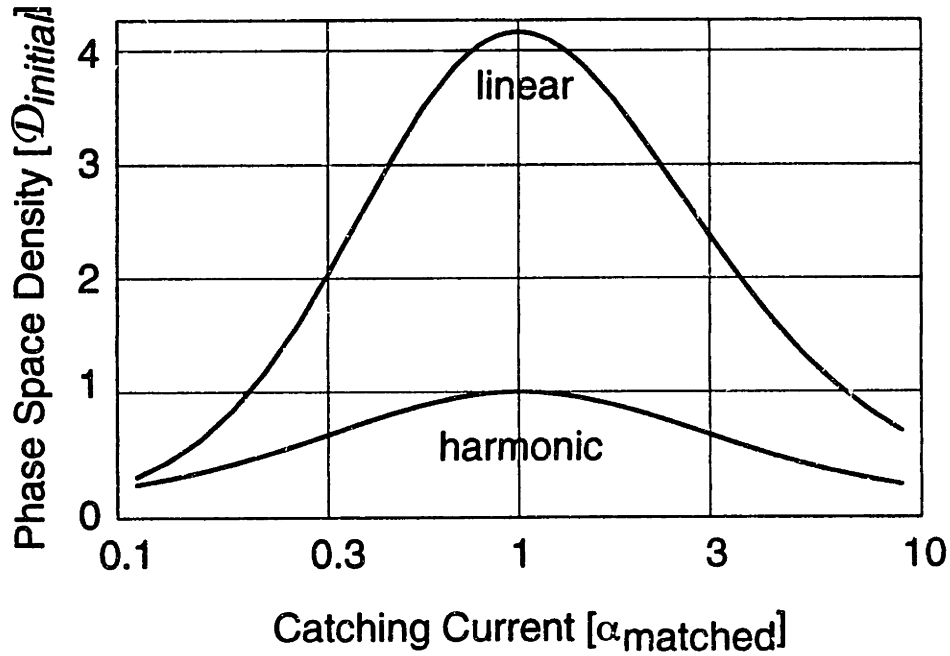

Fig.2.5 displays the peak phase space density $\mathcal{D}$ of laser-cooled atoms after transfer into a magnetic trap and collisional "relaxation". $\mathcal{D}$ is displayed as a function of the initial catching current. $\mathcal{D}$ is plotted in units of $\mathcal{D}_{initial}$, the peak phase space density of the sample right before the transfer. The catching current α is measured in units of the mode matched current $\alpha_{matched}$. The scale of the abscissa is logarithmic.

Aside from maximizing the phase space density, which is the ultimate figure of merit, we would like to maximize the elastic collision rate, which scales as $n_{peak}T^{1/2}$ according to Eq.(2.8). The collision rate after transfer normalized to the mode-matched case is

$$\tilde{\Gamma}_i = \frac{3^{5/2}\tilde{\alpha}_i^3}{(1+2\tilde{\alpha}_i)^{5/2}} \tag{2.14}$$

for a linear trap and

$$\tilde{\Gamma}_i = \frac{2\tilde{\alpha}_i^{3/2}}{1+\tilde{\alpha}_i} \tag{2.15}$$

in the harmonic potential. $\tilde{\alpha}_i$ is the renormalized catching current.

After "catching" the sample is adiabatically compressed. Adiabatic compression preserves entropy. If the power law of the potential is unchanged during compression the

phase space density remains constant during this process [24]. (A change in the power law of the potential during compression changes the phase space density and is discussed in chapter 4.1.4). An interesting question is whether we can trade off phase space density for elastic collision rate by catching at a non-mode matched current and then compressing to the maximum trap current. The advantage of such a trade off (if possible) would be a faster initial cooling rate. A faster cooling rate might allow us to cool more atoms into the quantum-degenerate regime on a shorter timescale. The increase in number would be due to fewer background gas collisions and a different evaporation path. We therefore investigate the final elastic collision rate as a function of initial catching current and final compression current. During adiabatic compression in the linear/ harmonic trap the phase space density is constant and given by Eq.(2.12)/ (2.13). The normalized collision rate after adiabatic compression in the linear trap is

$$\tilde{\Gamma}_f = \frac{3^{5/2}\tilde{\alpha}_f^2\tilde{\alpha}_i^{5/3}}{(1+2\tilde{\alpha}_i)^{5/2}} = \tilde{\Gamma}_i\tilde{\alpha}_f^2\tilde{\alpha}_i^{4/3} \tag{2.16}$$

and

$$\tilde{\Gamma}_f = \frac{2\tilde{\alpha}_f\sqrt{\tilde{\alpha}_i}}{1+\tilde{\alpha}_i} = \tilde{\Gamma}_i\tilde{\alpha}_i\tilde{\alpha}_f \tag{2.17}$$

describes the same quantity for the harmonic trap.

Fig.2.6 demonstrates that the final elastic collision rate is actually optimized in the case of a mode-matched transfer. The above considerations concerning a trade-off are therefore purely hypothetical. The conditions which optimize the phase space density also optimize the cooling rate. This is generally the case in an arbitrary power law potential, since the elastic collision rate $\Gamma(\mathcal{D},N)$ is a monotonic function of the phase space density $\mathcal{D}$. It is interesting to note how insensitive the collision rate is with respect to a mismatch of the initial catching current. A catching current mismatched by about a factor of three reduces the final collision rate by less than a factor of 2. This implies that an optimization of the transfer is only important if the initial collision rate is extremely marginal. A much more

important quantity is α_r. The final collision rate in a linear trap is proportional to the square of this quantity, while it increases proportional to it in a harmonic potential. In order to achieve a large collision rate we should design a linear trap which maximizes the confinement α_r.

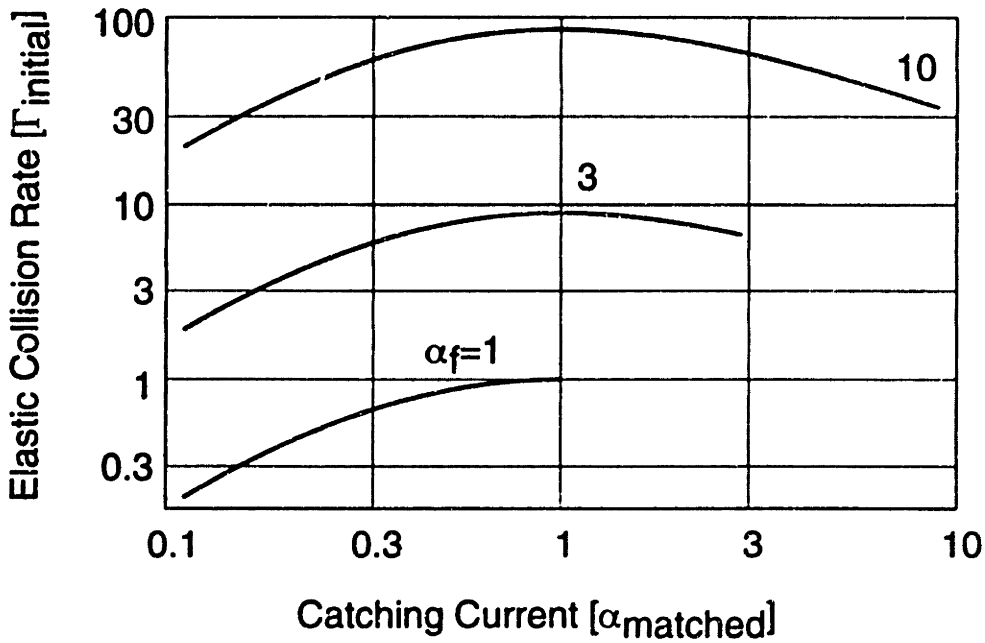

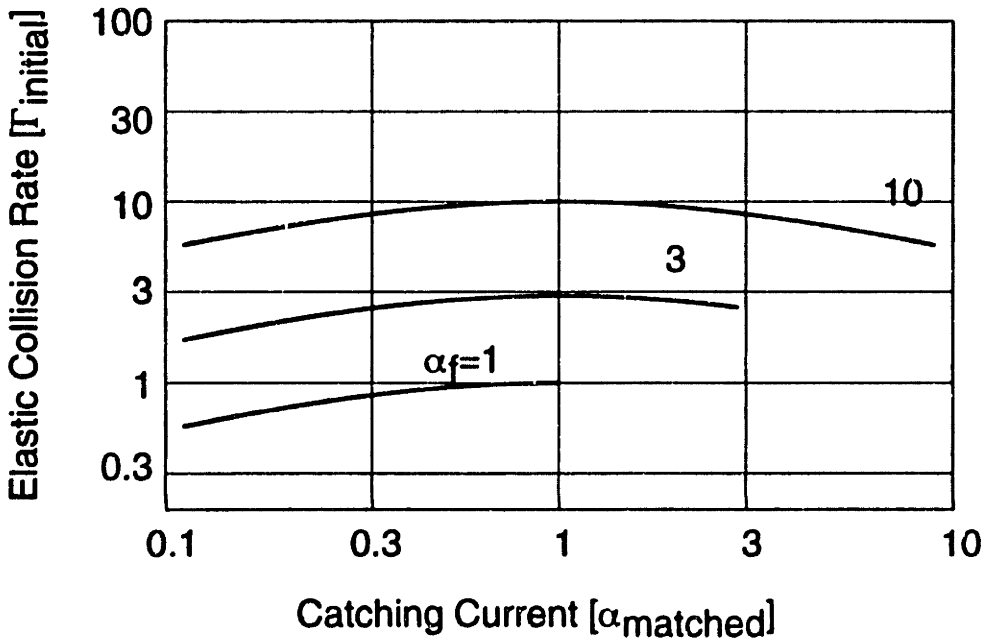

Fig.2.6 shows the elastic collision rate after transfer at the catching current α_i and adiabatic compression to the final current α_f. The plot on top displays the collision rate for the linear trap while the bottom plot shows the harmonic case. Both axis are logarithmic. The catching and final current are normalized to the "mode matched" case. The collision rate is normalized to the rate in a "mode matched" uncompressed cloud.

2.6 A Few Numbers

Table 2.1 summarizes the steps undertaken to cool sodium into quantum degeneracy. The listed numbers apply to our current Bose condensation setup, the "cloverleaf trap" (see chapter 4)[14]. The steps are listed in the order in which they are applied to the atoms (top to bottom). Δt is the duration of each step in the experiment. The experiment produces Bose condensates about every 25s. This result in a (pulsed) flux of more than $2x10^5$ coherent atoms/s. N is the number of trapped atoms present after each step. T and n are the temperature and the peak density respectively, while Γ is the peak elastic collision rate. $\mathcal{D}$ denotes the figure of merit: the peak phase space density of the sample. During the preparation the sample $\mathcal{D}$ is increased by more than *eighteen* orders of magnitude (sodium oven→pure condensate): We gain six orders in magnitude with laser cooling and trapping, another six orders through evaporation to the onset of condensation and the last six orders by cooling the cloud beyond the phase transition into a pure condensate. Coincidentally the densities in the sodium oven and in the condensate are similar, while the temperatures differ by more than 8 orders of magnitude.

	Δt [s]	N	T [K]	n [cm^{-3}]	Γ [Hz]	$\mathcal{D}$ [h^{-3}]
Sodium Oven	-	-	600	$\sim 10^{14}$	-	10^{-12}
Dark SPOT	2	$(5\text{-}10)x10^9$	10^{-3}	5×10^{11}	-	$\sim 3 \times 10^{-8}$
Dark Molasses	3×10^{-3}	$(5\text{-}10)x10^9$	10^{-4}	5×10^{11}	-	$\sim 10^{-6}$
Magnetic Trapping	10^{-1}*	2×10^9	10^{-4}	6×10^{10}	4	$\sim 10^{-6}$
After Compression	1	2×10^9	$\sim 2x10^{-4}$	$\sim 2 \times 10^{11}$	~16	$\sim 10^{-6}$
Rf Evaporation	16-25	↓	↓	↑	↑	↑
Onset of BEC	-	1.5×10^7	2×10^{-6}	1.5×10^{14}	10^3	2.6
Pure Condensate	-	5×10^6	-	3×10^{14}	-	5×10^6

Table 2.1 Preparation of ultra-cold atoms.

* eqilibration time after catching

2.7 Imaging Ultra Cold Atoms

We observe clouds of ultra-cold atoms by absorption imaging. For this purpose the magnetic trapping fields are extinguished in less then 100μs. The originally trapped atoms then ballistically expand and fall. After a adjustable time-of-flight between 0 and 50 ms the absorption of a 100μs-to-1 ms short weak near resonant laser pulse is imaged onto a charge coupled device (CCD) camera (Fig.2.7). The absorption can be adjusted by changing the detuning of the probe light. For a large time-of-flight the absorption images reflect the initial velocity distribution of the trapped cloud (an example is given in Fig. 2.8). This technique allows us to observe the condensation phenomenon in momentum space. In case of very slow expansion, such that the size of the initially trapped cloud is significant compared to the ballistic spreading of the cloud during the time-of-flight, the image displays a convolution of initial density distribution and the velocity distribution. (This is the case for the axial trapping direction for a condensate produced in the cloverleaf trap →chapter 4) Absorption imaging is destructive as the atoms are released from the trap and scatter photons. *Trapped* condensates and *trapped* ultra-cold clouds close to the transition are too small and dense for quantitative absorption imaging. For near resonant probe light these samples are completely absorptive and appear as "black" spots on the image. If we lower the absorption by detuning the probe light from resonance, dispersive effects become dominant and refraction of the sample limits the resolution [25]. We recently demonstrated a technique that can image trapped condensates "in-situ" and non-destructively through dispersive scattering of photons. [25] (also chapter 7.1).

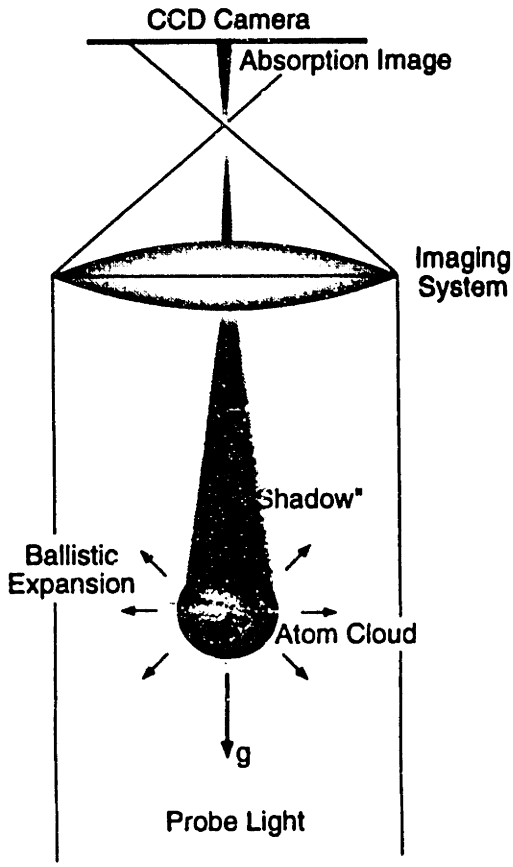

Fig.2.7 is illustrates the absorption imaging technique with which we study ultra-cold atoms. The initially trapped cloud is instantaneously released and ballistically expands for an adjustable time-of-flight of up to 50 ms. The absorption of a vertical near resonant probe beam is imaged onto a CCD camera . The probe pulse is short such that the atoms do not move significantly during the imaging. A typical probe pulse is 100μs long. The resolution of the imaging system is 5μm.

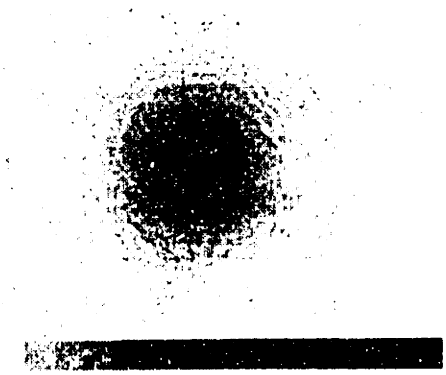

Fig.2.8 shows the absorption image of an ultra-cold atom cloud after 20 ms of free ballistic expansion. The horizontal width of the image is 6.2mm. The scale below is linear. "Black" corresponds to 100% absorption while areas with 100% transmission are "white". The image effectively maps the velocity distribution. Atoms near the center have small velocity while absorption further out correspond to high velocity atoms of in the distribution. [The dark oval peak in the center is due to the Bose condensed fraction of the cloud →chapter 3.2]

References in Chapter 2

1 M. A. Joffe, PhD thesis (Massachusetts Institute of Technology, Cambridge,MA, 1993).

2 K. B. Davis, PhD thesis (Massachusetts Institute of Technology, Cambridge, MA, 1995).

3 S. Giorgini, L. P. Pitaevskii, and S. Stringari, preprint (1996).

4 H. M. J. M. Boesten, A. J. Moerdijk, and B. J. Verhaar, preprint (1996).

5 K. B. Davis, M.-O. Mewes, M. A. Joffe, *et al.*, Physical Review Letters **74**, 5202-5205 (1995).

6 J. Lawall, S. Kulin, B. Saubamea, *et al.*, Physical Review Letters **75**, 4194 (1995).

7 N. Davidson, H.-J. Lee, M. Kasevich, *et al.*, Physical Review Letters **72**, 3158 (1994).

8 H. F. Hess, Physical Review B **34**, 3476 (1986).

9 H. Hess, G. P. Kochanski, J. M. Doyle, *et al.*, Physical Review Letters **59**, 672 (1987).

10 K. B. Davis, M.-O. Mewes, and W. Ketterle, Applied Physics B **60**, 155-159 (1995).

11 W. Ketterle and N. J. van Druten, in *Advances in Atomic, Molecular, and Optical Physics*, edited by B. Bederson and H. Walther (Academic Press, San Diego, 1996), Vol. 37.

12 D. W. Snoke and J. P. Wolfe, Physical Review B **39**, 4030 (1989).

13 K. B. Davis, M.-O. Mewes, M. R. Andrews, *et al.*, Physical Review Letters **75**, 3969 (1995).

14 M.-O. Mewes, M. R. Andrews, N. J. van Druten, *et al.*, Physical Review Letters **77**, 416-419 (1996).

15 D. E. Pritchard, K. Helmerson, and A. G. Martin, in *Atomic Physics 11*, edited by S. Haroche, J. C. Gay and G. Grynberg (World Scientific, Singapore, 1989), p. 179.

16 C. Cohen-Tannoudji, J. Dupont-Roc, and G. Grynberg, *Atom-Photon Interactions* (Wiley, New York, 1992).

17 J. R. Rubbmark, M. M. Kash, M. G. Littman, *et al.*, Physical Review A **23**, 3107 (1981).

18 E. Arimondo, W. D. Phillips, and F. Strumia, *Laser Manipulation of Atoms and Ions* (North-Holland, Amsterdam, 1992).

19 W. D. Phillips, J. V. Prodan, and H. J. Metcalf, Journal of the Optical Society of America B **2**, 1751 (1985).

20 E. L. Raab, M. Prentiss, A. Cable, *et al.*, Physical Review Letters **59**, 2631 - 2634 (1987).

21 M. A. Joffe, W. Ketterle, A. Martin, *et al.*, Journal of the Optical Society of America B **10**, 2257-2262 (1993).

22 W. Ketterle, K. B. Davis, M. A. Joffe, *et al.*, Physical Review Letters **70**, 2253 (1993).

23 P. D. Lett, R. N. Watts, C. I. Westbrook, *et al.*, Physical Review Letters **61**, 169 (1988).

24 D. M. Kurn, talk at DAMOP 1996, abstract SB3 (1996).

25 M. R. Andrews, M.-O. Mewes, N. J. van Druten, *et al.*, Science **273**, 84-87 (1996).

3. THE OPTICALLY PLUGGED TRAP

3.1. Majorana Flops

Evaporative cooling in a *linear* magnetic trapping potential does not extend into the quantum degenerate regime. This is due to the fact, that the magnetic field in the center of a linear magnetic trap vanishes. In regions of very small magnetic field, trapped atoms can undergo non-adiabatic transitions to the untrapped hyperfine ground states. These so called *Majorana Flops* constitute a temperature-dependent trap loss mechanism which results in a complete loss of the trapped sample during evaporative cooling far before the onset of BEC.

Majorana flops have been discussed in detail in Ken Davis' doctoral thesis [1]. The purpose of this section is to briefly explain the limitation with classical physical arguments and to motivate the following sections, which discuss ways around this loss problem.

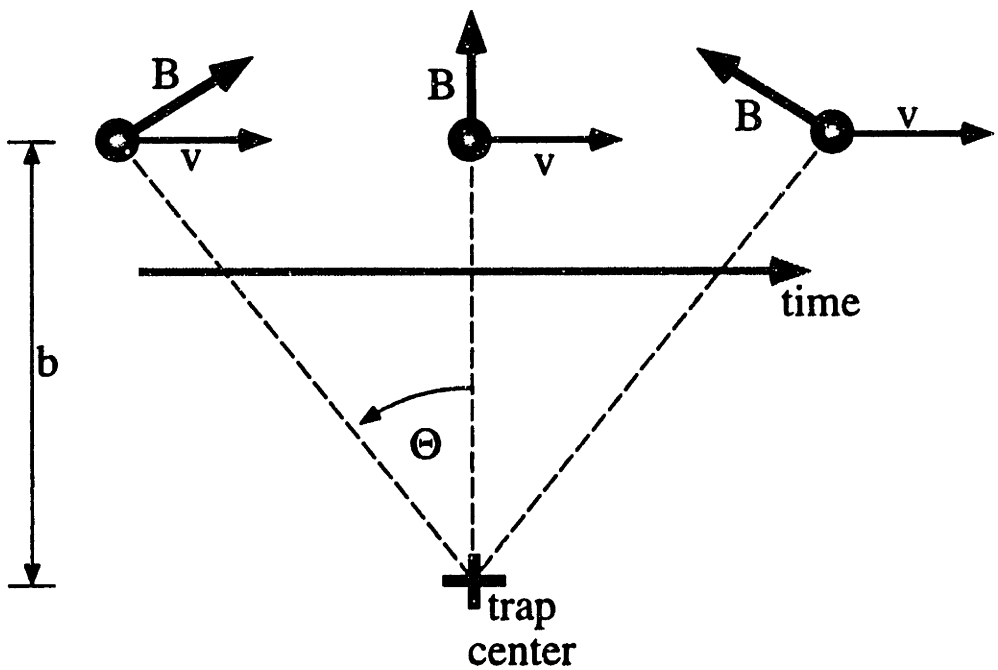

Fig.3.1 shows an atom moving near the center of a spherical quadrupole trap. (The sketch visualizes the quantities used on the following page.)

The trapped atoms are spinning magnetic dipoles which are precessing around the direction of the local magnetic field *B*. The Lamor precession frequency is proportional to |B| and therefore increases linearly with the distance from the trap center. In order for the atom to remain in trapped "weak-field seeking" state, the magnetic dipole moment of the atom has to adiabatically follow the magnetic field while the atom is oscillating in the trapping potential. The Lamor frequency ω_L is therefore required to be much larger than the rate of angular change $d\Theta/dt$ of the magnetic field direction in the reference frame of the atom. If this is not the case the atom can undergo Majorana flops to one of the untrapped hyperfine states. $d\Theta/dt$ is largest when the oscillating atom is closest to the trap center. $d\Theta/dt$ is then proportional to the atoms' speed v and is inversely proportional to the distance b from the trap origin: $d\Theta/dt \sim v/b$. Non-adiabatic spin flips are likely to occur if atoms atoms are oscillating through the area in which ω_L is comparable or smaller than $d\Theta/dt$. Since ω_L is proprtional to the magnitude of the magnetic field, which is in turn proportional to the distance b from the trap origin, the effective area A_{hole} of this "hole" scales as

$$A_{hole} \sim b^2 \sim v \sim T^{1/2} \tag{3.1}$$

where T is the temperature of the sample and v is the average speed of an atom.

According to the virial theorem the characteristic diameter of the magnetically trapped cloud in the linear potential is proportional to its temperature T and its projection onto the Majorana-loss "hole" scales as

$$A_{trap} \sim T^2. \tag{3.2}$$

From Eq.(3.1) and (3.2) it follows, that, as the cloud cools, its size decreases much more rapidly than the "hole" shrinks, evaporative cooling fades out and all the atoms will

eventually fall out of the trap. The temperature range (and phase space density) for which this occurs is well out of reach of BEC.

A classical estimate for the temperature dependent loss rate Γ in a spherical quadrupole potential is given in [1]:

$$\Gamma = \frac{\hbar \mu^2}{36\pi m}\left(\frac{B'}{k_B T}\right)^2 \tag{3.3}$$

where μ is the magnetic dipole moment of the atom and B' is the magnetic field gradient along the strongly confining direction of the potential. For the magnetic field gradient B' of 1000 G/cm used in our initial evaporative cooling experiment [2] this results in an order-of-magnitude estimate of the Majorana flop limited trapping time $1/\Gamma$:

$$(1/\Gamma)/[\mathrm{s}] = 1000\ T^2/[\mu\mathrm{K}]^2. \tag{3.4}$$

We observed a decrease of the trapping time from initially 30 sec (limited by background gas collisions) to a few seconds for a cloud evaporatively cooled to 80 μK [2]. This agrees well with the estimate (Eq.3.4).

3.2 Avoiding Majorana Flops

In order reach the BEC phase transition we had to find a way around this loss problem. As discussed in chapter 2, a linear potential is ideally suited for run-away evaporation [3]. We would therefore like to preserve the linearity of the potential for an energy range extending as close to the Bose-Einstein transition temperature as possible, while storing the atoms away form the low magnetic field near the center of the trap.

In order to achieve this goal the research group of Eric Cornell at JILA in Colorado adds a rotating magnetic bias field B_{rot} to the spherical quadrupole trap [4]. The bias field is rotating with a frequency ω_{rot} much larger than the oscillation frequency of the particles ω_{trap} but much slower than the Lamor precession frequency ω_{Lamor} of the stored atoms to assure stability against spin flips :

$$\omega_{trap} << \omega_{rot} << \omega_{Lamor} \tag{3.5}$$

This ac magnetic field causes the momentary zero-magnetic-field point to orbit on a circle around center of mass of the trapped cloud (Fig. 3.2).

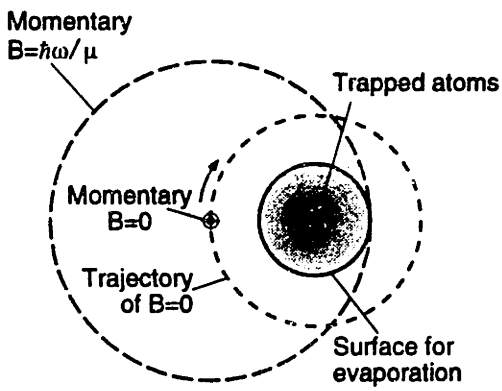

Fig. 3.2 is a schematic diagram of an atomic cloud trapped in the TOP trap. The *momentary zero-B-field* point is orbiting around the trapped atoms. The *momentary* $B=\hbar\omega/\mu$ shell orbits around the trapped atoms with the momentary B=0 as its center. The points on this shell closest to the center of the trapped cloud during the rotation define the surface of evaporation.

The atoms were consequently stored on the "slope" of an orbiting linear potential. The resulting time-averaged potential is mostly linear and only harmonic near the trap bottom with an effective field curvature of

$$B''=B'^2/(2B_{rot.}) \tag{3.6}$$

The Lamor frequency ω_{Lamor} of the atoms near the bottom of the effective potential is directly proportional to B_{rot}. Hence, the above constraints (Eq.3.5) impose a lower bound on B_{rot} and consequently limit the magnetic field curvature (Eq.3.6) and the confinement

of the TOP trap. This is discussed in more detail in the appendix of Chapter 4, our publication on the "cloverleaf" trap [5].

The JILA group observed Bose-Einstein condensation of Rubidium atoms in such a TOP (time-averaged orbiting potential) trap in June 1995 [6]. It was the first observation of this phase transition in a sample of weakly-interacting atoms. Condensates with 2000 atoms were obtained after 300s of loading and 70s of evaporation.

Contemporaneously our group at MIT took a different approach to "plugging" the Majorana flop "hole". We employed the conservative dipole force exerted on atoms in a light field to repel atoms from the "lossy" trap center. An atom in a light field experiences a conservative light shift potential U_{ac}, , the ac Stark shift :

$$U_{ac} = \frac{4\pi f_{osc} e^2 I(\vec{x})}{mc(\omega^2 - \omega_0{}^2)} \tag{3.7}$$

If the frequency ω of the light is larger than the resonance frequency ω_0 of the atomic transition, the resulting potential will be "repulsive", i.e. the atom is pushed towards the regions of low light intensity *I*. f_{osc} is the oscillator strength of the transition. In the case of sodium D-line this oscillator strength is very close to unity.

The ac Stark shift can be explained with a simple classical model. (In following we only discuss the far off-resonant case): We consider an atom as an "electron on a spring". Such an oscillator is driven by an electric field at a frequency ω far above its resonance frequency ω_0. The electron will oscillate with the frequency of the drive, but 180 degrees out-of-phase with the driving field. The amplitude of the oscillating dipole due to the driven electron is

$$\hat{\vec{p}} = -e\hat{\vec{x}}_e = -\frac{e^2 \hat{\vec{E}}}{m(\omega^2 - \omega_0{}^2)} \tag{3.8}$$

where $\hat{\vec{x}}_e$ is the amplitude of the oscillating electron, $\hat{\vec{E}}$ is the electric field amplitude of the driving field. The interaction of the oscillating dipole with the driving field gives rise to an time averaged potential

$$\begin{aligned}\langle U \rangle &= \left\langle -\vec{p} \cdot \vec{E} \right\rangle \\ &= \frac{e^2 \hat{\vec{E}}^2}{2m(\omega^2 - \omega_0{}^2)} \\ &= \frac{4\pi e^2 I}{mc(\omega^2 - \omega_0{}^2)}\end{aligned} \tag{3.9}$$

Eq. 3.7 and Eq. 3.9 differ by the oscillator strength f_{osc}, which accounts for deviations from the simple harmonic oscillator model. We can realize such an repulsive "optical plug" by focusing the green light of an argon ion laser (515 nm) into the "leaky" center of the spherical quadrupole trap. The frequency of this light is far detuned from the relevant resonance of the sodium atoms (589 nm). 3.5 Watts of green light are focused to beam waist with a gaussian waist parameter of 30 μm ($1/e^2$-radius of the intensity profile). By overlapping this focus with the center of the magnetic trap as illustrated in Fig. 3.3 we create a hybrid potential shown in Fig. 3.4.

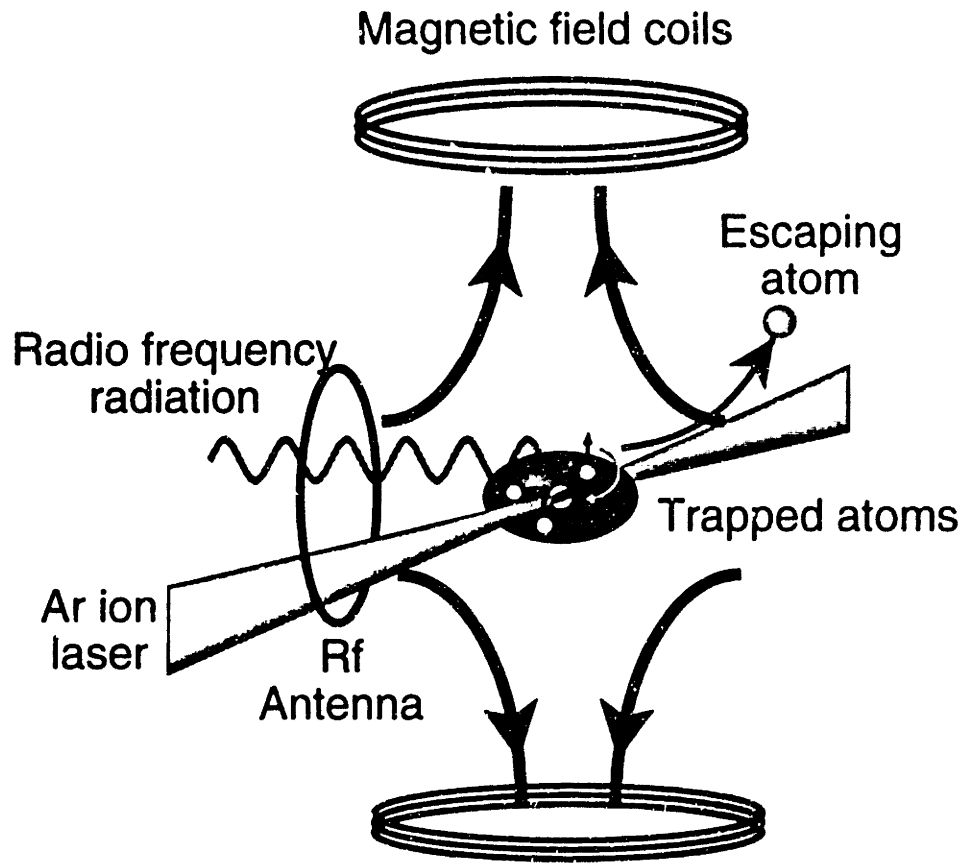

Fig.3.3 shows experimental setup of the optically plugged trap. The trapping potential is "customized" with a magnetic quadrupole field (to provide confinement), the Ar^{+}-ion laser beam (to plug the hole in the center) and rf radiation field (to adjust the depth of the trap for evaporation).

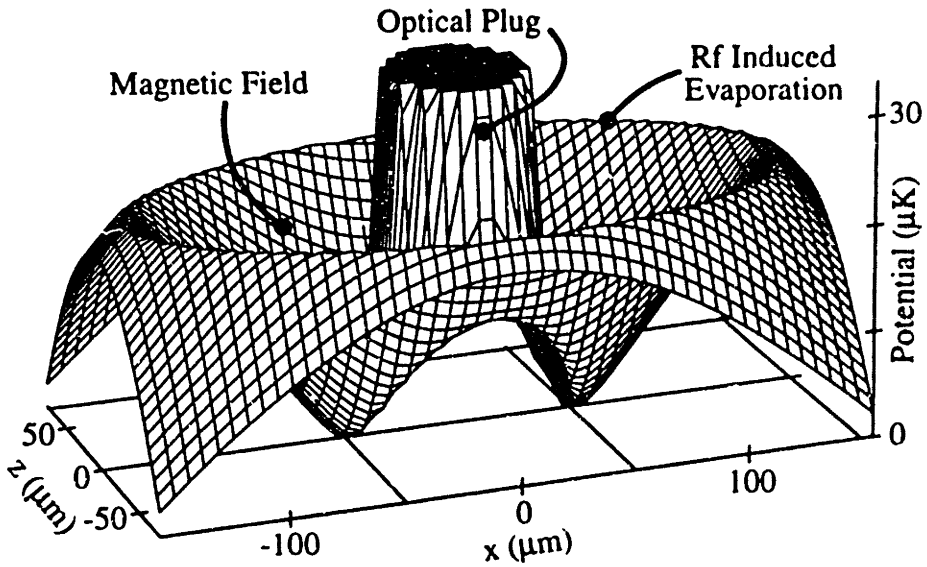

Fig. 3.4 is a cut through the three-dimensional adiabatic potential due to the magnetic quadrupole field, the optical plug and the rf. This cut is orthogonal to the propagation direction of the blue detuned light. The symmetry axis of the quadrupole field is the z axis. The potential has to two pockets due to the anisotropy of the quadrupole field. This causes a trapped atom cloud to split into two clouds at temperatures below 15μK.

The "light-plug" is detuned far enough from resonance to neglect spontaneous light forces and heating due to spontaneous scattering of photons. The spontaneous photon scattering rate for far off-resonant light for atoms trapped in the potential displayed in Fig. 3.4 is below one spontaneous photon in 50 seconds corresponding to a heating rates of a few 10nK/sec or less. Even for atoms in mK-energy range, such as samples before evaporation, the photon scattering rate does not exceed one photon in 10 seconds [1].

In the spring of 1995 we were able to evaporatively cool atoms in the optically plugged trap to 10μK at a density of 3.6×10^{13} cm^{-3}. The highest phase space densities achieved at that time were a factor of 30 above BEC [1]. When atoms were cooled below a

temperature of 15 μK at a gradient of 1000 G/cm in the optically plugged trap, they settled down in two spatially separated minima as shown in Fig. 3.5.

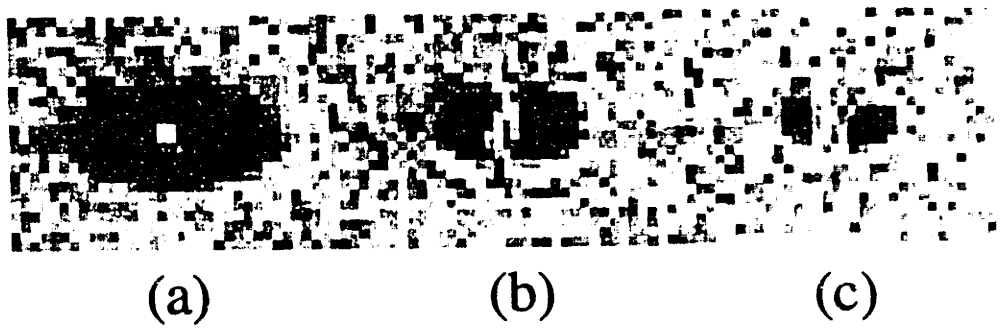

Fig.3.5 shows absorption images of atoms confined in an optically plugged magnetic quadrupole trap. The cloud in (a) has a temperature of 40μK and a 2:1 aspect ratio due to a magnetic field gradient which is twice as large along the vertical axis than along the horizontal direction . In (b) the atoms have reached a temperature of 15μK. They have "broken up" into two spatially separated clouds which are located at the two minima of the potential. (c) shows the clouds at a temperature T<10μK. The cloud size is smaller than the resolution limit of our imaging system (~8μm).

3.3 Observation of BEC in the Optically Plugged Trap

We tried to observe colder clouds and BEC in the Spring 95 by adiabatically expanding the potential during the last stages of evaporation and for observation. The clouds were expanded in order to (a) avoid inelastic loss or heating processes which might occur at densities exceeding $10^{14}cm^{-3}$ and (b) to optically resolve the clouds. Attempts to observe BEC this way were unsuccessful. This was possibly due to a heating rate which made evaporation inefficient and did not give us enough time for adiabatic expansion. Sources of the heating might have been vibrational motion of the plug relative to the magnetic field and collisions with the background gas at gracing incidence. The experiments up to this point are summarized in Ken Davis' thesis [1], who graduated in May 1995.

We did observe BEC in the plugged trap in September 1995 after minor[1] modification of the experimental apparatus. Possible sources of vibrations, such as turbo pumps, were eliminated[2].

[1] The changes were minor in terms of *physics* but quite labor-intensive.

The signature of Bose condensation in velocity space (as observed after ballistic expansion) is a sudden appearance of a bimodal velocity distribution below a critical temperature (Fig.3.6): a broad distribution due to the normal gas and a narrow distribution due to the condensate. Another striking feature is that the velocity distribution of the condensate fraction is anisotropic. This is caused by the "explosion" of the condensate due to mean-field interaction among the condensed atoms (see chapter 4.4). A detailed account of the first observation of BEC is given in the appendix of this chapter.

Fig. 3.7 is purely of historical interest. It is a time sequence of images detailing the ballistic expansion of the very first condensates we observed. We had instantaneously switched off the magnetic field while the potential due to the light plug remained. The condensates were sliding down the light plug potential like "ping pong balls" while expanding ballistically.

Fig.3.6 (on the following page): A three dimension rendering of two dimensional probe absorption images, after 6ms time of flight, showing evidence for BEC. The vertical axis represents the optical density. To the left is the velocity distribution of a cloud cooled to just above the transition point, in the middle the distribution just after the condensate appeared, and to the right is the distribution after further evaporative cooling has left an almost pure condensate.

[2] An active beam pointing stabilization of the Ar+-ion laser beam was not necessary.

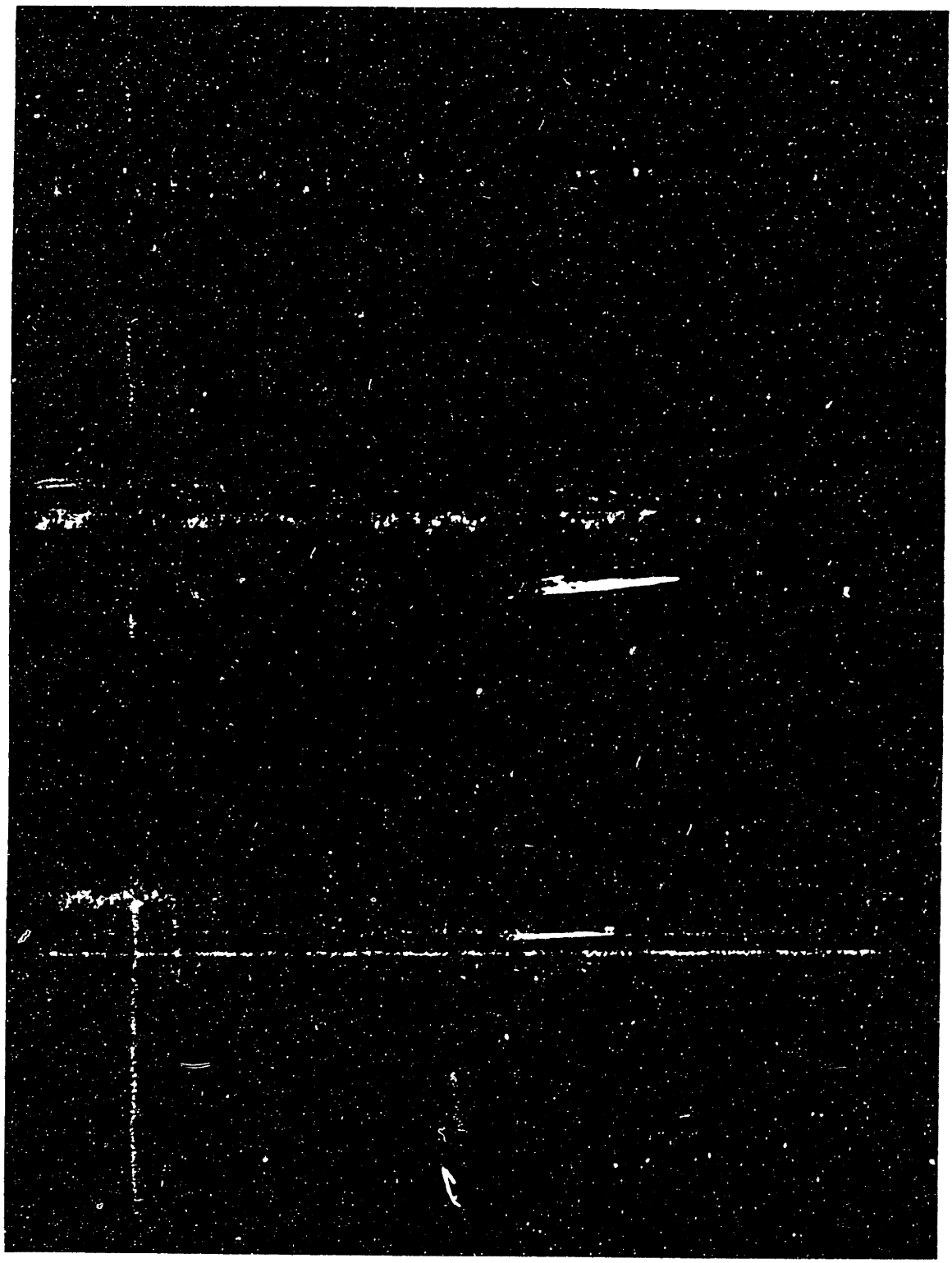

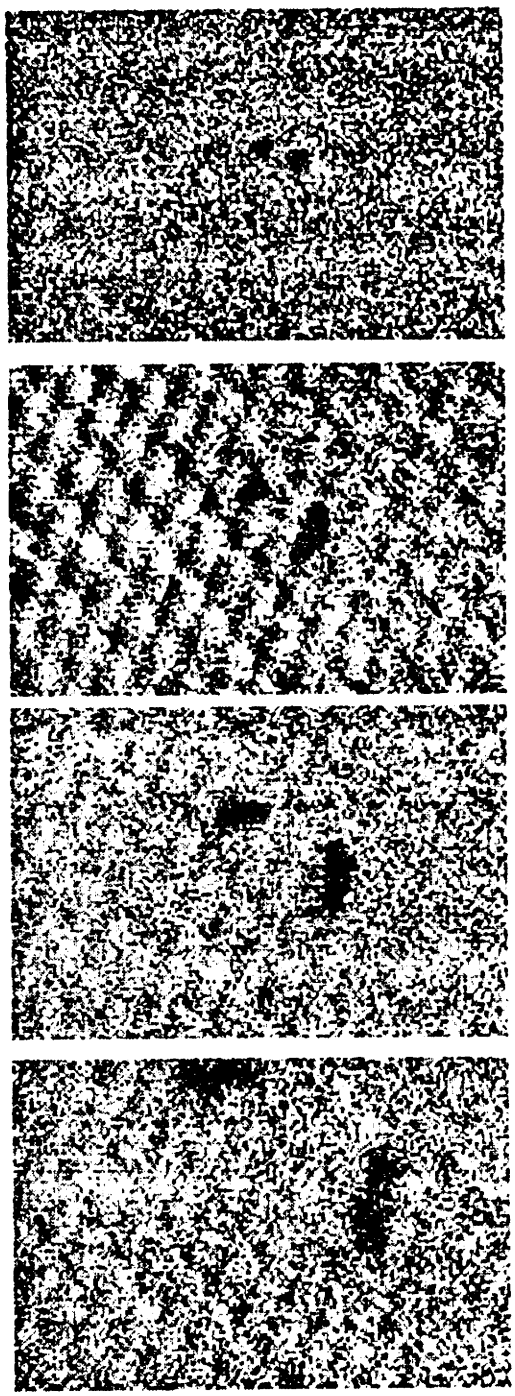

Fig.3.7 is the very first observation of BEC in the optically plugged trap. Depicted is sequence of absorption images which show the ballistic expansion of two condensates. The magnetic field was switched off instantaneously while the light plug remained switched on. The condensates are sliding down the plug potential while expanding.

References in Chapter 3

1 K. B. Davis, PhD thesis (Massachusetts Institute of Technology, Cambridge, MA, 1995).

2 K. B. Davis, M.-O. Mewes, M. A. Joffe, *et al.*, Physical Review Letters **74**, 5202-5205 (1995).

3 K. B. Davis, M.-O. Mewes, and W. Ketterle, Applied Physics B **60**, 155-159 (1995).

4 W. Petrich, M. H. Anderson, J. R. Ensher, *et al.*, Physical Review Letters **74**, 3352 (1995).

5 M.-O. Mewes, M. R. Andrews, N. J. van Druten, *et al.*, Physical Review Letters 77, 416-419 (1996).

6 M. H. Anderson, J. R. Ensher, M. R. Matthews, *et al.*, Science **269**, 198-210 (1995).

Appendix to Chapter 3

I conclude this chapter with the publication detailing the observation of *Bose-Einstein condensation in a gas of sodium atoms.*

PHYSICAL REVIEW
LETTERS

VOLUME 75 | 27 NOVEMBER 1995 | NUMBER 22

Bose-Einstein Condensation in a Gas of Sodium Atoms

K. B. Davis, M.-O. Mewes, M. R. Andrews, N. J. van Druten, D. S. Durfee, D. M. Kurn, and W. Ketterle
Department of Physics and Research Laboratory of Electronics, Massachusetts Institute of Technology, Cambridge, Massachusetts 02139
(Received 17 October 1995)

We have observed Bose-Einstein condensation of sodium atoms. The atoms were trapped in a novel trap that employed both magnetic and optical forces. Evaporative cooling increased the phase-space density by 6 orders of magnitude within seven seconds. Condensates contained up to 5×10^5 atoms at densities exceeding $10^{14}\,\mathrm{cm}^{-3}$. The striking signature of Bose condensation was the sudden appearance of a bimodal velocity distribution below the critical temperature of $\sim 2\ \mu\mathrm{K}$. The distribution consisted of an isotropic thermal distribution and an elliptical core attributed to the expansion of a dense condensate.

PACS numbers: 03.75.Fi, 05.30.Jp, 32.80.Pj, 64.60.–i

Bose-Einstein condensation (BEC) is a ubiquitous phenomenon which plays significant roles in condensed matter, atomic, nuclear, and elementary particle physics, as well as in astrophysics [1]. Its most striking feature is a macroscopic population of the ground state of the system at finite temperature [2]. The study of BEC in weakly interacting systems holds the promise of revealing new macroscopic quantum phenomena that can be understood from first principles, and may also advance our understanding of superconductivity and superfluidity in more complex systems.

During the past decade, work towards BEC in weakly interacting systems has been carried forward with excitons in semiconductors and cold trapped atoms. BEC has been observed in excitonic systems, but a complete theoretical treatment is lacking [1,3]. The pioneering work towards BEC in atomic gases was performed with spin-polarized atomic hydrogen [4,5]. Following the development of evaporative cooling [6], the transition was approached within a factor of 3 in temperature [7]. Laser cooling provides an alternative approach towards very low temperatures, but has so far been limited to phase-space densities typically 10^5 times lower than required for BEC. The combination of laser cooling with evaporative cooling [8–10] was the prerequisite for obtaining BEC in alkali atoms. This year, within a few months, three independent and different approaches succeeded in creating BEC in rubidium [11], lithium [12], and, as reported in this paper, in sodium. Our results are distinguished by a production rate of Bose-condensed atoms which is 3 orders of magnitude larger than in the two previous experiments. Furthermore, we report a novel atom trap that offers a superior combination of tight confinement and capture volume and the attainment of unprecedented densities of cold atomic gases.

Evaporative cooling requires an atom trap which is tightly confining and stable. So far, magnetic traps and optical dipole traps have been used. Optical dipole traps provide tight confinement, but have only a very small trapping volume ($10^{-8}\,\mathrm{cm}^3$). The tightest confinement in a magnetic trap is achieved with a spherical quadrupole potential (linear confinement); however, atoms are lost from this trap due to nonadiabatic spin flips as the atoms pass near the center, where the field rapidly changes direction. This region constitutes a "hole" in the trap of micrometer dimension. The recently demonstrated "TOP" trap suppresses this trap loss, but at the cost of lower confinement [8].

We suppressed the trap loss by adding a repulsive potential around the zero of the magnetic field, literally "plugging" the hole. This was accomplished by tightly focusing an intense blue-detuned laser that generated a repulsive optical dipole force. The optical plug was created by an Ar^+-laser beam (514 nm) of 3.5 W focused

0031-9007/95/75(22)/3969(5)$06.00

to a beam waist of 30 μm. This caused 7 MHz (350 μK) of light shift potential at the origin. Heating due to photon scattering was suppressed by using far-off-resonant light, and by the fact that the atoms are repelled from the region where the laser intensity is highest.

The experimental setup was similar to that described in our previous work [9]. Typically, within 2 s 10^9 atoms in the $F = 1$, $m_F = -1$ state were loaded into a magnetic trap with a field gradient of 130 G/cm; the peak density was $\sim 10^{11}$ cm^{-3}, the temperature ~ 200 μK, and the phase-space density 10^6 times lower than required for BEC. The lifetime of the trapped atoms was $\sim$ 30 s, probably limited by background gas scattering at a pressure of $\sim 1 \times 10^{-11}$ mbar.

The magnetically trapped atoms were further cooled by rf-induced evaporation [8,9,13]. rf-induced spin flips were used to selectively remove the higher-energy atoms from the trap resulting in a decrease in temperature for the remaining atoms. The total (dressed-atom) potential is a combination of the magnetic quadrupole trapping potential, the repulsive potential of the plug, and the effective energy shifts due to the rf. At the point where atoms are in resonance with the rf, the trapped state undergoes an avoided crossing with the untrapped states (corresponding to a spin flip), and the trapping potential bends over. As a result, the height of the potential barrier varies linearly with the rf frequency. The total potential is depicted in Fig. 1. Over 7 s, the rf frequency was swept from 30 MHz to the final value around 1 MHz, while the field gradient was first increased to 550 G/cm (to enhance the initial elastic-collision rate) and then lowered to 180 G/cm (to avoid the losses due to inelastic processes at the final high densities).

Temperature and total number of atoms were determined using absorption imaging. The atom cloud was imaged either while it was trapped or following a sudden switch-off of the trap and a delay time of 6 ms. Such time-of-flight images displayed the velocity distribution of the trapped cloud. For probing, the atoms were first pumped to the $F = 2$ state by switching on a 10 mW/cm^2 laser beam in resonance with the $F = 1 \rightarrow F = 2$ transition. 10 μs later the atoms were concurrently exposed to a 100 μs, 0.25 mW/cm^2 probe laser pulse in resonance with the $F = 2 \rightarrow F = 3$ transition, propagating along the trap's y direction. This probe laser beam was imaged onto a charge-coupled device sensor with a lens system having a resolution of 8 μm. Up to 100 photons per atom were absorbed without blurring the image due to heating.

At temperatures above 15 μK the observed trapped clouds were elliptical with an aspect ratio of 2:1 due to the symmetry of the quadrupole field. At the position of the optical plug they had a hole, which was used for fine alignment. A misalignment of the optical plug by ~ 20 μm resulted in increased trap loss and prevented us from cooling below 50 μK. This is evidence that the Majorana spin flips are localized in a very small region around the center of the trap. At temperatures below 15 μK, the cloud separated into two pockets at the two minima in the potential of Fig. 1. The bottom of the potential can be approximated as a three-dimensional anisotropic harmonic oscillator potential with frequencies $\omega_y^2 = \mu B'/(2mx_0)$, $\omega_z^2 = 3\omega_y^2$, $\omega_x^2 = \omega_y^2[(4x_0^2/w_0^2) - 1]$, where μ is the atom's magnetic moment, m the mass, B' the axial field gradient, w_0 the Gaussian beam waist parameter ($1/e^2$ radius) of the optical plug, and x_0 the distance of the potential minimum from the trap center. x_0 was directly measured to be 50 μm by imaging the trapped cloud, w_0 (30 μm) was determined from x_0, the laser power (3.5 W), and B' (180 G/cm). With these values the oscillation frequencies are 235, 410, and 745 Hz in the y, z, and x directions, respectively.

When the final rf frequency ν_{rf} was lowered below 0.7 MHz, a distinctive change in the symmetry of the velocity distribution was observed [Figs. 2(a) and 2(b)]. Above this frequency the distribution was perfectly spherical as expected for a thermal uncondensed cloud [14]. Below the critical frequency, the velocity distribution contained an elliptical core which increased in intensity when

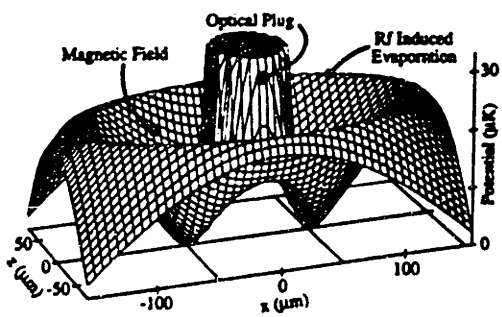

FIG. 1. Adiabatic potential due to the magnetic quadrupole field, the optical plug, and the rf. This cut of the three-dimensional potential is orthogonal to the propagation direction (y) of the blue-detuned laser. The symmetry axis of the quadrupole field is the z axis.

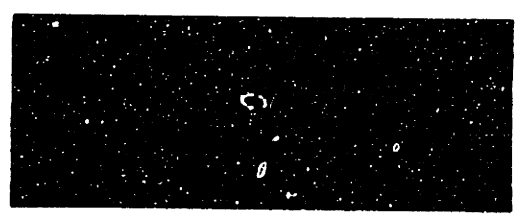

FIG. 2 (color). Two-dimensional probe absorption images, after 6 ms time of flight, showing evidence for BEC. (a) is the velocity distribution of a cloud cooled to just above the transition point, (b) just after the condensate appeared, and (c) after further evaporative cooling has left an almost pure condensate. (b) shows the difference between the isotropic thermal distribution and an elliptical core attributed to the expansion of a dense condensate. The width of the images is 870 μm. Gravitational acceleration during the probe delay displaces the cloud by only 0.2 mm along the z axis.

the rf was further swept down, whereas the spherical cloud became less intense. We interpret the elliptical cloud as due to the Bose condensate, and the spherical cloud as due to the normal fraction.

In the region just below the transition frequency one expects a bimodal velocity distribution: a broad distribution due to the normal gas and a narrow distribution due to the condensate. The cross sections of the time-of-flight images (Fig. 3) indeed show such bimodal distributions in this region. Figure 4 shows how suddenly the time-of-flight image changes below $\nu_{rf} = 0.7$ MHz. The effective area of the observed cloud becomes very small [Fig. 4(a)], while the velocity distribution is no longer Gaussian [Fig. 4(b)] and requires different widths for the condensate and the normal fraction [Fig. 4(c)].

At the critical frequency, a temperature of (2.0 ± 0.5) μK was derived from the time-of-flight image. An independent, though less accurate estimate of the temperature T is obtained from the dynamics of evaporative cooling. Efficient evaporation leads to a temperature which is about 10 times smaller than the depth of the trapping potential [15]. Since the speed of evaporation depends exponentially on the ratio of potential depth to temperature, we expect this estimate of $T = 2$ μK to be accurate to within a factor of 2.

The critical number of atoms N_c to achieve BEC is determined by the condition that the number of atoms per cubic thermal de Broglie wavelength exceeds 2.612 at the bottom of the potential [2]. For a harmonic oscillator potential this is equivalent to $N_c = 1.202(k_B T)^3/\hbar^3\omega_r\omega_z\omega_z$ [16]. For our trap and 2.0 μK, $N_c = 2 \times (1.2 \times 10^6)$, where the factor of 2 accounts for the two separated clouds. The predicted value for N_c depends on the sixth power of the width of a time-of-flight image and is only accurate to within a factor of 3. We determined the number of atoms by integrating over the absorption image. At the transition point, the measured number of 7×10^5 agrees with the prediction for N_c. The critical peak density n_c at 2.0 μK is 1.5×10^{14} cm^{-3}. Such a high density appears to be out of reach for laser cooling, and demonstrates that evaporative cooling is a powerful technique to obtain not only ultralow temperatures, but also extremely high densities.

An ideal Bose condensate shows a macroscopic population of the ground state of the trapping potential. This picture is modified for a weakly interacting Bose gas. The mean-field interaction energy is given by $n\tilde{U}$, where n is the density and $\tilde{U}$ is proportional to the scattering length a: $\tilde{U} = 4\pi\hbar^2 a/m$ [2]. Using our recent experimental result $a = 4.9$ nm [9], $\tilde{U}/k_B = 1.3 \times 10^{-21}$ K cm^3. At the transition point, $n_c\tilde{U}/k_B T_c = 0.10$. Consequently, above the transition point, the kinetic energy dominates over the interaction energy, and the velocity

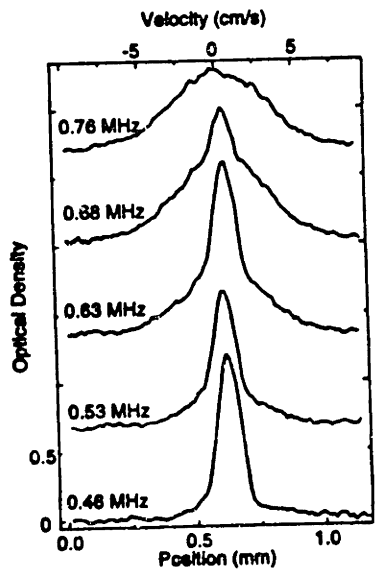

FIG. 3. Optical density as a function of position along the z axis for progressively lower values of the final rf frequency. These are vertical cuts through time-of-flight images like those in Fig. 2. For $\nu_{rf} < 0.7$ MHz, they show the bimodal velocity distributions characteristic of the coexistence of a condensed and uncondensed fraction. The top four plots have been offset vertically for clarity.

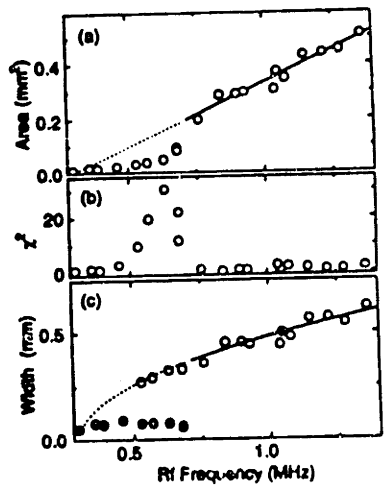

FIG. 4. Further evidence for a phase transition is provided by the sudden change of observed quantities as the final rf frequency ν_{rf} is varied. (a) Area of the cloud in the time-of-flight image versus ν_{rf}. The area was obtained as the ratio of the integrated optical density and the peak optical density. The area changes suddenly at $\nu_{rf} = 0.7$ MHz. Below the same frequency, the velocity distributions (Fig. 3) cannot be represented by a single Gaussian, as demonstrated by the χ^2 for a single Gaussian fit (b), and required different widths for the condensate (full circles) and noncondensate fraction (c). In (a) and (c) the lines reflect the behavior of a classical gas with a temperature proportional to the trap depth.

distribution after sudden switch-off of the trap is isotropic. For the condensate, however, the situation is reversed. As we will confirm below, the kinetic energy of the condensate is negligible compared to its interaction energy [17]. Furthermore, well below the transition point, the interaction with the noncondensate fraction can be neglected. In such a situation, the solution of the nonlinear Schrödinger equation reveals that the condensate density $n_0(\mathbf{r})$ is a mirror image of the trapping potential $V(\mathbf{r})$: $n_0(\mathbf{r}) = n_0(0) - V(\mathbf{r})/U$, as long as this expression is positive, otherwise $n_0(\mathbf{r})$ vanishes (see, e.g., Refs. [5,18]). For a harmonic potential, one obtains the peak density $n_0(0)$ for N_0 atoms in the condensate $n_0(0) = 0.118(N_0 m^3 \omega_x \omega_y \omega_z/\hbar^3 a^{3/2})^{2/5}$.

Typically, we could cool one-fourth of the atoms at the transition point into a pure condensate. For an observed $N_0 = 1.5 \times 10^5$, we expect the condensate to be 2 times more dense than the thermal cloud at the transition point, and about 6 times larger than the ground-state wave function. The kinetic energy within the condensate is $\sim \hbar^2/(2mR^2)$, where R is the size of the condensate [18], while the internal energy is $2n_0U/7$. Thus the kinetic energy of the condensed atoms is around 1 nK, much less than the zero-point energy of our trap (35 nK) and the calculated internal energy of 120 nK. This estimate is consistent with our initial assumption that the kinetic energy can be neglected compared to the interaction energy.

The internal energy is ~ 25 times smaller than the thermal energy $(3/2)k_BT_c$ at T_c. Consequently, the width of the time-of-flight image of the condensate is expected to be about 5 times smaller than at the transition point. This is close to the observed reduction in the width shown in Fig. 4(c). This agreement might be fortuitous because we have so far neglected the anisotropy of the expansion, but it indicates that we have observed the correct magnitude of changes which are predicted to occur at the BEC transition of a weakly interacting gas. In several cooling cycles, as many as 5×10^5 condensed atoms were observed; we estimate the number density in these condensates to be 4×10^{14} cm^{-3}.

A striking feature of the condensate is the nonisotropic velocity distribution [11,19]. This is caused by the "explosion" of the condensate due to repulsive forces which are proportional to the density gradient. The initial acceleration is therefore inversely proportional to the width of the condensate resulting in an aspect ratio of the velocity distribution, which is inverted compared to the spatial distribution. When we misaligned the optical plug vertically, the shape of the cloud changed from two vertical crescents to a single elongated horizontal crescent. The aspect ratio of the time-of-flight image of the condensate correspondingly changed from horizontal to vertical elongation. In contrast, just above the transition point, the velocity distribution was found to be spherical and insensitive to the alignment of the plug. However, we cannot account quantitatively for the observed distributions because we have two separated condensates which overlap in the time-of-flight images, and also because of some residual horizontal acceleration due to the switch-off of the trap, which is negligible for the thermal cloud, but not for the condensate [20].

The lifetime of the condensate was about 1 s. This lifetime is probably determined either by three-body recombination [21] or by the heating rate of 300 nK/s, which was observed for a thermal cloud just above T_c. This heating rate is much higher than the estimated 8 nK/s for the off-resonant scattering of green light and may be due to residual beam jitter of the optical plug.

In conclusion, we were able to Bose-condense 5×10^5 sodium atoms within a total loading and cooling cycle of 9 s. During evaporative cooling, the elastic collision rate increased from 30 Hz to 2 kHz resulting in a mean free path comparable to the dimensions of the sample. Such collisionally dense samples are the prerequisite for studying various transport processes in dense ultracold matter. Furthermore, we have reached densities in excess of 10^{14} cm^{-3}, which opens up new possibilities for studying decay processes like dipolar relaxation and three-body recombination, and for studying a weakly interacting Bose gas over a broad range of densities and therefore strengths of interaction.

We are grateful to E. Huang and C. Sestok for important experimental contributions, to M. Raizen for the loan of a beam pointing stabilizer, and to D. Kleppner for helpful discussions. We are particularly grateful to D. E. Pritchard, who not only contributed many seminal ideas to the field of cold atoms, but provided major inspiration and equipment to W. K. This work was supported by ONR, NSF, JSEP, and the Sloan Foundation. M.-O. M., K. B. D., and D. M. K. would like to acknowledge support from Studienstiftung des Deutschen Volkes, MIT Physics Department Lester Wolfe fellowship, and NSF Graduate Research Fellowship, respectively, and N. J. v. D. from "Nederlandse Organisatie voor Wetenschappelijk Onderzoek (NWO)" and NACEE (Fulbright fellowship).

[1] A. Griffin, D. W. Snoke, and S. Stringari, *Bose-Einstein Condensation* (Cambridge University Press, Cambridge, 1995).
[2] K. Huang, *Statistical Mechanics* (Wiley, New York, 1987), 2nd ed.
[3] J. L. Lin and J. P. Wolfe, Phys. Rev. Lett. 71, 1222 (1993).
[4] I. F. Silvera and M. Reynolds, J. Low Temp. Phys. 87, 343 (1992); J. T. M. Walraven and T. W. Hijmans, Physica (Amsterdam) 197B, 417 (1994).
[5] T. Greytak, in Ref. [1], p. 131.
[6] N. Masuhara *et al.*, Phys. Rev. Lett. 61, 935 (1988).
[7] J. Doyle *et al.*, Phys. Rev. Lett. 67, 603 (1991).
[8] W. Petrich, M. H. Anderson, J. R. Ensher, and E. A. Cornell, Phys. Rev. Lett. 74, 3352 (1995).

[9] K.B. Davis *et al.*, Phys. Rev. Lett. **74**, 5202 (1995).
[10] C.S. Adams *et al.*, Phys. Rev. Lett. **74**, 3577 (1995).
[11] M.H. Anderson *et al.*, Science **269**, 198 (1995).
[12] C.C. Bradley, C.A. Sackett, J.J. Tollett, and R.G. Hulet, Phys. Rev. Lett. **75**, 1687 (1995).
[13] D.E. Pritchard, K. Helmerson, and A.G. Martin, in *Atomic Physics 11*, edited by S. Haroche, J.C. Gay, and G. Grynberg (World Scientific, Singapore, 1989), p. 179.
[14] The measured $1/e$ decay time for the magnet current is 100 μs, shorter than the ω^{-1} of the fastest oscillation in the trap (210 μs). We therefore regard the switch-off as sudden. Any adiabatic cooling of the cloud during the switch-offtibs would result in a nonspherical velocity distribution due to the anisotropy of the potential.
[15] K.B. Davis, M.-O. Mewes, and W. Ketterle, Appl. Phys. B **60**, 155 (1995).
[16] V. Bagnato, D.E. Pritchard, and D. Kleppner, Phys. Rev. A **35**, 4354 (1987). This formula is derived assuming $k_B T_c \gg \hbar\omega_{x,y,z}$, which is the case in our experiment.
[17] Note that already for about 200 atoms in the ground state, the interaction energy in the center of the condensate equals the zero-point energy.
[18] G. Baym and C. Pethick (to be published).
[19] M. Holland and J. Cooper (to be published).
[20] These effects do not affect the vertical velocity distributions shown in Fig. 3.
[21] A.J. Moerdijk, H.M.J.M. Boesten, and B.J. Verhaar, Phys. Rev. A (to be published).

4. THE CLOVERLEAF TRAP

We first observed Bose-Einstein condensation of sodium atoms in the optically plugged (OP) trap [1](→Chapter 3). To avoid inelastic heating and loss processes predicted at densities much larger than 10^{14} atoms/cm^3 we weakened the trapping potential during the last stage of evaporation. Loosely spoken, the optically plugged trap is too tightly confining for evaporative cooling. However, the OP trap is an ideally suited trap to achieve the conditions for the onset of evaporation, while avoiding non-adiabatic spin flips (Majorana trap loss).

The magnetic traps used for evaporative cooling of ultra-cold atomic gases until spring 1996 had major disadvantages: The field of the TOP trap was time dependent. The OP trap was sensitive to the shape and the position of the optical plug. Traps employing permanent magnets [2] were inflexible and didn't allow for control of the field parameters, while traps that used superconducting coils [3] imposed serious constraints on the experimental environment.

4.1 The Cloverleaf Trap - A Tightly Confining DC Magnetic Trap

In order to not only observe but also study and manipulate Bose condensates, we have to be able to adjust the trap parameters fast and accurately. A purely magnetic trap operated with dc electromagnets can give us this flexibility.

4.1.1 The Field Configuration of the Ioffe-Pritchard Trap

We considered a magnetic trap of the Ioffe-Pritchard (IP) type [4]. This trapping configuration was initially suggested by David Pritchard for the confinement of cold atomic gases [5]. It was originally used for trapping hydrogen [6, 7] and sodium [8] in cryogenic traps. A similar field geometry (on a much larger scale) has been used earlier for plasma confinement as proposed by Ioffe[9]. The initially suggested trap geometry is

outlined in Fig.4.1. It consists of two "pinch" coils with parallel current and four parallel straight conductors with current in alternating directions. The trap has an axial bias field B_0 and axial confinement from a magnetic bottle field due to the two "pinch" coils. Transverse confinement is provided by a four-wire quadrupole focusing field. Because of a non-zero field in the center the Lamor frequency of even the coldest atoms can be larger than the orbital frequency, such that Majorana flops do not occur.

The value of the axial field B_z near the minimum of the trap can be described by the bias field B_0 and the axial curvature component B":

$$B_z(z,r)=B_0+B"/2\ z^2 \tag{4.1}$$

Close to the trap minimum the absolute value of the radial field B_r is linear in $r=(x^2+y^2)^{1/2}$ and vanishes in the center:

$$B_r(z,r)= B'r \tag{4.2}$$

The resulting value of the magnetic field can be expanded around its minimum and is

$$B(z,r)= B_0+[B'^2/(2B_0)]\ r^2+[B"/2]\ z^2 \tag{4.3}$$

4th or higher order terms in r,z are neglected. The resulting magnetic trapping field is harmonic near the trap center.

The geometric mean of the field curvatures $\left(B_x''B_y''B_z''\right)^{1/3}$ is the relevant figure of merit of a harmonic trap for evaporative cooling. The BEC transition temperature T_c is proportional to the square root of this quantity[1] (Eq.1.16) while the collision rate Γ after adiabatic compression in the purely harmonic trap increases linearly with

[1] The geometric mean of the trapping frequencies ϖ is given by $\sqrt{\mu/m}\left(B_x''B_y''B_z''\right)^{1/6}$.

$\left(B_x''B_y''B_z''\right)^{1/3}$ (Eq.2.20). The geometric mean of the curvatures therefore determines the efficiency of evaporation. In the IP trap it is

$$\left(B_x''B_y''B_z''\right)^{1/3} = \left(\frac{B''B'^4}{B_0^2}\right)^{1/3}. \tag{4.4}$$

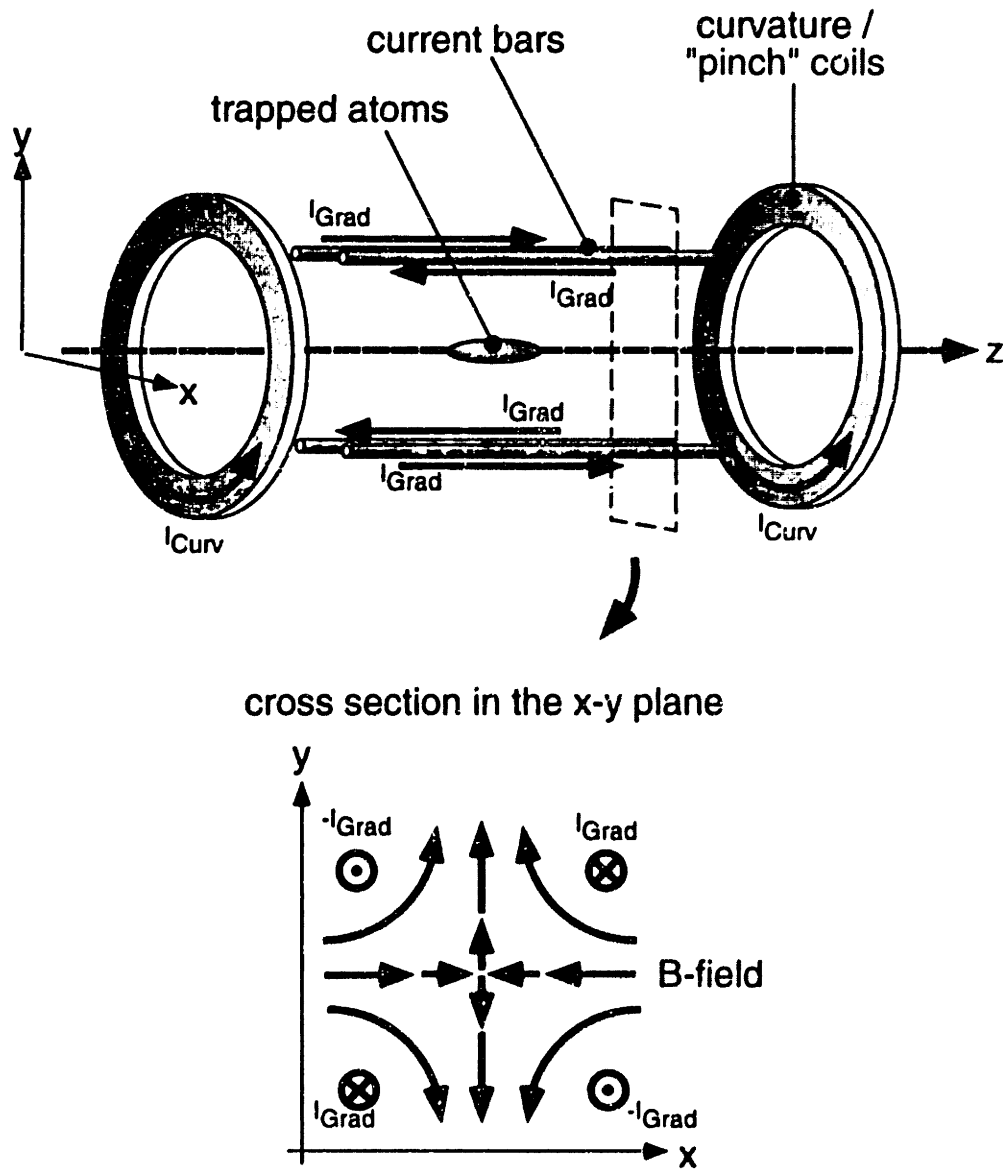

Fig.4.1 The Ioffe-Pritchard trap (top) is a magnetic trap based on dc electro magnets. Two coils with current in equal direction provide a magnetic "bottle" field which confines atoms along the axial (z) direction . The coils also produce a bias field. The four parallel wires with alternating currents provide radial confinement through a two-dimensional quadrupole field orthogonal to the z axis (bottom). Near the trap center the

magnitude of this field increases linearly with the distance from the symmetry axis z. The absolute values of both fields add in quadrature.

The ratio of the radial and axial trapping frequencies ω_r/ω_z is given as

$$\frac{\omega_r}{\omega_z} = \frac{B'}{\sqrt{B''B_0}} \tag{4.5}$$

For radial distances from the center larger than B_0/B' the potential is linear in the radial dimensions.

Eq.(4.3) thru (4.5) show that we can shape the power law , the aspect ratio and the curvatures of the trapping potential by adjusting the three field parameters B_0, B' and B". It is therefore desirable to have independent control of all three parameters. An adjustable bias field B_0 is crucial in order to achieve the maximum possible confinement. This can be realized by adding a Helmholtz coil pair to the trap geometry: The coils produce an axial bias field which is homogeneous over the whole trapping volume. This Helmholtz field can compensate the bias field produced by the "bottle" field coils without affecting the curvature B".

4.1.2 The Stabilty Against Majorana Spin Flips

In order to avoid trap loss due to Majorana spin flips (→Chapter 3), the Lamor precession frequency $\omega_{Lamor}=\mu B_0/\hbar$ of the atom near the trap center has to be much larger than the rate at which the atom "sees" the inhomogeneous trapping field rotate. This rate is less or equal to the atomic oscillation frequency along the strongly confining radial direction:

$$
\begin{aligned}
&\omega_{Lamor} >> \omega_r \\
&\Rightarrow \frac{\mu B_0}{\hbar} >> \sqrt{\frac{\mu}{m B_0}} B' \\
&\Leftrightarrow B_0 >> \left(\frac{\hbar^2}{m\mu}\right)^{1/3} B'^{2/3} \\
&\Rightarrow \underline{\underline{\frac{B_0}{[mG]} >> 0.2\left(\frac{B'}{[G/cm]}\right)^{2/3}}}
\end{aligned}
\tag{4.7}
$$

We estimate a ratio $\omega_{Lamor}/\omega_r=100$ to be sufficient to avoid Majorana flops. A gradient of 100G/cm would therefore necessitate a bias field on the order of a few hundred mG.

4.1.3 The Design of the Cloverleaf Trap

An important issue, which has not been considered so far is the optical access to the atomic cloud. The atoms are laser cooled and trapped magneto-optically before the transfer into the magnetic trap.

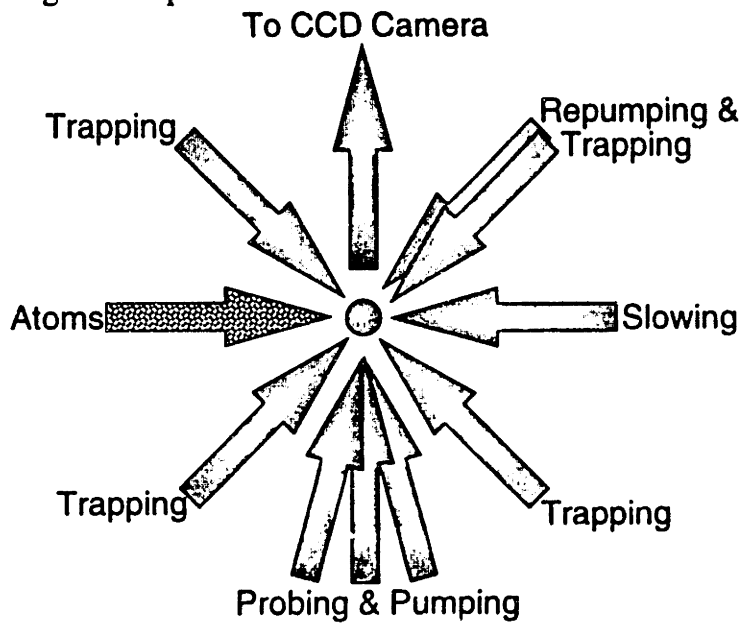

Fig.4.2 illustrates the optical access to the atomic sample (center) which is required to facilitate laser cooling and probing. The figure shows a vertical cut through the experimental setup along the axis of the horizontal atomic beam. The arrows labeled "Trapping" and "Repumping" represent laser beams required for magneto-optical trapping and polarization gradient cooling. "Pumping & Probing" are beams necessary for optical pumping and absorption imaging, while the arrow "To CCD camera" marks the imaging path to the camera. Labeled "Atoms" and "Slowing" are the atomic beam and the slowing light needed for Zeeman slowing. Additional access by two more trapping beams orthogonal to the depicted plane is also necessary.

In order to facilitate laser cooling and trapping as well as probing and imaging, up to 12 different laser beams have to be directed at the sample of atoms. Fig.4.2 illustrates these requirements. The four current bars of the IP Trap seriously constrain the optical access. We therefore produce the radial confining field without obstructing the space between the two "pinch" coils. I want to briefly explain the idea which lead to such a design:

Consider the field in the geometric center of a Helmholtz coil pair (Fig.4.3a). In this location the magnetic field is oriented along the symmetry axis. Radial field gradients resulting from each coil exactly compensate. If we break the cylindrical symmetry by pinching both coils along orthogonal directions (Fig.4.3b) the radial fields are imbalanced and a radial gradient results. Near the (former) symmetry axis the radial field is topologically identical to the two-dimensional quadrupole field produced by the current bars. This is a possibility to provide radial confinement without limiting optical access. We developed a design based on this idea and maximized the radial field gradients with the experimental constraints and technological limitations taken into account.

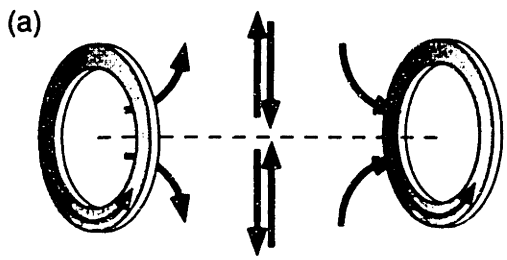

Fig.4.3a
The field on the symmetry axis (broken line) of a Helmholtz coil pair is oriented axially. In the center between the coils radial field gradients due to each of the coils exactly add up to 0 (black vertical arrows)

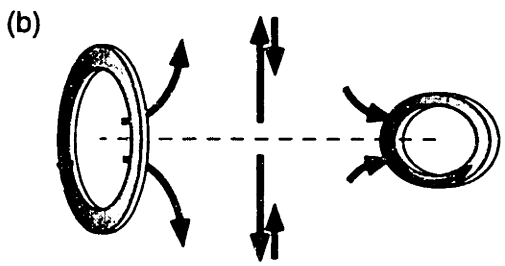

Fig.4.3b
The pair of coils is now pinched along orthogonal directions. The radial field gradients due to each of the coils no longer compensate each other. A radial B-field results which is topologically identical to a two-dimensional radial quadrupole field near the symmetry axis.

Fig.4.5 shows the evolution of the "cloverleaf" -design. At first the pinched coil (Fig.4.4a) is split up into three components (Fig.4.4b). The outer two coils dominantly contribute to the radial gradient field while the coils in the center are largely responsible for the field on axis. The radial gradient can be doubled by adding an extra pair of coils (Fig4.4c). This design is now optimized by deforming the current loops. Note that the segments of the coils which carry current flowing radially away or towards the symmetry axis as well as the part of the coils which is closest to the symmetry axis are contributing

most efficiently to the radial field. The outermost part of the loops produces a field which subtracts from the radial field. The final result resembles a cloverleaf. Extra coils are added to provide the axial *curvature* field and reduce the on-axis *bias* field.

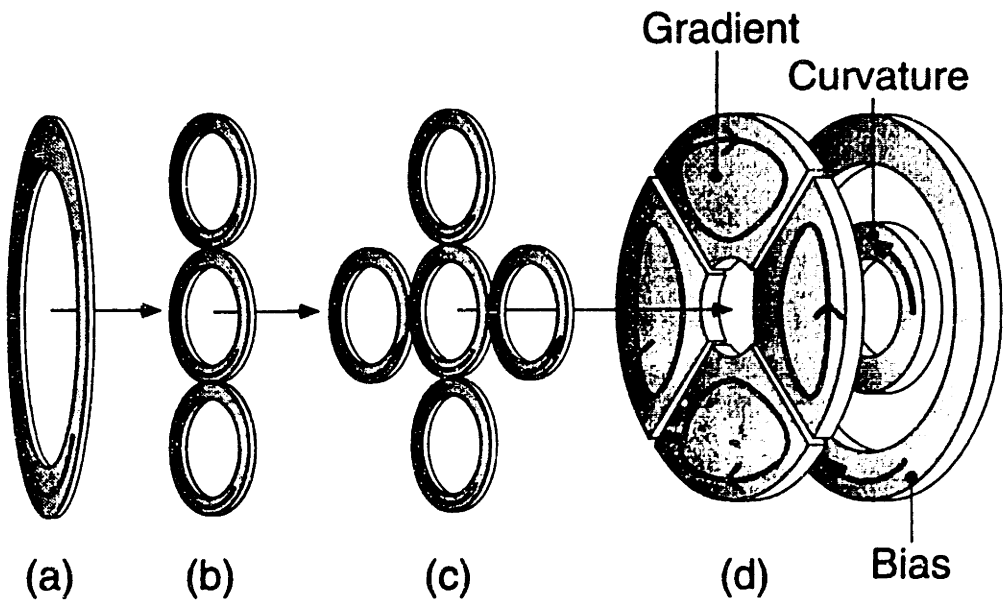

Fig.4.4 The evolution of a single "pinched" coil (a) into a "cloverleaf". The coil is segmented (b) to separate parts which mostly contribute to axial curvature and radial gradient respectively. The radial gradient field is enhanced by adding an extra set of coils (c). After optimization a design results which resembles a "cloverleaf". Additional coils provide independent control of bias and curvature fields. Note that the figure shows just one of the two cloverleaves which make up the trap.

Fig.4.5 shows the cloverleaf coils, which produce the radial gradient, the curvature coils, which are responsible for the axial curvature and a bias field coil pair, which makes the on-axis bias field adjustable. All three trapping parameters are therefore independently controllable. The cloverleaves are separated by 2.5 cm. The outer diameter of each "cloverleaf" consisting of four coils is 10 cm. The diameter of the inner hole which allows access for the horizontal trapping beams, is 2.5 cm. Contrary to what the figure shows, the curvature and bias field coils touch the clover leaf coils in order to be positioned as close to the atomic sample as possible.

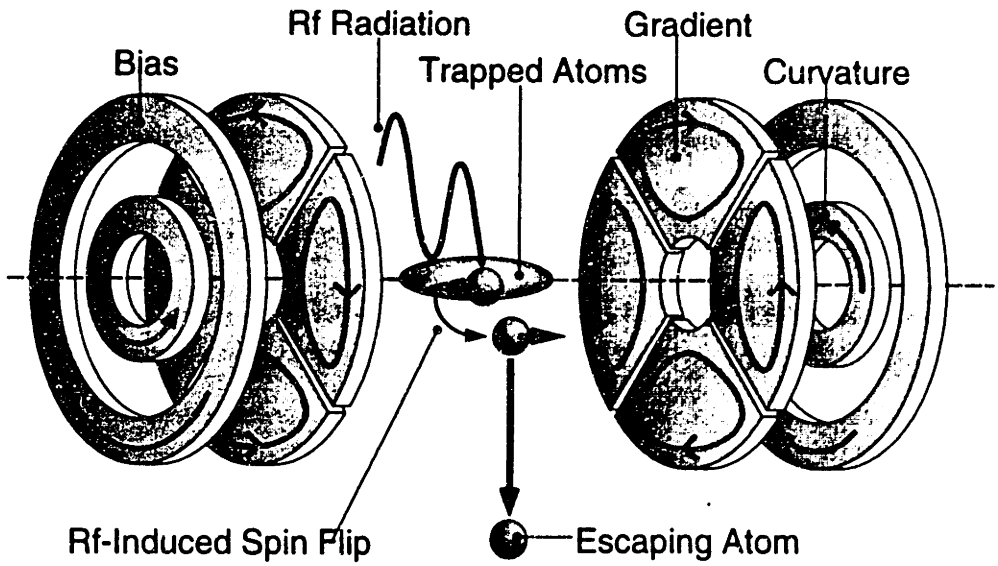

Fig.4.5 shows the experimental setup of the cloverleaf trap. The *gradient* coils produce the radial gradient B' in the trap center while the *curvature* coils provide the axial curvature B". The *bias* coils compensate for the axial bias field in the center added by the curvature coils. All three relevant trap parameters B', B" and B_0 are independently adjustable. The two gradient producing "clover leafs" are separated by one inch. The space between the coils is accessible to the laser beams required for optical cooling and detection. An rf antenna inside the vacuum chamber produces the rf field which evaporates atoms by means of electron spin resonance.

With the "cloverleaf" -setup we can realize a maximum curvature of 125 G/cm^2, a gradient of up to 170 G/cm and a bias field between 0 and 100G. This leads to a geometric mean of the field curvatures of 5 kG/cm^2 for a bias field of 1G. In order to achieve these parameters, trap currents of up to 270A are necessary. The coils have to dissipate up to 10kW. The trapping field can be switched on within 1 ms and extinguished within less than 100 μs.

The parameters B' and B_0 enable us to adjust the radial confinement over the extend of a trapped cloud from nearly linear (B_0/B'<<cloud size) in two dimensions to largely harmonic and isotropic (B"B_0=B'^{2}).

4.1.4 Mode Matching and Compression in the Cloverleaf Trap

To "mode-match" the magnetic trap to the almost spherically symmetric laser-cooled cloud, we have to provide nearly isotropic confinement. The axial curvature is

adjusted, to provide mode-matched axial confinement. With the two parameters B_0 and B' the radial curvature is then matched to the axial curvature. The depth of the trap is maximized[2] by choosing a radial gradient B', which is as large as possible, and by adjusting the bias field B_0 accordingly. We would mode match to a 100μK cloud which has a 3mm rms diameter with a curvature B"=125 G/cm^2, a gradient B'=170 G/cm and a bias field B_0=217 G. Our available bias field is limited to ~100 G. We therefore slightly "over-match" the radial trapping frequency by a factor of 1.5. This mismatch causes insignificant heating and does not affect the onset of evaporation. This illustrates the point made in Chapter 2.5, namely that phase space density and collision rate are not very sensitive to a mismatched transfer.

The transferred cloud is then compressed by decreasing the bias field adiabatically to ~1 Gauss. This method of compressing the cloud differs from the model discussed in Chapter 2.5, where we do not consider a change of the power law of the potential. As the bias field is decreased, the confining potential turns from nearly isotropic and harmonic (over the size of the cloud) into a potential which is linear along the radial direction.

This has a subtle implication for the phase space density during adiabatic compression: It increases by a factor of e=2.73 as the entropy remains constant [10, 11]. This increase requires elastic collisions to keep the sample thermalized. It has very recently been observed experimentally with spin-polarized hydrogen [11]. In our experiment we compress the sample to a mean geometric curvature of 5 kG/cm^2. Due to radial compression the ratio of the radial and axial trapping frequencies increases to approximately 15.

4.1.5 The Dimensionality of Evaporation

Such a large aspect ratio has important implications for rf evaporation in such a trap: As discussed briefly in Chapter 2.3, rf evaporation can become one-dimensional, if

[2] The dependence of the trap depth on trap parameters was discussed by [10].

the potential energy due to gravity across the rf truncation-shell is larger than k_BT. This means that gravity pulls the cloud towards a larger magnetic field at the trap bottom, such that only atoms at the very bottom of the cloud are in resonance with the rf. It leads to a truncation which is energy selective in one instead of three dimensions and hence greatly depreciates the evaporation efficiency [12]. The temperature T_{1D}, at which this effect occurs for sodium, is given by [12]

$$T_{1D}/[\mu K] \sim 10(B''_{vertical}/[kG/cm^2])^{-1} \qquad (4.7)$$

The above formula assumes an rf truncation at ~10 k_BT. $B''_{vertical}$ is the curvature along the vertical axis of the trap. According to the considerations above, the most strongly confining axis of a magnetic trap should therefore be vertical. For the trap parameters described in section 4.1.4 ($B''_{vertical}=B'^2/B_0=(170G/cm)^2/1G$) one dimensional evaporation would set in at a temperature T~100μK if the axial direction of the "cloverleaf " trap is oriented vertically. The trap is however oriented horizontally, which leads to one-dimensional evaporation at temperature ~ 400nK, well below the onset of BEC [13].

4.2 Bose-Einstein Condensation in the Cloverleaf Trap

We observed BEC in the cloverleaf trap in March 1996 [13]. The procedure and the evidence are similar to the OP trap experiment [1]. The detailed publication on BEC in the cloverleaf trap is presented in the appendix of this chapter.

The fact that the confinement is purely magneto-static and that the fields are highly stable allowed us to adjust the temperature of a Bose condensed sample such that it was possible to map out the condensate fraction as a function of (normalized) temperature across the transition [13]. The measurement of this fraction in superfluid

helium was a major accomplishment which took many decades to complete. A fascinating historical account and a description of the measurement is given in Sokol [14].

Evaporation in the cloverleaf trap lead to an order of magnitude increase in the number of condensed atoms ($5x10^6$ atoms) over the OP trap experiment [1]. This increase is probably due a lower heating rate because of less vibrations. The adjustability of the potential parameters also allowed us to adiabatically expand a trapped condensate [15] and excite collective excitations [16] in subsequent experiments. The reduction in curvature, compared to the extremely tight confinement of the OP trap, resulted only in a doubling of the evaporation time to ~20s.

4.3 A Summary of different Bose-Einstein Condensation experiments

Table 4.1 is a short comparison of the BEC experiments reported thus far [1, 2, 13, 17, 18]. The table does not include the observation of BEC of rubidium 87 in a modified "Baseball" trap which was reported very recently by JILA [19]. The first report of the Rice group [2] is not considered as the observation of BEC in a gas of atomic lithium but rather a report of cooling lithium into the quantum degenerate regime.

	JILA 95	MIT 95	MIT 96	Rice 96
Atom	^{87}Rb	Na	Na	^{7}Li
Scattering length [nm]	+ 6 nm	+ 5 nm	+ 5 nm	- 1.5 nm
Trap	TOP	Opt. plugged mag. trap	Cloverleaf mag. trap	Permanent mag. trap
$(B''_x B''_y B''_z)^{1/3}$[k G/cm^2]	3	150	5	1
first BEC	June 95	Sept. 95	March 96	(July 95) summer 96
Evidence for BEC	TOF	TOF	TOF direct imaging	(Halo) direct imaging
N_c	$2x10^4$	$2x10^6$	$15x10^6$	$2x10^5$
T_c [nK]	100	2,000	1,500	400
n_c [cm^{-3}]	$2x10^{12}$	$1.5x10^{14}$	$1x10^{14}$	$2x10^{12}$
N_0	2,000	$5x10^5$	$5x10^6$	2000
Cooling Time	6 min.	9 s	20 s	5 min.
condensed atoms/s	6	60,000	200,000	6
lifetime	≈ 15 s	≈ 1 s	≈ 20 s	≈ 20 s

Tab.4.1: Comparison of BEC experiments reported thus far.

4.4 The Weakly-Interacting Bose-Einstein Condensate

This section will briefly explain the mean-field which arises due to the weak interactions between atoms in the condensate. It will also introduce the Thomas-Fermi approximation and its implications on the condensates shape, the density distribution and the dependence of the mean-field energy on the number of condensed atoms.

The many-body wave function of a condensate which contains $5x10^6$ atoms in the fully compressed cloverleaf trap is about 17 μm wide radially and extends over 300 μm axially [13]. The ground state wave function of a *single* atom in the same trap on the other hand would have an rms width of 1.7 μm and 7 μm along the radial and axial direction respectively. A condensate of ideal *non-interacting* bosons would have the size of the single-particle ground state. The large extent of the condensate is due to weak repulsive interactions between the condensed atoms. The characteristic length scale for these interactions is the s-wave scattering length for sodium atoms in the F=1 hyperfine groundstate. The value of this scattering length was determined spectroscopically to be a=2.70(3)nm [20], much shorter than the expectation value of the distance between two atoms in the condensate which is on the order of 100 nm. The wavefunction of the condensed atoms on the other hand extends over the full size of the condensate. These atoms therefore "overlap" and experience a mean-field potential U_{mf} due to the mutual repulsion which is proportional to the condensate density ρ(z,r) [21-23]:

$$U_{mf}(r,z) = \frac{4\pi\hbar^2 a}{m}\rho(r,z) \tag{4.8}$$

The mean-field is a result of the large extent of the ground state wave function. It is *not* a time averaged potential which arises due to frequent elastic collisions between atoms. In fact, the condensate ground state is stationary and the mean field results from *collisionless* interactions, a manifestation of quantum mechanics.

The physics of such a weakly-interacting condensate is governed by the non-linear Schrödinger equation (NLSE) (also referred to a Grosz-Pitaevskii equation [24, 25]):

$$i\hbar\frac{\partial}{\partial t}\Phi(r,t) = \left(-\frac{\hbar^2\nabla^2}{2m} + U_{trap}(r) + \frac{4\pi\hbar^2 a}{m}|\Phi(r,t)|^2\right)\Phi(r,t) \tag{4.9}$$

$\Phi(r,t)$ is the macroscopic order parameter of the system and the expectation value of the density is given by

$$\rho(r,t) = |\Phi(r,t)|^2 \tag{4.10}$$

For a large number of condensed atoms N we can obtain a very good approximation to the ground state wave function by neglecting the kinetic energy term in the NLSE. This approximation is called the Thomas-Fermi limit and applies to condensates in the cloverleaf trap: The mean field of $5\text{x}10^6$ atoms in a condensate with a peak density $\rho_{peak}=3.0\text{x}10^{14}\text{cm}^{-3}$ is on the order of 100 nK while the zero-point energy in the ground state is a approximately 16nK [13]. The density distribution $\rho_0(r,z)$ resembles an inverted "image" of the trapping potential and is given by

$$\begin{aligned}\rho_0(r,z) &= \frac{m}{4\pi\hbar^2 a}\left(\mu - U_{trap}(r,z)\right) \\ &= \frac{m}{4\pi\hbar^2 a}\left(\mu - \tfrac{1}{2}m\omega_r^2 r^2 - \tfrac{1}{2}m\omega_z^2 z^2\right)\end{aligned} \tag{4.11}$$

as long as this expression is positive and vanishes otherwise. μ is the chemical potential of the condensate given by

$$\mu = \frac{15^{2/5}}{2}\left(\frac{\hbar^2 a\varpi^3 N}{m}\right)^{2/5} \tag{4.12}$$

where $\varpi = (\omega_z\omega_r^2)^{1/3}$ is the geometric mean of the trapping frequencies. The ground state wavefunction is shaped such that the potential due to the mean field exactly cancels the trapping potential. This is illustrated in Fig. 4.6.

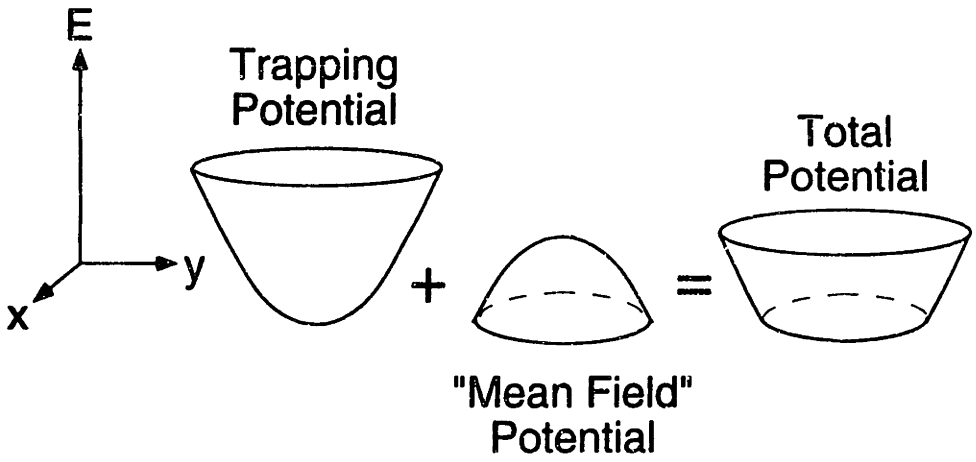

Fig.4.6 In the Thomas-Fermi limit the kinetic energy of condensed atoms is negligible compared to the mean-filed energy. The contribution to the potential due to the mean-field is directly proportional to the local density. The resulting ground state density distribution is a "mirror image" of the potential, which flattens out the bottom of the total potential.

The solution is not a good approximation at the "boundary" of the wave function where the density vanishes and the kinetic energy term becomes comparable to the mean field. Far outside the boundary, where the mean-field is negligible, the wavefunction falls off like a gaussian in analogy to the single particle wavefunction [26].

The peak density of the condensate in the Thomas-Fermi is by a factor $8/(15^{2/5}\pi^{1/2})\ N^{3/5}(a/a_{osc})^{3/5}$ smaller than the peak density of a non-interacting condensate with the same number of atoms [27]. $a_{osc}=(\hbar/m\omega)^{1/2}$ is the oscillator length. The aspect ratio of the condensate α, the ratio of the axial to the radial extend of the wavefunction, is the reciprocal ratio of the corresponding trapping frequencies: $\alpha=\omega_r/\omega_z$.[3] The wave function spreads out due to repulsive mean field interaction. In fact, the linear extent of the condensate in the Thomas-Fermi limit is proportional to $N^{1/5}$. The volume which the condensate occupies consequently scales as $N^{3/5}$ while the peak density increases proportional to $N^{2/5}$ (Eq.4.11 and Eq.4.12). The mean-field energy stored in the condensate should therefore scale as $N^{7/5}(\sim \int dx^3\rho^2)$ and the mean field energy *per atom in the condensate* E_{mf} increases as $N^{2/5}$. From Eq.4.11 and Eq.4.12 follows

[3] The effects of the anisotropy of the potential are much more pronounced than in non-interacting case, where $\alpha=(\omega_r/\omega_z)^{1/2}$.

$$E_{mf} = \frac{15^{2/5}}{7}\left(\hbar^2 m^{1/2} a \varpi^3 N\right)^{2/5} \tag{4.14}$$

Dalfovo *et al.* [26] derive a simple estimate for the ratio between the mean field energy and the kinetic energy of a particle in the many-body condensate ground state. According to that estimate the mean-field (~100nK) energy is more than two orders of magnitude larger than the kinetic energy of the particles in the condensate (<1nK). We consequently expect the mean field to play a significant role in the dynamics of the ground state.

In fact, if the trap is switched instantaneously, atoms will be accelerated due to the mean-field repulsion and the "explosively" released mean-field energy will be the dominant contribution to the kinetic energy of the atoms in ballistic expansion. We were able to confirm the $N^{2/5}$ dependence of the mean-field energy per particle by recording the ballistic expansion of condensates with a variable number of condensed atoms [13] (→appendix of this chapter).

In ballistic expansion the mean-field energy is predominantly released in the direction of strongest confinement (the radial direction in case of the cloverleaf trap): The local mean-field scales as the condensate density and the initial acceleration due to the mean-field after the switch-off of the confinement is proportional to the density gradient in the cloud. This gradient is largest along the strongly confining directions.

Castin and Dum predicted that a ballistically expanding condensate, which was initially trapped in a harmonic trap and in the Thomas-Fermi limit, does not change its characteristic shape of an inverted 3-dimensional parabola [28]. It only rescales width and peak density. Such a dependence is apparent in the absorption images of ballistically expanding clouds [13] (→ appendix of this chapter).

The Thomas-Fermi approximation often simplifies a theoretical description tremendously, which permits quantitative analytical predictions of the condensate

dynamics (see e.g. [29]). If the kinetic energy is *not* negligible compared to the mean field energy a theoretical treatment can become very complex and require numerical approaches (see e.g. [30]).

References for Chapter 4:

1 K. B. Davis, M.-O. Mewes, M. R. Andrews, *et al.*, Physical Review Letters **75**, 3969 (1995).

2 C. C. Bradley, C. A. Sackett, J. J. Tollet, *et al.*, Physical Review Letters **75**, 1687 (1995).

3 T. J. Greytak, in *Bose-Einstein Condensation*, edited by A. Griffin, D. W. Snoke and S. Stringari (Cambridge University Press, Cambridge, 1995), p. 131-159.

4 T. Bergeman, G. Erez, and H. Metcalf, Physical Review A **35**, 1535 (1987).

5 D. E. Pritchard, Physical Review Letters **51**, 1336 (1983).

6 H. Hess, G. P. Kochanski, J. M. Doyle, *et al.*, Physical Review Letters **59**, 672 (1987).

7 R. van Roijen, J. J. Berkhout, S. Jaakkola, *et al.*, Physical Review Letters **61**, 931-934 (1988).

8 V. S. Bagnato, G. P. Lafyatis, A. G. Martin, *et al.*, Physical Review Letters **58**, 2194 (1987).

9 Y. V. Gott, M. S. Ioffe, and V. G. Tel'kovskii, Nucl. Fusion, 1962 Suppl., Pt. 3 , 1045 and1284 (1962).

10 D. M. Kurn, talk at DAMOP 1996, abstract SB3 (1996).

11 P. W. H. Pinske, A. Mosk, M. Reynolds, *et al.*, preprint (1996).

12 W. Ketterle and N. J. van Druten, in *Advances in Atomic, Molecular, and Optical Physics*, edited by B. Bederson and H. Walther (Academic Press, San Diego, 1996), Vol. 37.

13 M.-O. Mewes, M. R. Andrews, N. J. van Druten, *et al.*, Physical Review Letters 77, 416-419 (1996).

14 P. E. Sokol, in *Bose-Einstein Condensation*, edited by A. Griffin, D. W. Snoke and S. Stringari (Cambridge University Press, Cambridge, 1995), p. 51-85.

15 M. R. Andrews, M.-O. Mewes, N. J. van Druten, *et al.*, Science **273**, 84-87 (1996).

16 M.-O. Mewes, M. R. Andrews, N. J. van Druten, *et al.*, Physical Review Letters (1996).

17 M. H. Anderson, J. R. Ensher, M. R. Matthews, *et al.*, Science **269**, 198-210 (1995).

18 C. C. Bradley, C. A. Sackett, and R. G. Hulet, preprint (1996).

19 C. J. Myatt, E. A. Burt, R. W. Ghrist, *et al.*, preprint (1996).

20 E. Tiesinga, C. J. Williams, P. S. Julienne, *et al.*, Journal of Research of the National Institute of Standards and Technology **101**, 505-520 (1996).

21 P. Nozières and D. Pines, *The theory of quantum liquids* (Addison-Wesley, Redwood City, CA, 1990).

22 V. V. Goldman, I. F. Silvera, and A. J. Leggett, Physical Review B **24**, 2870-2873 (1981).

23 D. A. Huse and S. E. D., Journal of Low Temperature Physics **46**, 137 (1982).

24 V. L. Ginzburg and L. P. Pitaevskii, Sov. Phys. JETP **7**, 858 (1958).

25 L. P. Pitaevskii, Sov. Phys. JETP **13**, 451 (1961).

26 F. Dalfovo, L. Pitaevskii, and S. Stringari, Physical Review A **54**, 4213 (1996).

27 G. Baym and C. Pethick, Physical Review Letters **76**, 6 (1996).

28 Y. Castin and R. Dum, preprint (1996).

29 S. Stringari, Physical Review Letters 77, 2360 (1996).

30 M. Edwards, P. A. Ruprecht, K. Burnett, *et al.*, preprint (1996).

Appendix to Chapter 4:

This appendix contains the publication which describes the observation of Bose-Einstein condensation of atomic sodium in the cloverleaf trap.

Bose-Einstein Condensation in a Tightly Confining dc Magnetic Trap

M.-O. Mewes, M. R. Andrews, N. J. van Druten, D. M. Kurn, D. S. Durfee, and W. Ketterle
Department of Physics and Research Laboratory of Electronics, Massachusetts Institute of Technology, Cambridge, Massachusetts 02139
(Received 17 May 1996)

Bose-Einstein condensation of sodium atoms has been observed in a novel "cloverleaf" trap. This trap combines tight confinement with excellent optical access, using only dc electromagnets. Evaporative cooling in this trap produced condensates of 5×10^6 atoms, a tenfold improvement over previous results. We measured the condensate fraction and the repulsive mean-field energy, finding agreement with theoretical predictions. [S0031-9007(96)00729-6]

PACS numbers: 03.75.Fi, 05.30.Jp, 32.80.Pj, 64.60.-i

Einstein predicted in 1925 that an ideal quantum gas would undergo a phase transition when the thermal de Broglie wavelength becomes larger than the mean spacing between particles [1]. For many years, this phenomenon, now known as Bose-Einstein condensation (BEC), was regarded as a mathematical artifact, until London "rediscovered" it in 1938 to explain the superfluidity of liquid helium [2]. However, in liquid helium, the purely quantum-statistical nature of the BEC transition is complicated by strong interactions [3]. BEC was recently created in excitons, which behave similarly to a gas of particles [4]. Bose-Einstein condensation in dilute atomic gases was first pursued in spin-polarized hydrogen [5], and last year was finally observed in alkali vapors at JILA and MIT [6,7]. A third group, at Rice University, reported cooling of lithium atoms into the quantum-degenerate regime [8]. These experiments led to renewed experimental and theoretical interest in the study of quantum-degenerate gases [9].

In this Letter, we report a detailed study of the properties of a weakly interacting condensate and a comparison with theory [10]. These experiments were carried out in a novel atom trap which overcame major limitations of the traps used so far for evaporative cooling and BEC: the time-dependent field in the case of the TOP trap [11], the sensitivity to shape and position of the optical plug in the optically plugged trap [7], the inflexibility of a trap that uses permanent magnets [8], or the constraints of a cryogenic environment for a trap that employs superconducting coils [5].

Our new trap is of the Ioffe-Pritchard (IP) type, suggested in Refs. [12,13] and originally used for trapping hydrogen [14,15] and sodium [16] in cryogenic traps. In contrast, our trap is built with normal electromagnets. Previously, it had been concluded that IP traps are inferior in confinement compared to the TOP trap [11], which uses a static spherical quadrupole field and a rotating bias field. However, the previous analysis was incomplete, and we point out here that spin flips induced by the rotating field limit the confinement of a TOP trap to below the value that can be achieved in an IP trap. Tight confinement is crucial because evaporative cooling [17] (the technique used to attain BEC in atomic gases) requires densities high enough that the thermalization time is much shorter than the lifetime of the sample.

The design of our trap was based on the following considerations. The magnetic trapping potential μB is given by the effective magnetic moment μ of the atom and the absolute value B of the magnetic field. Both the TOP and IP traps are harmonic and cylindrically symmetric near the minimum of the potential, with different radial and axial curvatures. The geometric mean of the curvatures is the relevant figure of merit of a trap for evaporative cooling [18]. The radial curvature B''_{IP} in an IP trap varies with the radial gradient B' and the bias field B_0 as $B''_{\mathrm{IP}} = B'^2/B_0$. In the TOP trap, one obtains for the curvature $B''_{\mathrm{TOP}} = B'^2/2B_{\mathrm{rot}}$, where B_{rot} is the amplitude of the rotating bias field. Stability against spin flips requires the Larmor frequency (which is proportional to B_0 or B_{rot}) to be much higher than ω_{rot}, the frequency at which the moving atom sees the inhomogeneous magnetic field rotate. For an IP trap, ω_{rot} is less than or equal to the atomic oscillation frequency, whereas in a TOP trap, the frequency of the rotating field ω_{rot} must be much higher than the atomic oscillation frequency (in Ref. [6], for example, the ratio of ω_{rot} to the radial trap frequency was 150). As a consequence, the minimum B_{rot} of a TOP trap must be much larger than B_0 of an IP trap. This limits the radial curvature of the TOP trap to be about 2 orders of magnitude weaker than that of an IP trap with comparable radial gradient B'. In the axial direction, the TOP trap creates a B'' which can be a hundred times larger than in an IP trap; however, the product of the three curvatures is higher for an optimized IP trap. The above discussion assumes that the curvature does not change over the extent of the cloud and is thus valid for cold samples.

A somewhat different discussion applies when a warmer cloud of temperature T is loaded into a magnetic trap. In the TOP trap, B_{rot} must be larger than $20kT/\mu$ to maintain a trap depth larger than $5kT$, determined by the rotating zero of the magnetic field. The resulting

 0031-9007/96/77(3)/416(4)$10.00

radial curvature of $\mu B'^2/40kT$ is much lower than the effective curvature $\mu B'^2/kT$ of the IP trap [17]. Again, the IP trap has a higher mean curvature.

The usual configuration of the IP trap, using the so-called "Ioffe bars" or the baseball winding pattern [19], limits optical access to the trapping region. This was solved by a novel winding pattern, allowing full 2π optical access in the symmetry plane of the trap: each of the two axial coils (the so-called "pinch coils" [19]) was surrounded by four coils, in the form of planar cloverleaves, which created the radial quadrupole field. Two larger axial coils were added to reduce the bias field. The twelve coils of the "cloverleaf" trap allowed independent and almost orthogonal control over the three important parameters of the trapping field: axial bias field, axial curvature, and radial gradient. Additional coils generated bias fields along the x, y, and z directions, allowing accurate overlap of the centers of the light trap and the magnetic trap.

The experimental procedure was as follows. A high density of magnetically trapped sodium atoms was obtained in a multistep procedure similar to that described in our previous works [7,20]. Using a Zeeman slower and a dark SPOT [21], within 2 s typically $(5-10) \times 10^9$ atoms were confined at densities of 5×10^{11} cm^{-3}. *In situ* loading of the magnetic trap was accomplished by extinguishing the laser-cooling light quickly and switching on the cloverleaf trap with the maximum values of axial curvature ($\approx$125 G/cm^2), radial gradient ($\approx$170 G/cm), and axial bias field ($\approx$100 G) within 1 ms. The trapping potential was approximately isotropic and provided confinement at about the same temperature and size as the initial laser-cooled cloud. This resulted in typically 2×10^9 trapped atoms in the $F = 1, m_F = -1$ state, at a peak density of 6×10^{10} cm^{-3} and a phase space density $\approx 10^6$ times lower than required for BEC. The elastic collision rate in the center of the cloud was about 20 Hz, based upon an elastic collision cross section of 6×10^{-12} cm^2 [20]. Subsequently, the cloud was radially compressed by reducing the bias field to 1 G. The lifetime of the trapped atoms was approximately 1 min, probably limited by background-gas scattering at a pressure of typically 3×10^{-11} mbar. From Hall-probe measurements of the magnetic fields, the axial and radial trapping frequencies were calculated to be $\omega_z = 2\pi \times 18$ Hz and $\omega_r = \omega_y = 2\pi \times 320$ Hz, respectively.

The atoms were further cooled by rf-induced evaporation [11,17,20,22]. The rf frequency was swept from 30 MHz to a variable final value, typically around 1 MHz. The sweep time (between 15 and 26 s) was longer than in our previous experiment [7], where such a long evaporation time did not result in more efficient cooling. This suggests that some additional heating process was present in our previous trap.

After evaporation, the atom cloud was allowed to thermalize in the magnetic trap for 100 ms, with the rf switched off. Finally, following a sudden switch-off of the trap and a variable delay time, the atom cloud was imaged using the same method as in our previous work [7]. The probe laser beam was directed vertically through the atom cloud, along a radial axis of the trap, and the probe absorption was imaged onto a charge-coupled device sensor with a system of lenses having a resolution of 5 μm. The vertical absorption beam allowed for delay times of up to 50 ms (corresponding to a drop distance of 1.2 cm). No refocusing was necessary due to the expansion of the falling cloud. Density, temperature, and total number of atoms were determined from these absorption images, as will be described below.

As in our previous work [7], the BEC phase transition was observed as the sudden appearance of a bimodal distribution in time-of-flight images when the final rf frequency was lowered below a critical value of typically 1.1 MHz. Examples of time-of-flight images are shown in Fig. 1, for varying delay times; they show the expansion of the initially pencil-shaped cloud. The normal component expands isotropically, whereas the condensate expands predominantly along the radial direction.

For the longer flight times, the image reflects the velocity distribution of the expanding thermal cloud because the initial spatial extent is negligible. We analyzed such images taken with a 40 ms time of flight, and a varying final rf frequency. At the transition temperature and below, the velocity distribution of the normal component is isotropic and proportional to $g_{3/2}[\exp(-mv^2/2kT)]$ where $g_{3/2}$ is the familiar Bose function. On the other hand, in the Thomas-Fermi regime (see below) the density distribution of the expanding condensate is anisotropic

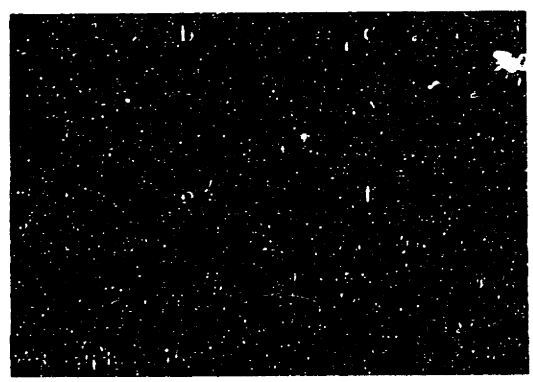

FIG. 1(color) Time-of-flight images of expanding mixed clouds. Flight times for (a)–(f) are 1, 5, 10, 20, 30, and 45 ms, respectively. The normal component expands isotropically [most clearly seen in (d) and (e), the light-blue spherical cloud], whereas the condensate expands much faster in the radial than in the axial direction. The earliest image shows the pencil-like shape of the initial cloud. In the early phase of the expansion, the clouds appear larger than their true sizes due to complete absorption of the probe laser light. The width of the field of view is 1.6 mm.

and predicted to maintain its parabolic shape [23]. Full two-dimensional images were fitted assuming this model for the expansion of the cloud. The shape of the condensate was clearly non-Gaussian and was fitted well by the parabolic function. The relatively low optical density of the normal fraction limited the determination of an accurate temperature to clouds with condensate fractions smaller than 50%.

Theoretically, one expects a critical temperature T_c of [24]

$$kT_c = \hbar\bar{\omega}(N/1.202)^{1/3}, \quad (1)$$

with N the number of atoms and $\bar{\omega}$ the geometric mean of the harmonic trap frequencies $\bar{\omega} = (\omega_x\omega_y\omega_z)^{1/3}$. Below the critical temperature, the condensate fraction should vary as [24]

$$N_0/N = 1 - (T/T_c)^3. \quad (2)$$

In Fig. 2, the condensate fraction is plotted versus normalized temperature $T/N^{1/3}$ (both determined from the fits) and compared to the theoretical prediction, Eq. (2). As the temperature was lowered by evaporative cooling, the number of atoms N decreased. The data were plotted in terms of $T/N^{1/3}$ to account for the scaling of T_c with N, Eq. (1). The scatter in the experimental data is consistent with our estimated statistical and systematic errors. Comparing the horizontal scales of the theoretical and experimental data yields [using Eq. (1)] $\bar{\omega} = 2\pi \times 142$ Hz, in reasonable agreement with $\bar{\omega} = 2\pi \times 120$ Hz, as determined from the Hall-probe measurements.

Note that Eqs. (1) and (2) are equivalent to $N - N_0 = 1.202(kT/\hbar\bar{\omega})^3$, expressing that the normal component behaves as a saturated vapor where the interaction energy is much smaller than the thermal energy. Therefore, the condensate fraction is only weakly affected by interactions between the atoms.

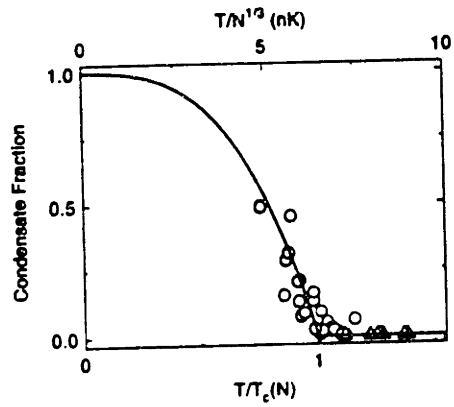

FIG. 2. Condensate fraction versus normalized temperature $T/T_c \propto T/N^{1/3}$. Solid line theoretical curve, Eq. (2). The experimental data were determined from fits to time-of-flight images (see text); Δ: clouds with no detectable condensate, O: clouds with both condensate and normal fraction visible.

Typical values for the number of atoms and temperature at the phase transition were $N_c = 15 \times 10^6$ and $T_c = 2\ \mu$K, respectively. The critical peak density at 2 μK was 1.5×10^{14} cm^{-3}. Pure condensates with up to 5×10^6 atoms have been observed, a factor of 10 improvement over our previous result [7], which is ascribed to the more efficient evaporative cooling in the cloverleaf trap.

If the density of condensed atoms is high, the kinetic energy of the condensate is negligible compared to its interaction energy $n_0\tilde{U}$ (Thomas-Fermi approximation), where n_0 is the peak condensate density, and $\tilde{U}$ is proportional to the scattering length a [25]: $\tilde{U} = 4\pi\hbar^2 a/m$ ($\tilde{U}/k = 1.3 \times 10^{-21}$ K cm^3). In this regime, the condensate density distribution is given by $n_0(\mathbf{r}) = n_0 - V(\mathbf{r})/\tilde{U}$, where $V(\mathbf{r})$ is the trapping potential [and $n_0(\mathbf{r})$ vanishes where $V(\mathbf{r}) > n_0\tilde{U}$]. This results in a peak condensate density

$$n_0 = 0.118(N_0 m^3\bar{\omega}^3/\hbar^3 a^{3/2})^{2/5}. \quad (3)$$

For typical parameters of our experiment, $n_0 = 3.0 \times 10^{14}$ cm^{-3}, and the mean-field energy per atom, $2n_0\tilde{U}/7$, is 110 nK, much larger than the zero-point energy of 16 nK. Consequently, the assumption of negligible kinetic energy is justified.

In the Thomas-Fermi approximation, the aspect ratio of the condensate is the ratio of radial and axial trapping frequencies, which is approximately 20. The initial acceleration after switch-off of the trap is determined by the gradient of the interaction energy and is inversely proportional to the width of the condensate. Consequently, the aspect ratio of the velocity distribution is inverted compared to the initial spatial distribution. In our case, nearly all the interaction energy is released in the radial expansion. The axial expansion corresponds to a temperature around 0.2 nK, and is small compared to the initial length. The radial kinetic energy obtained from the time-of-flight images corresponds therefore to the interaction energy of the condensate.

In Fig. 3, the interaction energy is plotted versus the number of atoms in the condensate. N_0 was varied by only partially condensing the cloud, or by using rf evaporation to remove atoms from a pure condensate. As can be seen from the figure, the expansion of the condensate did not depend on whether a normal component was present. This indicates that interactions with the normal fraction did not affect the expansion of the condensate. The mean-field energy per condensed atom is proportional to $N_0^{2/5}$, as predicted by Eq. (3). From the proportionality constant a value for the scattering length was obtained.

To eliminate errors due to uncertainty in the trapping frequencies and absolute measurements of atom numbers, $\bar{\omega}^3$ in Eq. (3) was expressed by using Eqs. (1) and (2). In this way we find $a = 65 \pm 30$ bohr, which agrees well with $a = 92 \pm 25$ bohr, the value previously determined from thermal relaxation times [20]. The determination of the released energy per atom, $2n_0\tilde{U}/7$, provides a direct

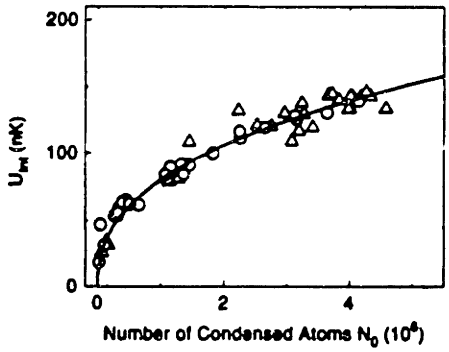

FIG. 3. Mean-field energy per condensed atom versus the number of atoms in the condensate. △: clouds with no visible normal fraction. ○: clouds with both normal and condensed fractions visible. The solid line is a fit proportional to $N_0^{2/5}$.

measurement of the peak density n_0 of the condensate, and, combined with N_0, of the size of the condensate. For $N_0 = 5 \times 10^6$, the Thomas-Fermi approximation gives a density distribution of the condensate which is nonzero within 17 μm in the radial direction and 300 μm axially [25]. Note that these widths are much larger than the rms widths of the ground state, $\sqrt{2\hbar/m\omega}$, which are 1.7 μm in the radial and 7.0 μm in the axial directions.

The condensate had a lifetime of about 20 s when the rf radiation was left on. This lifetime decreased to about 1 s when the rf field was turned off. This reduced lifetime might be caused by grazing-incidence collisions with 300 K background-gas atoms, which excite trapped atoms to an energy comparable to the trap depth of about 5 mK. If these hot atoms are kept in the trap, they rapidly heat up the condensate. If the rf is left on, it skims off such atoms. A more detailed study is needed to accurately characterize the decay of the condensate.

In conclusion, we have achieved Bose-Einstein condensation of sodium atoms in a novel cloverleaf trap, a purely magnetic trap using only dc electromagnets. The variable confinement and aspect ratio of the cloverleaf trap are ideal for studying various properties of the condensate. In the present case the condensate had an aspect ratio of ≈20 and a maximum length of 300 μm. The kinetic energy of the axial motion is about 1 pK. An elongated condensate is advantageous for several experiments. For instance, it is possible to spatially resolve the shape of the condensate amidst the normal fraction [26]. Also, an elongated condensate can easily be cut with a sheet of far-off-resonant blue-detuned light [7]. This configuration might realize an atomic Josephson junction, or can be used to perform interference experiments with two condensates, demonstrating the existence of a macroscopic wave function and superfluidity.

We are grateful to Dan Kleppner for helpful comments on the manuscript. This work was supported by ONR, NSF, JSEP, and the Sloan Foundation. M.-O. M. and D. M. K. acknowledge support from Studienstiftung des Deutschen Volkes and an NSF Graduate Research Fellowship, respectively, and N. J. v. D. from "Nederlandse Organisatie voor Wetenschappelijk Onderzoek (NWO)" and NACEE (Fulbright fellowship).

[1] A. Einstein, Sitz. K. Preuss. Akad. Wiss. **1925**, 3 (1925).
[2] F. London, Nature (London) **141**, 643 (1938).
[3] *Bose-Einstein Condensation*, edited by A. Griffin, D. W. Snoke, and S. Stringari (Cambridge University Press, Cambridge, UK, 1995).
[4] Jia Ling Lin and J. P. Wolfe, Phys. Rev. Lett. **71**, 1222 (1993).
[5] T. J. Greytak, in Ref. [3], pp. 131–159.
[6] M. H. Anderson *et al.*, Science **269**, 198 (1995).
[7] K. B. Davis *et al.*, Phys. Rev. Lett. **75**, 3969 (1995).
[8] C. C. Bradley, C. A. Sackett, J. J. Tollett, and R. G. Hulet, Phys. Rev. Lett. **75**, 1687 (1995).
[9] Book of Abstracts, Workshop on Collective Effects in Ultracold Atomic Gases, Les Houches, France, 1996 (to be published).
[10] Related results were obtained at JILA (to be published).
[11] W. Petrich, M. H. Anderson, J. R. Ensher, and E. A. Cornell, Phys. Rev. Lett. **74**, 3352 (1995).
[12] Y. V. Gott, M. S. Ioffe, and V. G. Telkovsky, in *Nuclear Fusion, 1962 Suppl., Pt. 3* (International Atomic Energy Agency, Vienna, 1962), pp. 1045–1049, 1284.
[13] D. E. Pritchard, Phys. Rev. Lett. **51**, 1336 (1983).
[14] H. F. Hess *et al.*, Phys. Rev. Lett. **59**, 672 (1987).
[15] R. van Roijen, J. J. Berkhout, S. Jaakkola, and J. T. M. Walraven, Phys. Rev. Lett. **61**, 931 (1988).
[16] V. S. Bagnato *et al.*, Phys. Rev. Lett. **58**, 2194 (1987).
[17] W. Ketterle and N. J. van Druten, in Advances in Atomic, Molecular and Optical Physics, edited by B. Bederson and H. Walther (Academic Press, San Diego, to be published), Vol. 37.
[18] The BEC transition temperature and the collision rate after adiabatic compression are proportional to this quantity which therefore determines the efficiency of evaporative cooling [17].
[19] T. Bergeman, G. Erez, and H. J. Metcalf, Phys. Rev. A **35**, 1535 (1987).
[20] K. B. Davis *et al.*, Phys. Rev. Lett. **74**, 5202 (1995).
[21] W. Ketterle *et al.*, Phys. Rev. Lett. **70**, 2253 (1993).
[22] Originally suggested by D. E. Pritchard, K. Helmerson, and A. G. Martin, in *Atomic Physics 11*, edited by S. Haroche, J. C. Gay, and G. Grynberg (World Scientific, Singapore, 1989), pp. 179–197, and first realized by W. Ketterle *et al.*, in Proceedings of the OSA Annual Meeting, Toronto, Canada, 1993 (unpublished).
[23] R. Dum and Y. Castin (to be published).
[24] S. R. de Groot, G. J. Hooyman, and C. A. ten Seldam, Proc. R. Soc. London A **203**, 266 (1950).
[25] G. Baym and C. J. Pethick, Phys. Rev. Lett. **76**, 6 (1996), and references therein.
[26] M. R. Andrews *et al.*, Science (to be published).

5. COLLECTIVE EXCITATIONS OF A BOSE CONDENSATE

This chapter is centered around the publication on the observation of collective excitations in a weakly-interacting Bose condensate (→appendix). It starts with a historical note on how the theory of collective excitations helped to establish the link between superfluidity in He II and Bose statistics. The chapter then continues with a brief derivation of low-lying collective condensate modes that can be observed in the cloverleaf trap. A short section on the observation of a strong condensate excitation is added as a supplement

.

5.1 Collective Excitations and Superfluidity

Superfluidity describes a range of experimental phenomena in ultracold liquid helium such as frictionless and persistent flow, wave propagation on liquid surfaces and other kinetic effects. We understand less about the physics of these complex phenomena than we understand about Bose condensation itself which can be directly derived from the basic principles in quantum statistical mechanics (appendix chapter 2).

Collective quantum excitations played a key role in determining and understanding the superfluid behavior of helium. In fact, it was the theory of these collective excitations that helped to establish the link between Bose statistics and superfluidity. I briefly sketch the historical steps towards this insight. A comprehensive overview of superfluid quantum systems is given in [1]. A thorough treatment of Bose-Einstein Condensation and superfluidity can be found in [2, 3].

As early as 1938 Fritz London realized that the discontinuity in the derivative of the specific heat of an ideal Bose gas resembles the λ–point of helium [4]. He suspected that atoms in superfluid helium might move in a "self consistent periodic field formed by the other atoms" similar to the description of electrons in the Bloch theory of a metal. Drawing upon these analogies he pointed out that the condensation phenomenon in Bose statistics (BEC) might be the underlying mechanism of superfluidity in helium. Until that time Einstein's prediction of BEC[5] had been considered purely a mathematical oddity

and had not been taken serious as a physical phenomenon. London's insight, however, did not catch on right away. In fact, Landau opposed any connection of superfluidity with BEC and in 1941 he used the theory of elementary excitations of the quantum liquid to explain excited states of superfluid helium [6]. The excitations are also called quasiparticles and are phonons in the long wave length limit. He argued that a system with only phonon excitations would flow without friction, since they cannot absorb an arbitrary small amount of energy or momentum. His theory enabled him to understand various thermodynamic and transport properties of He II, such as the propagation of second sound. Landau's phenomenological approach to the subject was based on quantum hydrodynamics. Earlier, in 1938, Tisza had predicted second sound by using another empirical approach, the "two fluid" model [7]. Landau was not aware of Tisza's results due a lack of scientific communication during the second world war. It was Bogoliubov, who finally reconciled Landau's approach with London's suggestion in 1947[8] . He showed that in a weakly interacting system which obeys Bose-Einstein statistics the single-particle energy spectrum is modified by a macroscopic population of the ground state, the *Bose-Einstein condensate.* This modification leads to the low-lying phonon states predicted by Landau earlier. From 1953 to 1957 Feynman enforced this link between superfluidity and Bose statistics by thoroughly describing the nature of the macroscopic wavefunction. He argued that Bose statistics excludes *any* low lying excitations except density fluctuations in the immediate neighborhood of the ground state. He was able to explain the excitation spectrum well enough that it agreed with experimental data obtained through neutron scattering [1]. An interesting popular overview over Feynman's contributions to the theory of superfluidity can be found in [9]. He also explained the creation of quantized vortex lines [10] by linking it to the critical velocity of superfluids.

The observation of Bose-Einstein condensation in weakly interacting atomic gases requires a quite different approach to the relationship with superfluidity and collective excitations: in contrast to superfluid helium, it was rather easy to provide evidence for the

existence of a Bose condensate once the quantum degenerate regime was reached [11-13]. The determination of the Bose condensed fraction as a function of temperature [13, 14] was simple compared to the decade-long effort necessary for the measurement in superfluid helium [15]. However, the direct evidence for superfluidity in a quantum degenerate atomic gas has not been observed. (It is also not well understood what *superfluidity* in a small trapped sample implies.) The accumulation of a macroscopic fraction of the atoms in the groundstate of the system is a direct consequence of the *complete symmetric* many-body wave function. It would be desirable to observe the quantum mechanical character of the system on a macroscopic scale: the coherence of the condensed "matter waves". The observation of superfluidity or the interference of two independent condensates would be a major step in this direction.

Until the observation of BEC in exciton systems [16] and in dilute atomic gases [11-13, 17] superfluid helium has been the only bosonic system that exhibits a macroscopic quantum behavior. It took long to achieve a detailed theoretical understanding of this phenomenon, since quantum statistical effects are entangled with strong (and not only binary) interparticle interactions. A dilute Bose system, on the other hand is an ideal testing ground for theories. It might permit a complete understanding and could lead to an improved theory for superfluidity in more complex systems. The observation of phonon-like collective excitations is a first step towards establishing superfluid behavior in atomic gases. The observation of vortex states or second sound would be a step further.

There have been numerous theoretical papers which discuss aspects of collective excitations in dilute Bose condensates (e.g.[18-22]), and there have been three experimental studies so far[23-25], one of which is presented in this chapter [23].

5.2. Theory of Collective Excitations in the Cloverleaf Trap

A trapped Bose condensate of *non-interacting* atoms can exhibit collective shape oscillations. The oscillations are due to synchronous *uncoupled* motion of single particles

and the frequencies of the modes therefore have to be multiples of the trapping frequencies. In the weakly-interacting condensate on the other hand the particles are coupled by the quantum-mechanical mean-field (see chapter 4.4) which significantly modifies the shape and the frequency of these lowest-energy condensate excitations.

In this section I will derive the properties of the collective excitations for a weakly-interacting Bose condensate in a magnetic trap. The derivation is not a general theory of collective excitations. It is aimed at understanding the physics of the low-lying excitations measured in the cloverleaf trap. I will therefore focus on "our" experimental parameters: A pure condensate in an anisotropic harmonic trapping potential with axial symmetry and a number of condensed atoms which is deeply in the Thomas Fermi limit. The following derivation similar to the analytical treatment presented by Stringari [21].

The physics of a weakly interacting condensate is governed by the non-linear Schrödinger equation (NLSE) which has been already introduced in chapter 4.4:

$$i\hbar\frac{\partial}{\partial t}\Phi(r,t)=\left(-\frac{\hbar^2\nabla^2}{2m}+U_{trap}(r)+\frac{4\pi\hbar^2 a}{m}|\Phi(r,t)|^2\right)\Phi(r,t) \qquad (5.1)$$

The non-linear term

$$\frac{4\pi\hbar^2 a}{m}|\Phi(r,t)|^2$$

accounts for the repulsive (a>0) interaction between the condensed atoms. $\Phi(r,t)$ is the macroscopic order parameter of the system and the expectation value of the density is given by

$$\rho(r,t)=|\Phi(r,t)|^2.$$

The NLSE (Eq.5.1) can be reexpressed in terms of quantum hydrodynamic equations

$$\frac{\partial}{\partial t}\rho(r,t)+\nabla(\mathbf{v}\rho)=0 \qquad (5.2)$$

$$m\frac{\partial}{\partial t}\mathbf{v}+\nabla(\delta\mu+\tfrac{1}{2}m\mathbf{v}^2)=0$$

The "velocity"-field of the condensate v(r,t) is defined as

$$\mathbf{v}(\mathbf{r},t)=\frac{\Phi^*(\mathbf{r},t)\nabla\Phi(\mathbf{r},t)-\Phi(\mathbf{r},t)\nabla\Phi^*(\mathbf{r},t)}{2im|\Phi(\mathbf{r},t)|^2} \tag{5.3}$$

and δμ is the change in the chemical potential with respect to the chemical potential μ of the ground state

$$\delta\mu=V_{ext}+\frac{4\pi\hbar^2a}{m}\rho-\frac{\hbar^2}{2m\sqrt{\rho}}\nabla^2\sqrt{\rho}-\mu \tag{5.4}$$

(The chemical potential of the ground state has been described in Eq.4.14.) The hydrodynamic equations have *exactly the same* structure as the equations governing the dynamics of superfluids at T=0 [1].

As long as we are in the Thomas-Fermi limit, where the pressure due to the kinetic energy

$$\frac{\hbar^2}{2m\sqrt{\rho}}\nabla^2\sqrt{\rho}$$

is negligible compared to the contribution of the mean field

$$\frac{4\pi\hbar^2a}{m}\rho,$$

the perturbation to the chemical potential can be simplified:

$$\delta\mu=U_{trap}+\frac{4\pi\hbar^2a}{m}\rho-\mu \tag{5.5}$$

We substitute the density distribution of the ground state (see also Eq.4.12)

$$\rho_0(\mathbf{r})=\frac{m}{4\pi\hbar^2a}\left(\mu-U_{trap}(\mathbf{r})\right) \tag{5.6}$$

into Eq.5.5 and obtain a proportionality between the perturbations to the chemical potential $\delta\mu$ and the density perturbations of the ground state distribution

$$\delta\mu = \frac{4\pi\hbar^2}{m}(\rho - \rho_0) \tag{5.7}$$

This implies that, in the Thomas-Fermi limit, collective excitations are fluctuations of the mean field, i.e. density perturbations to the ground state of the condensate. By expressing $\delta\mu$ in terms of its normal spectral components

$$\delta\mu \equiv \frac{4\pi\hbar^2}{m} e^{-i\omega t}\delta\rho(\mathbf{r}) \tag{5.8}$$

and linearizing the hydrodynamic equations in Eq. 5.2 we obtain the "wave" equation for Bose condensates at T=0 in the Thomas-Fermi regime:

$$\omega^2\delta\rho - \frac{1}{ma}\nabla\delta\rho\nabla(\mu - U_{trap}(\mathbf{r})) = 0 \tag{5.9}$$

This equation is solved for an anisotropic harmonic potential

$$U_{trap}(r,z) = \tfrac{1}{2}m\omega_r^2\left(r^2 + \omega_z^2/\omega_r^2 z^2\right). \tag{5.10}$$

In an *isotropic* harmonic potential normal modes of Eq.5.9 have a polynomial dependence along the radial direction while the angular dependence of the solutions is given by spherical harmonics Y_{lm} (l=1,2,3,.., |m|=0,1,2,..,l). "Our" *anisotropic* trapping potential on the other hand only has cylindrical symmetry. In this case $Y_{l,\pm l}$ and $Y_{l,\pm(l-1)}$ (l=1,2,3,..) are the only spherical harmonics which solve the "wave" equation. These solutions are

$$\delta\rho_{l,\pm l} = (r/R)^l Y_{l,\pm l}(\theta,\phi) \qquad (5.11)$$
$$\omega_{l,\pm l} = \sqrt{l}\omega_r$$

and

$$\delta\rho_{l,\pm(l-1)} = (r/R)^l Y_{l,\pm(l-1)}(\theta,\phi) \qquad (5.12)$$
$$\omega_{l,\pm(l-1)} = \sqrt{(l-1)\omega_r^2 + \omega_z^2}$$

where r is the renormalized radial coordinate $r=(x^2/R^2+y^2/R^2+z^2/Z^2)^{1/2}$ and 2R and 2Z give the radial and axial extend of the condensate respectively, while (r,θ,ϕ) is the spherical representation of the renormalized Cartesian coordinates (x/R,y/R,z/Z). Other excitations are given by more complicated superpositions of spherical harmonics (each multiplied by polynomials in r). For now we are only interested in the low-lying excitations, the modes with the lowest oscillation frequencies.

In order to excite a collective mode the condensate in the harmonic trap has to be temporarily deformed such that its density perturbations overlap with the perturbation associated with the mode of interest. The condensate is deformed by a brief perturbation in the trapping potential. Due to the field geometry of our trapping potential there a low lying modes which we cannot excite by simply changing the current through on of the trap coils:

Among the excitations we were able to excite and study are the modes $\delta\rho_{1,\pm1}$ and $\delta\rho_{1,0}$ .These modes oscillate with the radial and axial trapping frequencies ω_r and ω_z respectively. They are *"sloshing"* modes, center-of-mass oscillations which do not involve a deformation of the condensate density. These "sloshing" modes therefore *do not* reveal any mean-field effects. However, a measurement of these frequencies characterizes the trapping potential.

The most interesting two low-lying excitations we can observe are *"shape"* oscillations which correspond to density perturbations that are of superpositions of m=0-solutions for the isotropic case:

$$\delta\rho_{l=2,m=0} = AP_0^{(2)}(r/R) + B(r/R)^2 Y_{2,0}(\theta,\phi) \qquad (5.13)$$

$$\omega^{\pm}{}_{l=2,m=0} = \omega_r \sqrt{2 + \tfrac{1}{2}\left(\tfrac{\omega_z}{\omega_r}\right)^2 \mp \tfrac{1}{2}\sqrt{9\left(\tfrac{\omega_z}{\omega_r}\right)^4 - 16\left(\tfrac{\omega_z}{\omega_r}\right)^2 + 16}}$$

$P_0^{(2)}$ is a Legendre polynomial in r/R of order 2. Both, the *"slow"* shape oscillation and the *"fast"* oscillation, are depicted in Fig. 5.1. In case of the extreme aspect ratio of the cloverleaf trap (α~15) their respective frequencies are $\omega^+=(5/2)^{1/2}\omega_z$ and $\omega^-=2\omega_r$. The corrections due to Eq.5.13 are less than 0.1%.

Among the inaccessible modes are the $\delta\rho_{2,\pm 2}$ excitations which propagate with the frequency $2^{1/2}\omega_r$. They are *"football"* modes, which involve a compression of the condensate along an axis orthogonal to the symmetry axis. This compression axis rotates with the frequency $2^{1/2}\omega_r$ either clockwise or counter-clockwise. A superposition of both modes with equal weight results in a mode which compresses along one radial direction and extends along the orthogonal radial direction and vice versa. Fig. 5.1 depicts this mode. It was observed in the TOP trap at JILA [25].

It is important to note that the hydrodynamic equations with a structure similar to Eq. 5.2 also govern the collective modes of a trapped classical gas in the hydrodynamic regime [26, 27]. In this case, classical elastic collisions give rise to the coupling term. These equations predict surface modes which have the same dispersion relations as those for oscillations of a Bose condensate at T=0 within the Thomas-Fermi approximation. The frequency spectrum of low-lying collective excitations is therefore not a distinctive feature of Bose condensation. The existence of collective excitation of a Bose condensate is however a manifestation of the quantum mechanical mean field interaction.

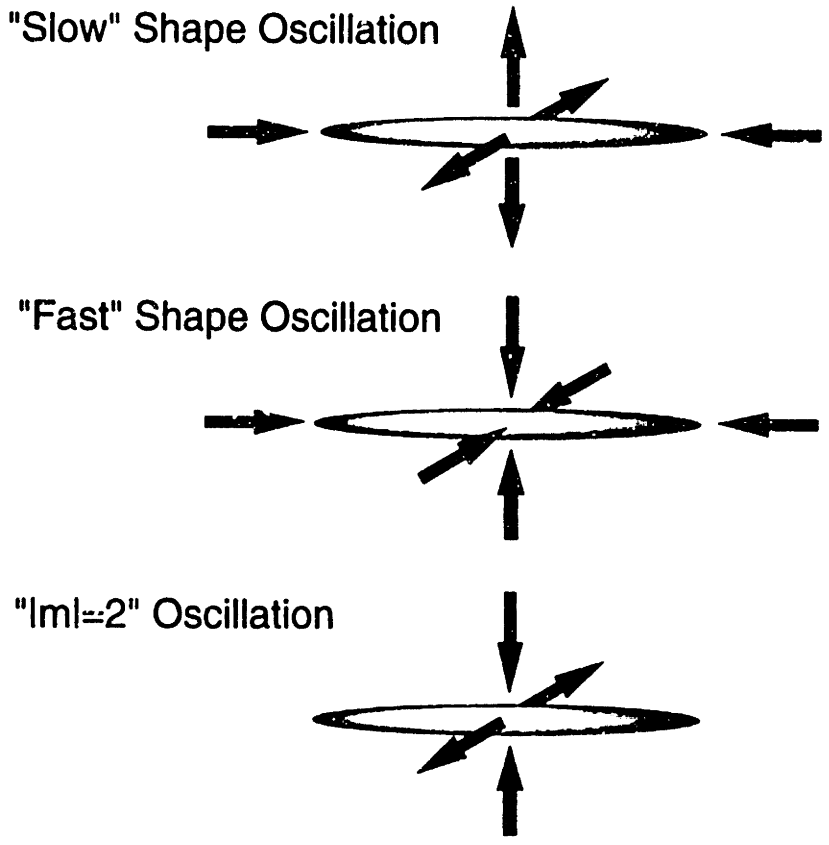

Fig. 5.1 illustrates some of the low-lying collective excitations of a condensate in the Thomas-Fermi regime at T=0 in a cylindrically symmetric anisotropic trap. The black arrows indicate the directions of compression or expansion during the oscillation. (The arrows reverse orientation twice during an oscillation period.) For the extreme aspect ratio of the cloverleaf trap the "slow" shape oscillation oscillates with $(5/2)^{1/2}$ times the axial trapping frequency, while the "fast" oscillation has twice the radial frequency. The $|m|=2$ oscillation is a superposition of two counter rotating "football" modes.

Appendix to Chapter 5

Attached is the publication which details the observation of collective excitations in weakly interaction Bose condensate. It also reports on the observation of "sound" waves in a dense ultra-cold but uncondensed trapped sample.

Collective Excitations of a Bose-Einstein Condensate in a Magnetic Trap

M.-O. Mewes, M. R. Andrews, N. J. van Druten, D. M. Kurn, D. S. Durfee, C. G. Townsend, and W. Ketterle
Department of Physics and Research Laboratory of Electronics, Massachusetts Institute of Technology, Cambridge, Massachusetts 02139
(Received 19 June 1996)

Collective excitations of a dilute Bose condensate have been observed. These excitations are analogous to phonons in superfluid helium. Bose condensates were created by evaporatively cooling magnetically trapped sodium atoms. Excitations were induced by a modulation of the trapping potential, and detected as shape oscillations in the freely expanding condensates. The frequencies of the lowest modes agreed well with theoretical predictions based on mean-field theory. Before the onset of Bose-Einstein condensation, we observed sound waves in a dense ultracold gas. [S0031-9007(96)00900-3]

PACS numbers: 03.75.Fi, 05.30.Jp, 32.80.Pj, 64.60.-i

In 1941 Landau introduced the concept of elementary excitations to explain the properties of superfluid helium [1]. This phenomenological approach, based on quantum hydrodynamics, gave a quantitative description of the thermodynamic properties and transport processes in liquid helium. Landau rejected any relation to Bose-Einstein condensation (BEC). A microscopic derivation of the elementary excitation spectrum for a weakly interacting Bose gas was given by Bogoliubov in 1947 [2] and for He II by Feynman in 1955 [3], emphasizing the role of Bose statistics [3] and reconciling Landau's approach with London's explanation of superfluidity as being due to BEC [2,4].

The elementary excitations determine the spectrum of density fluctuations in a Bose liquid, and have been directly observed in He II by neutron scattering [5]. The low-frequency excitations are phonons, long-wavelength collective modes of the superfluid. So far, a satisfactory microscopic theory for an interacting bosonic system exists only for the dilute quantum gas. The recent realization of BEC in dilute atomic vapors [6–8] has opened the door to test this theory experimentally. In this paper we report on the observation of shape oscillations of a trapped Bose condensate, modes analogous to phonons in homogeneous systems [9].

The experimental setup for creating Bose condensates was the same as in our previous work [10]. Briefly, sodium atoms were optically cooled and trapped, and transferred into a magnetic trap where they were further cooled by rf-induced evaporation [11,12]. Every 30 s, condensates containing 5×10^6 sodium atoms in the $F = 1, m_F = -1$ ground state were produced. Evaporative cooling was extended well below the transition temperature to obtain a condensate without a discernible normal component. The condensate was confined in a cloverleaf magnetic trap which had cylindrical symmetry with trapping frequencies of 19 Hz axially and 250 Hz radially (see below). The trapping potential is determined by the axial curvature of the magnetic field $B'' = 125\ \mathrm{G\,cm^{-2}}$, the radial gradient $B' = 150\ \mathrm{G\,cm^{-1}}$, and the bias field $B_0 = 1.2$ G.

The condensate was excited by a time-dependent modulation of the trapping potential. First, we used a sudden step in the gradient B' to identify several collective modes of the condensate and to find their approximate frequencies. B' was decreased by 15% for a duration of 5 ms with a transition time of about 1 ms, and then returned to its original value. A variable time delay was introduced between the excitation and the observation of the cloud. In this way, we strobed the free time evolution of the system after the excitation. The cloud was observed by absorption imaging after a sudden switch off of the magnetic trap and 40 ms of ballistic expansion. No trap loss was observed during the interval over which the delay was varied. The images were similar to the series shown in Fig. 1. Four modes were identified from the measured center-of-mass positions and the widths of the condensate. The radial and axial center-of-mass oscillations (dipole modes) were excited because a change in B' displaced the center of the trap slightly due to asymmetries in the field-producing coils. A fast shape oscillation predominantly showed up as a sinusoidal modulation of the radial width while a slow sinusoidal shape oscillation was observed in the axial width. When a strong parametric drive (see below) was used to excite the slow shape oscillation, a weak oscillation of the radial width was also detected. Note that the widths were observed after ballistic expansion and reflect a convolution of the initial spatial and velocity

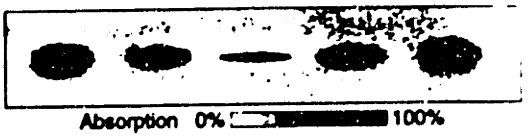

FIG. 1. Shape oscillation of a Bose-Einstein condensate. After excitation the condensate was allowed to freely oscillate in the trap for a variable time, ranging from 16 ms (left) to 48 ms (right). The absorption images were taken after a sudden switch-off of the trapping potential and 40 ms of ballistic expansion. The horizontal width of each cloud is 1.2 mm.

 0031-9007/96/77(6)/988(4)$10.00

distributions, further complicated by the acceleration due to the repulsive mean field.

From these "kicked" excitation experiments, we determined $\nu_\rho = 250(5)$ Hz [13] for the radial trapping frequency and $\nu = 510(15)$ Hz for the faster shape oscillation. The slower shape oscillation was studied further in the following manner. A better "mode selectivity" in the excitation was obtained by modulating B'' at 30 Hz sinusoidally for five full cycles. The amplitude of the parametric drive was varied between 0.5% and 6% of the dc field strength. Axial and radial widths of the cloud were then determined as a function of delay time. The axial widths were fitted with an exponentially decaying sine function. For the smallest drive an improved fit was obtained by fitting the aspect ratio of the cloud instead of the width itself (Fig. 2); this procedure eliminated the effect of fluctuations of the number N_0 of condensed atoms, which were about 20%. Note that in the hydrodynamic limit the frequencies of the normal modes are independent of N_0 (see below). The amplitudes of the axial width modulation Δw_z, after a time Δt of ballistic expansion, varied from 77.8 for the smallest drive to 527 μm for the largest drive. From $\Delta w_z/(2\Delta t)$ we obtained an upper bound for the kinetic energy of the collective mode, which ranged from 1.3 to 60 nK. The highest value is comparable to the typical mean-field energy per atom in our experiment [10]. It is, therefore, remarkable that the frequency of the collective excitation was found not to depend on the strength of the drive (Fig. 3). For the smallest amplitudes, the frequency was determined to be 30.0(2) Hz which will be compared below to a theoretical prediction for small oscillations. An accurate value of 19.28(11) Hz for the axial trapping frequency was obtained by using a five-cycle sinusoidal modulation of B' at 18 Hz. In this way, the simultaneous excitation of the radial dipole mode at 250 Hz was suppressed.

We first discuss the nature of the shape oscillations for a noninteracting gas and a weakly interacting condensate in the simplest case of an isotropic harmonic potential. For a noninteracting ideal gas (both in the normal and in the Bose-condensed states), all modes have frequencies which are integer multiples of the harmonic trapping frequency ν_0. In particular, the lowest quadrupole oscillation occurs at a frequency of $2\nu_0$. In a homogeneous weakly interacting Bose condensate of density n_0, the lowest frequency excitations are phonons propagating at the speed of sound $c = \sqrt{n_0 U/m}$ at $T = 0$ [2,14]. $U = 4\pi\hbar^2 a/m$ characterizes the interactions of bosons with mass m and scattering length a. In a sample of size d, the lowest frequency ν of a phonon is obtained from the dispersion relation $\nu = c/\lambda$ with $\lambda = 2d$. In the Thomas-Fermi approximation the condensate wave function is nonvanishing over a size $d = (1/\pi\nu_0)\sqrt{2n_0 U/m}$ [14,15] resulting in $\nu = (\pi/2^{3/2})\nu_0$. For an inhomogeneous condensate this result is only an estimate, but it correctly shows that the lowest excitation frequencies are proportional to ν_0. These frequencies should be independent of the number of atoms N_0 in the condensate since the dependences of the sound velocity and of the size of the condensate on N_0 exactly cancel.

The normal modes of the inhomogeneous interacting condensate are obtained by solving the corresponding wave equation which is the nonlinear Schrödinger equation, as recently discussed by several groups [5,14, 16–21]. Stringari presented the analytical solution for an isotropic harmonic potential in the Thomas-Fermi regime which gave $\sqrt{2}\,\nu_0$ as the frequency of the lowest normal mode, aside from the center-of-mass oscillation [16]. The normal modes of the condensate are classified by quantum numbers (n, l, m) where n is the radial quantum number and l, m denote quantum numbers for the total angular momentum and its axial projection,

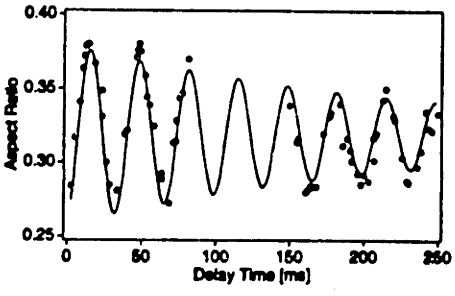

FIG. 2. Analysis of the "quadrupole" oscillation at 30 Hz. The aspect ratio of the expanding cloud is plotted against the free oscillation time between excitation and switch off of the trap. Damping of the harmonic oscillations was observed with a decay time of 250 ms. Note that the analagous mode in the non-interacting ideal gas occurs at $2\nu_z = 38.6$ Hz.

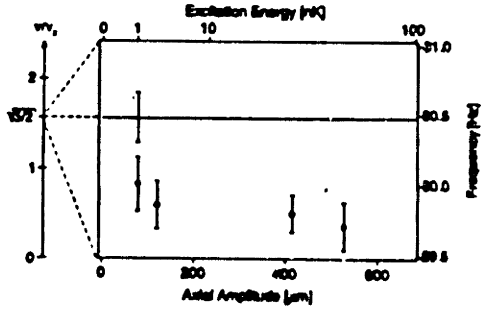

FIG. 3. Frequency of the collective excitation at 30 Hz as a function of driving amplitude. The abscissa shows the amplitude of the axial width modulation after 40 ms of ballistic expansion, which is used to estimate the excitation energy. The solid line is the theoretical prediction of Stringari [16] when combined with the measured axial trapping frequency.

respectively. For cylindrical symmetry (as in our trap), m is still a good quantum number, but l is not. Thus, the normal modes are superpositions of wave functions with the same m. Since our excitation scheme preserves the axial symmetry of the trapping potential, we expect to observe only $m = 0$ modes. (However, the excitation of the dipole modes shows that slight asymmetries in the trapping coils also excite $m = 1$ modes.) Stringari discussed an anisotropic harmonic potential with axial symmetry in the Thomas-Fermi limit [16]. He showed that the lowest $m = 0$ modes are coupled excitations of (0,2,0) (which is a quadrupolar surface oscillation) and (1,0,0) symmetries. For a cigar-shaped condensate with a large aspect ratio, these lowest modes were predicted at frequencies $\sqrt{5/2}\,\nu_z$ and $2\nu_\rho$, where ν_z and ν_ρ are the axial and radial trapping frequencies, respectively [16,22].

The observed ratio $\nu/\nu_z = 1.556(14)$ is in good agreement with the predicted ratio of $\sqrt{5/2} = 1.581$. It is the main result of the present paper and should be regarded as a critical quantitative test of the mean-field theory describing excited states of a Bose condensate. The fast collective excitation which was observed is probably the high frequency mode of the mixed (0,2,0) and (1,0,0) excitations for which a frequency of $2\nu_\rho$ was predicted [16], in good agreement with our measurement of $2.04(6)\nu_\rho$. Note that a noninteracting condensate also has a mode at $2\nu_\rho$.

The solutions of the linearized Gross-Pitaevskii equation are the normal modes of the condensate, also called the elementary excitations or quasiparticles of the macroscopic quantum system [5,19]. The collective excitations which we have observed, such as in Fig. 1, are large-scale density fluctuations which obey the hydrodynamic equation for superfluid flow at zero temperature [5,16]. They are a coherent excitation of many quasiparticles at the frequency of the normal mode. The lifetime of the quasiparticles can thus be determined from the damping of the shape oscillations.

Damping may be caused either by interactions between collective and thermal excitations, or by nonlinear interactions which couple the normal modes of the condensate [20]. For a nearly pure condensate ($T \approx 0$), the damping due to thermal excitations should be negligible. In our experiment, we observed a damping time of 250(40) ms for the collective excitation at 30 Hz (Fig. 2). So far there is no theoretical prediction for the damping of collective excitations of a trapped condensate.

Similar excitation experiments were performed on a thermal cloud at $T/T_c \approx 2$. For an ideal gas at low density one expects quadrupole oscillations at $2\nu_0$, the damping of which is described by a Q factor given by $Q = \pi\tau\nu \sim l/d$, where d is the size of the sample, l is the mean-free path between elastic collisions, and τ is the amplitude damping time. Our experiments were carried out at a density of 10^{14} cm^{-3} and an axial rms sample length of 300 μm. Using our recent determination of the cross section for elastic collisions of 6×10^{-12} cm^2 [11], we obtain 4 kHz for the elastic collision rate in the center of the cloud, and 12 μm for the mean-free path, much shorter than the size of the cloud. We are therefore well in the hydrodynamic regime, where the normal modes of the cloud are sound waves. One can estimate the frequency ν of the lowest mode from the speed of sound which is $c = \sqrt{5k_BT/3m}$ for a monatomic ideal gas, and the rms diameter d of the thermal cloud $d = (1/\pi\nu_0)\sqrt{k_BT/m}$. These give a lowest mode frequency of $\nu = c/2d \approx 2\nu_0$. This estimate agrees coincidentally with the frequency obtained in the collisionless regime. Damping in a classical gas is due to thermal conduction and shear viscosity, with each mechanism contributing almost equally for an ideal gas [23]. From the kinetic theory of gases we obtain the Q factor for a sound wave of wavelength λ as $Q = \pi\tau\nu \approx (1/2\pi)\lambda/l$. The damping therefore decreases with increasing density in the hydrodynamic regime, in contrast to the behavior at low density. For our experimental conditions this estimate gives an amplitude damping time of about 100 ms. Our measurements on a thermal cloud are in agreement with these predictions. We observed oscillations in the axial width at a frequency of 35(4) Hz $= 1.8(2)\nu_z$ and a damping time of about 80 ms, much longer than the collision time.

Theoretical discussions of collective excitations of a condensate have emphasized that the frequency shift of the normal modes compared to the uncondensed atoms is clear evidence for the order parameter associated with BEC [19]. We point out that the normal modes of dense clouds can show frequency shifts even above T_C, due to the hydrodynamic propagation of sound waves. It will be interesting to study the behavior of such shifts across the BEC phase transition. For the accurate comparison to theory we have normalized the frequencies of the condensate with the center-of-mass oscillation frequencies which are unshifted and identical to the single-particle trapping frequencies.

The results reported above were all obtained at small and medium drive amplitudes. At larger amplitude, we observed striations in the time-of-flight pictures of Bose condensates parallel to the radial direction. We conjecture that these interferencelike structures are the self-diffraction of an excited macroscopic matter wave and might reflect the nodal structure of a strongly driven condensate.

This paper is only the first step of a systematic study of the elementary excitations of a Bose condensate. The ultimate goal is a complete survey of the spectrum of collective excitations, including the lifetimes of the quasiparticles and the behavior at different temperatures and higher excitation energies. For excitation frequencies larger than the mean interaction energy (typically 2 kHz or 100 nK in our samples) one expects a transition from collective to single-particle behavior [5]. One limitation of the current experiment is that the

time-of-flight probing technique is intrinsically destructive. We have recently demonstrated dispersive imaging as a nondestructive technique to spatially resolve Bose condensates [24]. Combining this technique with a high-speed camera should enable us to observe collective modes of a Bose condensate *in situ* and in real time.

The authors are grateful to S. Stringari for helpful discussions. This work was supported by ONR, NSF, and JSEP. D. M. K. would like to acknowledge support from an NSF Graduate Research Fellowship, N. J. v. D. from "Nederlandse Organisatie voor Wetenschappelijk Onderzoek (NWO)" and NACEE (Fulbright fellowship), and C. G. T. from a NATO Science Fellowship.

[1] L. D. Landau, J. Phys. (Moscow) **5**, 71 (1941).
[2] C. N. Bogoliubov, J. Phys. (Moscow) **11**, 23 (1947).
[3] R. P. Feynman, in *Progress in Low Temperature Physics*, edited by C. J. Gorter (North-Holland, Amsterdam, 1955), Vol. 1, p. 17.
[4] F. London, Nature (London) **141**, 643 (1938).
[5] P. Nozieres and D. Pines, *The Theory of Quantum Liquids* (Addison-Wesley, Redwood City, CA, 1990), Vol. 2.
[6] M. H. Anderson *et al.*, Science **269**, 198 (1995).
[7] C. C. Bradley *et al.*, Phys. Rev. Lett. **75**, 1687 (1995). Note that some results of this paper have been corrected (R. Hulet, presented at the DAMOP meeting in Ann Arbor, MI, 1996).
[8] K. B. Davis *et al.*, Phys. Rev. Lett. **75**, 3969 (1995).
[9] First results of this study were presented at the DAMOP meeting in Ann Arbor, MI, 1996. At the same meeting the JILA group gave a report on unsubmitted related work. See D. S. Jin *et al.*, Phys. Rev. Lett. **77**, 420 (1996).
[10] M.-O. Mewes *et al.*, Phys. Rev. Lett. **77**, 416 (1996).
[11] K. B. Davis *et al.*, Phys. Rev. Lett. **74**, 5202 (1995).
[12] W. Ketterle and N. J. van Druten, in Advances in Atomic, Molecular and Optical Physics, edited by B. Bederson and H. Walther (to be published), Vol. 37, and references therein.
[13] All quoted experimental uncertainties in this paper correspond to 1 standard deviation in the fit.
[14] G. Baym and C. J. Pethick, Phys. Rev. Lett. **76**, 6 (1996).
[15] V. V. Goldman, I. F. Silvera, and A. J. Leggett, Phys. Rev. B **24**, 2870 (1981).
[16] S. Stringari, Report No. cond. mat. 9603126 (to be published).
[17] L. You *et al.* (to be published).
[18] A. L. Fetter, Phys. Rev. A **53**, 4245 (1996).
[19] M. Edwards *et al.* (to be published).
[20] P. A. Ruprecht *et al.*, Phys. Rev. A **51**, 4704 (1995).
[21] M. Marinescu and A. F. Starace (to be published).
[22] This prediction for $\nu_\rho/\nu_z \to \infty$ is good to 10^{-3} accuracy for $\nu_\rho/\nu_z = 13$.
[23] P. M. Morse and K. U. Ingard, *Theoretical Acoustics* (Princeton University Press, Princeton, NJ, 1986).
[24] M. R. Andrews *et al.*, Science **273**, 84 (1996).

Supplement to Chapter 5: A Strongly Excited Condensate

For large drives we recorded striations in the time of flight pictures which are parallel to the radial direction of the trap, as shown in Fig.5.2.

We observed the striations with about $2x10^6$ condensed atoms. The condensate was stored in the axially symmetric potential of the cloverleaf trap with an axial trapping frequency of 21Hz and a radial trapping frequency of 310 Hz. We instantaneously lowered the radial trapping frequency to 230 Hz for 0.5 ms and then switched back to the original confinement for 15 ms. Then we completely switched off the trap instantaneously and observed the falling cloud after 75 ms time-of-flight through absorption imaging.

These patterns might be due to self interference of the expanding matter waves which reflects the nodal structure of a strongly driven condensate. This is a tentative explanation as of yet and no theoretical description for this phenomenon has been developed so far.

Fig. 5.2 Ballistic expansion of a strongly driven condensate. The time-of-flight image shows high contrast striations. The image was taken after 75 ms of ballistic expansion and has a horizontal width of 3 mm.

References in Chapter 5

1 P. Nozières and D. Pines, *The theory of quantum liquids* (Addison-Wesley, Redwood City, CA, 1990).

2 A. Griffin, D. W. Snoke, and S. Stringari, *Bose-Einstein Condensation* (Cambridge University Press, Cambridge, 1995).

3 K. Huang, in *Bose-Einstein Condensation*, edited by A. Griffin, D. W. Snoke and S. Stringari (Cambridge University Press, Cambridge, 1995), p. 31-50.

4 F. London, Nature **141**, 643 (1938).

5 A. Einstein, Sitzungsberichte der preussischen Akademie der Wissenschaften, Bericht 3 , 18-25 (1925).

6 L. D. Landau, J. Phys. (USSR) **5**, 71 (1941).

7 L. Tisza, Nature **141**, 913 (1938).

8 N. N. Bogoliubov, J. Phys. (USSR) **11**, 23 (1947).

9 D. Pines, Physics Today, February 1989, p.61-66.

10 R. P. Feynman, in *Progress in Low Temperature Physics*, edited by C. J. Gorter (North-Holland, Amsterdam, 1955), Vol. 1, p. 17.

11 M. H. Anderson, J. R. Ensher, M. R. Matthews, *et al.*, Science **269**, 198-210 (1995).

12 K. B. Davis, M.-O. Mewes, M. R. Andrews, *et al.*, Physical Review Letters **75**, 3969 (1995).

13 M.-O. Mewes, M. R. Andrews, N. J. van Druten, *et al.*, Physical Review Letters **77**, 416-419 (1996).

14 J. R. Ensher, D. S. Jin, M. R. Matthews, *et al.*, preprint (1996).

15 P. E. Sokol, in *Bose-Einstein Condensation*, edited by A. Griffin, D. W. Snoke and S. Stringari (Cambridge University Press, Cambridge, 1995), p. 51-85.

16 J. L. Lin and J. P. Wolfe, Physical Review Letters **71**, 1222 (1993).

17 C. C. Bradley, C. A. Sackett, and R. G. Hulet, preprint (1996).

18 M. Edwards, P. A. Ruprecht, K. Burnett, *et al.*, preprint (1996).

19 M. Edwards, P. A. Ruprecht, K. Burnett, *et al.*, preprint (1996).

20 P. A. Ruprecht, M. Edwards, K. Burnett, *et al.*, preprint (1996).

21 S. Stringari, Physical Review Letters **77**, 2360 (1996).

22 L. You, W. Hoston, M. Lewenstein, *et al.*, preprint (1996).

23 M.-O. Mewes, M. R. Andrews, N. J. van Druten, *et al.*, Physical Review Letters (1996).

24 D. S. Jin, J. R. Ensher, M. R. Matthews, *et al.*, preprint (1996).

25 D. S. Jin, J. R. Ensher, M. R. Matthews, *et al.*, Physical Review Letters 77, 420 (1996).

26 Y. Kagan, E. L. Surkov, and G. V. Shlyapnikov, preprint (1996).

27 A. Griffin, W.-C. Wu, and S. Stringari, preprint (1996).

6. AN OUTPUT COUPLER FOR BOSE CONDENSED ATOMS

6.1 Introduction

There has been a lot of theoretical and experimental interest in bright sources of atoms with a very narrow energy spread. The quest for such sources is driving atom cooling and trapping research. A promising concept is the atom-optical equivalent of the laser, a source of *coherent, spectrally pure* matter waves [1][1-4]. Such a "laser-like" source of atoms, a striking example for the intrinsic wave nature of matter, would be an ideal object for fundamental tests of quantum theory and the interactions of coherent atoms with a radiation field. As a superior source of monochromatic atoms it might have significant impact on atom optics similar as the laser changed optics and spectroscopy. Diffraction limited atomic beams might push atom lithography to new limits.

One could define a laser-like source by the key elements and mechanisms that lead to the emission of a laser-like particle beam. According to [1] a laser consists of three elements: A cavity allowing the build-up of radiative energy in a cavity mode, an irreversible pumping and gain process through which photons can accumulate in this mode, and an output mechanism enabling the controlled extraction of coherent light from the cavity and allowing for above threshold operation[2].

The equivalent to the optical cavity in the recent BEC experiments [5-9] is the magnetic trapping potential, in which the sample of atoms is confined and evaporatively cooled. The pumping process is rather complex: Bosonic atoms are loaded into the magnetic trap from an incoherent laser-cooled source. The atoms are further cooled by evaporation to a temperature right above Bose-Einstein transition temperature T_c. The energy distribution is then truncated such that the average energy per particle corresponds

[1] The idea of the atom "laser" is an adaptation of the quantum optical formalism for the laser to atoms. Despite many publications, there is no seminal reference on the subject.

[2] Wiseman's definition only applies to a cw source. We use a more general definition and also include pulsed lasers: In *pulsed operation* the output coupler should permit a cavity finesse such that radiative energy can build up in the lasing mode between pulses.

to a temperature *below* T_c. This non-equilibrium situation is the analog to the *inversion* in a laser. Thermal equilibration through elastic collisions and quantum statistics *stimulate* atoms into the ground state of the system: This is the *gain* mechanism. The last missing element is the analog of a partially transmissive mirror which enables us to couple atoms coherently out of the ground state.

A more functional definition of a laser-like atomic beam was suggested by Eric Cornell [10]: An atom -"laser" could be realized by an atomic Bose condensate in combination with a device which coherently removes atoms from the condensate "little by little" such that a quasi-continuous beam results. Since the outcoupled atoms are coherent, it would imply that the beam is coherent on a scale much larger than the size of the cavity, i.e. the trapped condensate.

Both definitions suggest that, in order to turn a Bose condensate of magnetically trapped atoms into a laser-like particle source, two steps are essential:

1) An extraction mechanism has to be implemented, which acts on the condensate just like an optical beamsplitter acts on light: It couples an adjustable fraction of the coherent condensate atoms into a coherent untrapped state without affecting the coherence or the phase of the condensate.
2) One has to establish proof for the coherent properties of the extracted atoms. This can be done by recording the interference of pulses released from different condensates.

One of the goals of the research in our group is to experimentally realize these steps. In this chapter, I will present an output coupler for condensed "single mode" atoms, based on the interaction of the condensate with an rf field. Atoms were extracted by coupling the condensed atoms into a superposition of trapped and untrapped hyperfine states. A similar process is employed for rf induced evaporation [11]. This method should allow us to create coherent pulses of atoms from a condensate.

6.2 Theory

6.2.1 A Simple Model for Two-Level Atoms

We first discuss the basic principle of the atomic output coupler and therefore consider a Bose condensate of non-interacting two-level atoms in a trap. The internal states of each atom are labeled $|1\rangle$ and $|2\rangle$ respectively. State $|1\rangle$ is confined while the other state $|2\rangle$ is expelled. A resonant rf pulse of frequency ω_0 and duration τ couples the two states. The coupling matrix element in the interaction picture is given by $\omega_R/2$. The trap frequency and the variation of the two level resonance over the size of the condensate are negligible compared to $1/\tau$ which makes the rf coupling position independent. During the interaction the initially confined particle oscillates between the trapped and untrapped state with the Rabi frequency ω_R. It evolves from the trapped state $|1\rangle$ into the superposition $t|1\rangle+r|2\rangle$ with the coefficients

$$\begin{aligned} r &= \sin(\tfrac{1}{2}\omega_R\tau) \\ t &= \sqrt{1-r^2} = \cos(\tfrac{1}{2}\omega_R\tau). \end{aligned} \tag{6.1}$$

The wave function of a condensate with N atoms is then given by the symmetric product

$$(t|1\rangle + r|2\rangle)^N = \sum_{n=0}^{N} \sqrt{\frac{N!}{n!(N-n)!}} r^n t^{N-n} |N-n\rangle \otimes |n\rangle \tag{6.2}$$

where $|N-n\rangle \otimes |n\rangle$ is an number state with N-n trapped and n untrapped atoms. The fraction of atoms coupled out of the condensate oscillates with the single-particle Rabi frequency ω_R

$$\frac{\langle n\rangle}{N} = r^2 = \sin^2(\tfrac{1}{2}\omega_R\tau) \tag{6.3}$$

while its relative rms fluctuations are given by

$$\frac{\sqrt{\langle \Delta n^2 \rangle}}{\langle n \rangle} = \sqrt{\frac{1}{\langle n \rangle} - \frac{1}{N}}. \tag{6.4}$$

An alternative output coupler for atoms is a non-adiabatic sweep of the rf through resonance. If the sweep range is much greater than the variation $\Delta\omega_0$ of the resonance frequency over the size of the condensate and the sweep rate $d\omega_{rf}/dt$ is larger than $\frac{1}{2\pi}\omega_0\Delta\omega_0$, the coupling is again position independent. The sweep, like the rf pulse, puts an initially trapped atom into the superposition $t|1> + r|2>$ with

$$\begin{aligned} |t|^2 &= e^{-2\pi\Gamma} \\ |r|^2 &= 1 - e^{-2\pi\Gamma}. \end{aligned} \tag{6.5}$$

The Landau-Zener parameter Γ is given by [12]

$$\Gamma = \frac{\omega_R^{\,2}}{4\frac{d\omega_{rf}}{dt}}. \tag{6.6}$$

Equ.(6.2)-(6.4) describe the effects of the sweep on the condensate and the untrapped fraction

$$\frac{\langle n \rangle}{N} = \left(1 - e^{-2\pi\Gamma}\right) \tag{6.7}$$

can be varied by adjusting Γ. In the adiabatic case, i.e. $\Gamma >> 1$, the whole condensate is coupled out. In contrast to the rf pulse coupler, the extracted fraction is not affected by drifts in the resonance $\Delta\omega_{drift}$ due to slow fluctuations of the trapping potential, provided we sweep over a range much larger than $\Delta\omega_{drift}$

6.2.2 Optical Analogies

The rf based output coupler is the exact atomic analog to a beamsplitter in optics (Fig.6.1).

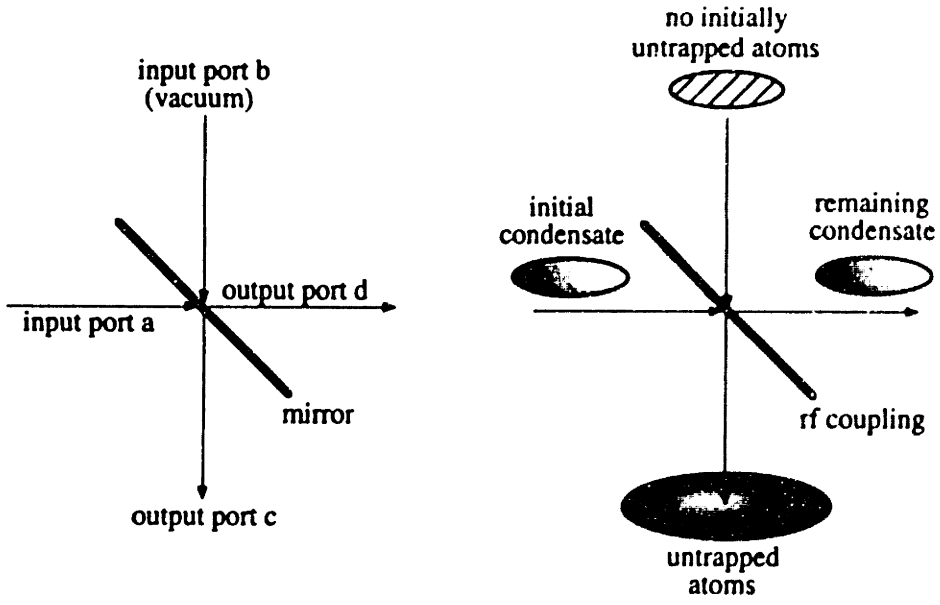

Fig. 6.1 Analogy between a beam splitter for light (left) and an output coupler for Bose condensed atoms (right).

We can understand the close analogy between atoms and photons better, if we make use of annihilation and creation operators for the input port and output port modes of the optical beamsplitter: The Hamiltonian of the uncoupled photon modes is

$$H = \tfrac{1}{2}\hbar\omega_0(a^+a + aa^+ + b^+b + bb^+ + c^+c + cc^+ + d^+d + dd^+) \tag{6.8}$$

a,a^+ and b,b^+ are the creation and annihilation operators for photons in the two "input" modes, while c,c^+ and d,d^+ annihilate and create photons in the two "output" modes. The creation operators are proportional to the electric field operators for these modes. The beam splitter connects the fields a,b for the "input" modes to the "output " mode operators c,d with a unitary transformation

$$\begin{pmatrix} a \\ b \end{pmatrix} = \begin{pmatrix} r & t \\ -t & r \end{pmatrix}\begin{pmatrix} c \\ d \end{pmatrix} \quad . \tag{6.9}$$

t in this case is the transmission of the mirror, while r represents its reflectivity. The mirror is non-absorptive, i.e. $|r|^2 + |t|^2 = 1$.

A Fock state of N photons in mode a and no photons in mode b

$$|N\rangle\otimes|0\rangle_{input}=\frac{a^{+N}}{\sqrt{N!}}|0\rangle\otimes|0\rangle_{input} \tag{6.10}$$

is coupled to state

$$\begin{aligned}&\frac{(rc^{+}+td^{+})^{N}}{\sqrt{N!}}|0\rangle\otimes|0\rangle_{output}\\&=\sum_{n=0}^{N}\sqrt{\frac{N!}{n!(N-n)!}}r^{n}t^{N-n}|N-n\rangle\otimes|n\rangle_{output}\end{aligned} \tag{6.11}$$

A state similar to this state was previously obtained in Eq.6.2 for Bose condensed atoms. The states $|p\rangle\otimes|q\rangle_{input(output)}$ denote number states with p photons in the input mode a (output mode b) and q photons in mode c (d) respectively.

The physics of the two-level atomic output coupler and the four-port beam splitter is consequently analogous. As in optics, a condensate, which is initially in a "classical" coherent state $|\alpha>$, remains in a coherent state $|t\alpha>$ (with a "field" amplitude attenuated by a factor t) while the outcoupled pulse of atoms will also be a coherent state $|r\alpha>$:

$$|\alpha\rangle\xrightarrow{\eta}|t\alpha\rangle\otimes|r\alpha\rangle \tag{6.12}$$

Since the outcome factorizes into coherent states of trapped and untrapped atoms, a subsequent measurement of the trapped fraction does *not* affect the quantum state of the outcoupled pulse. The phase imposed on the pulse by the condensate before the rf interaction remains preserved. It should therefore be possible to consecutively launch multiple pulses in a state of definite phase from the same initially coherent condensate and have them interfere with each other or even with coherent pulses launched from other condensates of the same boson. The rf based output coupler could therefore realize a pulsed atom- laser.

On the other hand, if the condensate is initially *not* in a coherent state, but for example in a pure number-state (Fock state), then the extracted pulse of atoms is

entangled with the remainder in the trap as shown in Eq.(6.2). Any measurement performed on the trapped fraction also affects the state of the outcoupled atoms. Therefore, if we only perform a measurement on the outcoupled fraction , we perform a trace with a statistical operator over the reservoir and the outcoupled pulse will just be a *statistical* ensemble of atoms.

6.2.3 Magnetically trapped sodium atoms

We now apply the formalism derived for a two-level system in sections 6.2.1 and 6.2.2 to Bose condensed sodium atoms that are magnetically confined in the $F=1,m_F=-1$ groundstate. F and m_F are the quantum numbers of the total angular momentum and its projection onto the local magnetic field respectively. An rf field couples the trapped state $|-1\rangle$ with the untrapped $F=1,m_F=0$ level $|0\rangle$ and the latter with the magnetically repelled $F=1,m_F=1$ state $|1\rangle$. The physics of such a spin 1 system is similar to the two level picture presented in 6.2.1. After the rf coupling an initially trapped atom will have evolved into a superposition $t|-1\rangle + r_1|0\rangle + r_2|1\rangle$ where the coefficients t, r_1 and r_2 are determined by the specific interaction with the rf field. The energy of the three m_F substates in a local magnetic field B_0 is given by $m_F g_L B_0 h$ to first order in B_0. $g_L B_0$ is the Lamor frequency of a trapped sodium atom. An rf field that couples the $m_F=-1$ and $m_F=0$ levels resonantly is consequently also resonant with the $m_F=0 \rightarrow m_F=1$ transition. The condensate of N atoms after the interaction can be again described by the symmetric product of the single particle wave functions similar to Eq.6.1

$$\left(t|-1\rangle + r_1|0\rangle + r_2|1\rangle\right)^N = \sum_{n=0}^{N}\sum_{m=0}^{N-n}\sqrt{\frac{N!}{n!m!(N-n-m)!}}r_1^n r_2^m t^{N-n-m}|N-n-m\rangle\otimes|n\rangle\otimes|m\rangle \qquad (6.?)$$

$|N-n-m\rangle\otimes|n\rangle\otimes|m\rangle$ is a number state with n and m atoms coupled into the untrapped $m_F=0$ and $m_F=1$ states respectively, while N-n-m atoms remain confined. For the resonant

case the coupling matrix element in the interaction picture is $\hbar\frac{\omega_R}{\sqrt{2}}$[3]. A short resonant rf pulse of duration τ gives

$$\begin{aligned} t &= \cos^2\omega_R\tau/2, \\ r_1 &= i/2^{1/2}\sin\omega_R\tau, \\ r_2 &= -\sin^2\omega_R\tau/2 \end{aligned} \tag{6.14}$$

while the coefficients for a non-adiabatic rf sweep have been calculated numerically [13] and can be approximated to better then 0.1% by the formulas

$$\begin{aligned} |t|^2 &= e^{-2\pi\Gamma}, \\ |r_1|^2 &= 2e^{-\pi\Gamma}(1-e^{-\pi\Gamma}), \\ |r_2|^2 &= (1-e^{-\pi\Gamma})^2 \end{aligned} \tag{6.15}$$

The Landau-Zener parameter Γ for the Spin 1 system is given by

$$\Gamma = \frac{\omega_R^2}{2\frac{d\omega_0}{dt}}. \tag{6.16}$$

The rf pulse duration τ as well as the range and the rate $d\omega_f/dt$ of the rf sweep should satisfy the conditions for position independent coupling discussed in the two-level case. The average number of atoms coupled into the m_F=0 state and the m_F=1 state are given by

$$\begin{aligned} \langle n\rangle &= N|r_1|^2, \\ \langle m\rangle &= N|r_2|^2 \end{aligned} \tag{6.17}$$

Hence, in case of the rf pulse the population is periodically transferred between the trapped m_F=-1 state and the magnetically expelled m_F=1 state with the Rabi frequency ω_R

[3] ω_R was chosen such, that it describes the frequency with which the system oscillates between the states |-1> and |1> if a Rabi pulse is applied.

while the m_F=0 occupation oscillates between 0 and 50% with $2\omega_R$. The rf coupler for condensates of spin 1 atoms also has an optical equivalent just like in the two-level atom picture. The corresponding optical element is a six-port beamsplitter [14] with three input and three output ports as shown in Fig. 6.2. Two of the three input ports couple to the vacuum.

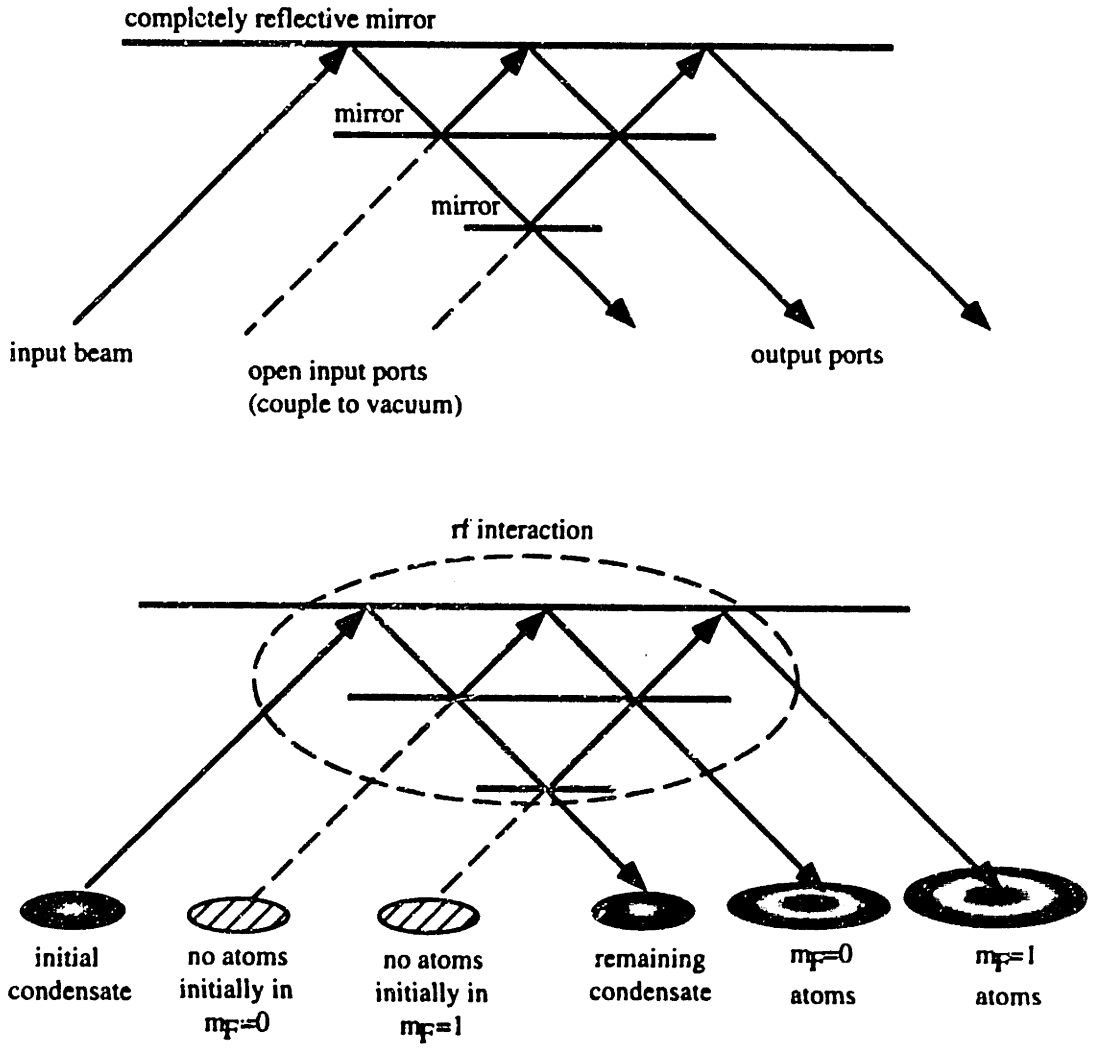

Fig.6.2 The analogy between a 6-port beam splitter for light (top) and the rf output coupler for a condensate of spin-1 atoms (bottom).

6.3 The experiment

The rf output coupler experiment and its results are thoroughly discussed in the manuscript "An output coupler for Bose condensed atoms" in the appendix of this chapter. This section is complementary to the paper. It illustrates the evolution of a condensate which was coupled into a superposition of all three F=1 hyperfine states in a magnetic trap.

A magnetically confined condensate of sodium atoms in the F=1, m_F=-1 ground state was subject to an rf sweep. The rf sweep parameters were chosen such that the sweep produced a condensate of atoms in a superposition of all three F=1 hyperfine states. This multi-particle state evolved in the magnetic trapping field for an adjustable delay time. By recording absorption images for different delay times we were able to study how the pulse of different hyperfine states evolved in the presence of the magnetic field.

The initially confined F=1, m_F=-1 state and the expelled F=1, m_F=1 ground state both experience a linear Zeeman shift in the presence of a magnetic field. m_F=-1 atoms remain trapped in the trapping potential. m_F=1 atoms evolve in the inverted (and therefore repulsive) potential. In contrast, the m_F=0 state only experiences a very weak quadratic Zeeman shift of -1.3kHz/G^2. This results in an only slightly repulsive magnetic potential: For typical trap parameters (B'=170G/cm), about 1.5 mm away from the trap center (in the radial direction) the m_F=0 atoms experience a repulsive force which is 10 times weaker than the radial force experienced by the m_F=1 atoms. Fig 6.3 shows a time sequence of the pulse evolution.

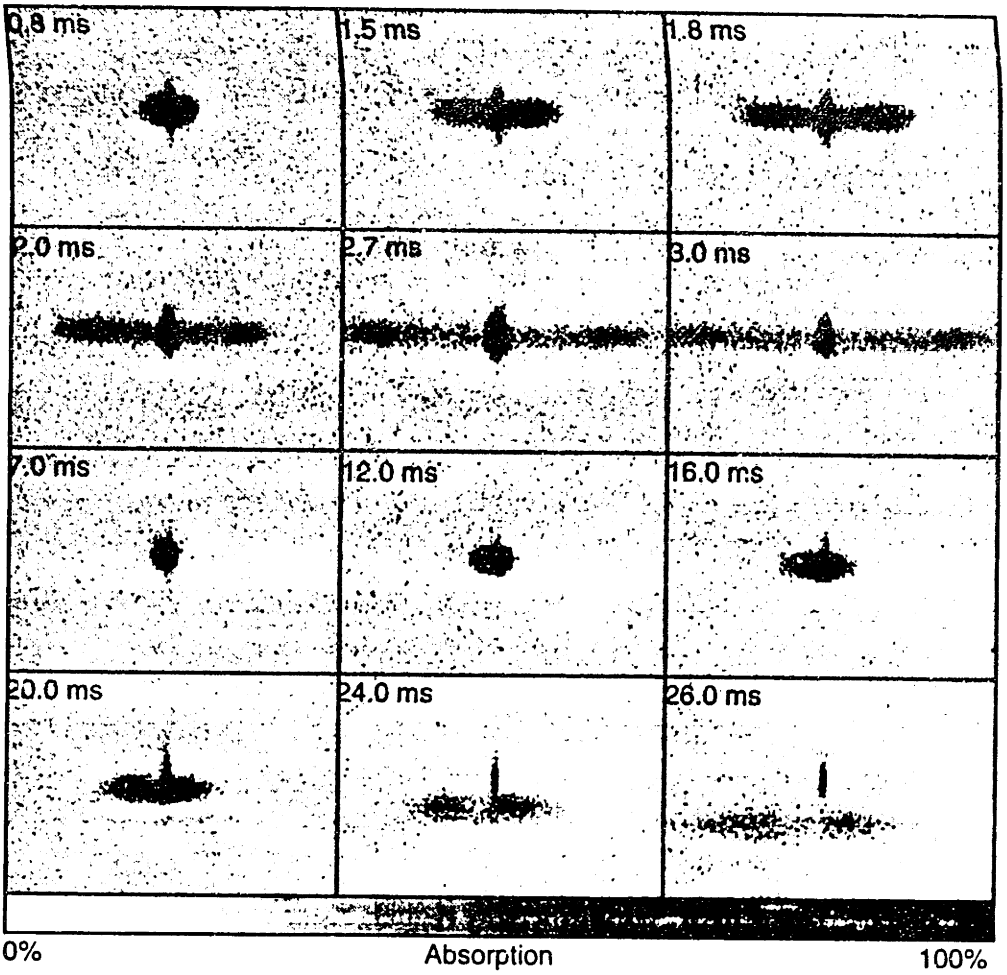

Figure 6.3 Time evolution of the outcoupled pulses of atoms in the magnetic trapping field. The images are absorption shadows of the atomic sample imaged onto a CCD array. The images present a view from the top, i.e. gravity points into the picture. Because of the small angle between the observation axis and gravity the falling pulses appear to move towards the bottom of the image. (see Fig. 6.4). After the start of a 1ms long a non-adiabatic rf sweep the atoms remained in the trapping potential for a variable delay time indicated in the image. The central cigar shaped shadow in the image is the trapped fraction of atoms. In the first 3 ms the pulse of atoms in the m_F=1 state escapes from the sample. It is repelled by the inverted trapping potential (Fig.5.3a). The m_F=0 atoms slowly "sneak" out in the following 25 ms until finally only the trapped fraction remains. The width of each image is 3.1 mm.

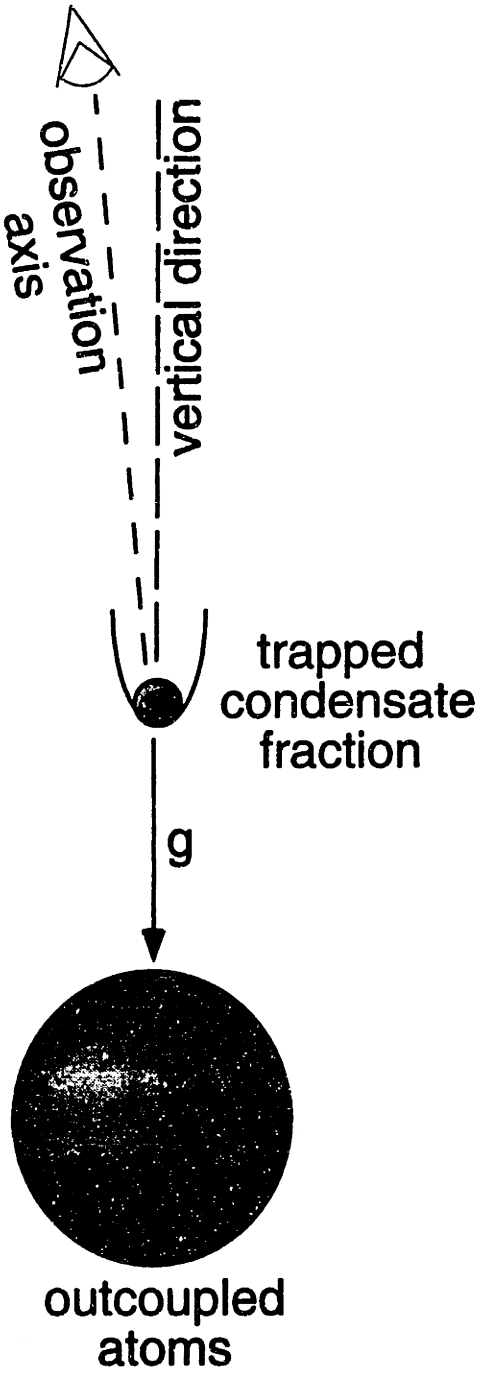

Figure 6.5 The shadows of the falling pulses and the trapped condensate are imaged onto a CCD array. The observation axis is at a small angle with respect to the vertical axis. The pulses are therefore moving slightly toward the bottom of the CCD images as they are falling (see also Fig.6.3)

References for Chapter 6

1 H. Wiseman, A. Martins, and D. Walls, Quantum Semicl. Optics **8**, 737 (1996)

2 R. J. C. Spreeuw, T. Pfau, U. Janicke, *et al.*, Europhysics Letters **32**, 469 (1995)

3 M. Holland, K. Burnett, C. Gardiner, *et al.*, Physical Review A **54**, (1996).

4 M. Olshanii, Y. Castin, and J. Dalibard, in *Proceedings of the 12th International Conference on Laser Spectroscopy*, edited by M. Inguscio, M. Allegrini and A. Sasso (World Scientific, Singapore, 1995), p.7

5 M. H. Anderson, J. R. Ensher, M. R. Matthews, *et al.*, Science **269**, 198-210 (1995).

6 K. B. Davis, M.-O. Mewes, M. R. Andrews, *et al.*, Physical Review Letters **75**, 3969 (1995).

7 M.-O. Mewes, M. R. Andrews, N. J. van Druten, *et al.*, Physical Review Letters **77**, 416-419 (1996).

8 C. C. Bradley, C. A. Sackett, and R. G. Hulet, preprint (1996).

9 C. J. Myatt, E. A. Burt, R. W. Ghrist, *et al.*, preprint (1996).

10 E. Cornell, Journal of Research of the National Institute of Standards and Technology **101**, 419-434 (1996).

11 D. E. Pritchard, K. Helmerson, and A. G. Martin, in *Atomic Physics 11*, edited by S. Haroche, J. C. Gay and G. Grynberg (World Scientific, Singapore, 1989), p. 179.

12 J. R. Rubbmark, M. M. Kash, M. G. Littman, *et al.*, Physical Review A **23**, 3107 (1981).

13 J. Holley, private communication (1996)

14 D. M. Greenberger, M. A. Horne, and A. Zeilinger, in *Physics Today*, August 1993, p.22-29.

Appendix to Chapter 6

Attached is the manuscript which details the experiment with the rf output coupler. It was accepted for publication in Physical Review Letters.

An output coupler for Bose condensed atoms

M.-O. Mewes, M.R. Andrews, D.M. Kurn, D.S. Durfee, C.G. Townsend, and W. Ketterle
Department of Physics and Research Laboratory of Electronics,
Massachusetts Institute of Technology, Cambridge, MA 02139
(To appear as *Phys. Rev. Lett.* 78 582 (1997))

We have demonstrated an output coupler for Bose condensed atoms in a magnetic trap. Short pulses of rf radiation were used to create Bose condensates in a superposition of trapped and untrapped hyperfine states. The fraction of out-coupled atoms was adjusted between 0 and 100% by varying the amplitude of the rf radiation. This configuration produces output pulses of coherent atoms and can be regarded as a pulsed "atom laser".

PACS numbers: 03.75.-b 03.75.Fi, 05.30.Jp, 32.80.Pj

The recent realization of Bose-Einstein condensation (BEC) in atomic gases [1–4] provides samples of atoms with a macroscopic population in the ground state of the system. This population forms a coherent matter wave and is described by a macroscopic wavefunction, which is the solution of the non-linear Schrödinger equation [5]. Recently, several papers have discussed the analogies between coherent matter waves and coherent photons and have worked out the theory for an "atom laser" [6–10]. An atom trap is the atomic analog to an optical cavity, and evaporative cooling into the Bose-Einstein phase transition represents a gain mechanism through which bosonic atoms accumulate in a single mode of the trap. A condensate released from the trap propagates according to a "single-mode" wave equation [11–13]. Theoretical discussions of the atom laser have considered the case in which atoms are fed into and coupled out of the "lasing mode" continuously [6–10]. In comparison to the photon case, the coherence of the atom laser is complicated by the dispersion of particles with finite rest mass and the presence of collisions [6–8].

In this paper, we do not deal with the subtle issue of coherence, but demonstrate methods to couple a Bose condensate out of a magnetic trap. The rf-induced output mechanisms discussed here provide a controlled, non-dissipative way of coupling the trapped Bose condensate to propagating modes. Gravitational acceleration gives the output a distinct direction. Output coupling realizes a crucial element in turning a Bose condensate into an atom laser [14], although the sudden release of a condensate by switching off the trapping potential can already be regarded as a crude form of such a laser. The creation of a controlled, quasi-continuous output from a Bose condensate would allow one to monitor the phase of a condensate and study phase diffusion and other decoherence processes, as recently suggested by several authors [12,15–20].

Our output coupling scheme is most easily discussed for the case of a two-level system consisting of state $|1\rangle$, a magnetically trapped state, and state $|2\rangle$, an untrapped state. Consider a Bose condensate of atoms in state $|1\rangle$. A resonant rf pulse of duration τ couples states $|1\rangle$ and $|2\rangle$ with the matrix element $\hbar\omega_R/2$, where ω_R is the Rabi frequency. State $|1\rangle$ evolves into the superposition $t|1\rangle + r|2\rangle$ with $t = \cos(\omega_R\tau/2)$ and $r = \sin(\omega_R\tau/2)$. The N-particle wave function of the Bose condensate is then given by the symmetric product

$$(t|1\rangle + r|2\rangle)^N = \sum_{n=0}^{N} \sqrt{\frac{N!}{n!(N-n)!}}\, t^{N-n} r^n |N-n, n\rangle \quad (1)$$

where $|N-n, n\rangle$ is a state with $N-n$ trapped and n untrapped atoms. The fraction of atoms coupled out of the condensate oscillates with the single-particle Rabi frequency ω_R as $\langle n\rangle/N = |r|^2 = \sin^2(\omega_R\tau/2)$.

The superposition state in Eq. (1) can also be achieved by sweeping the rf through resonance. The populations of trapped and untrapped states can be controlled by adjusting the sweep parameters from diabatic (no transfer of population) to adiabatic (complete transfer by adiabatic passage). In the case of a sweep with constant rate $d\omega_{rf}/dt$, one has $|r|^2 = 1 - e^{-\frac{1}{2}\pi\Gamma}$ and $|t|^2 = e^{-\frac{1}{2}\pi\Gamma}$, with the Landau-Zener parameter $\Gamma = \omega_R^2(4d\omega_{rf}/dt)^{-1}$ [21]. The sweep scheme has the advantage that it is not affected by small drifts in the resonance frequency, for example due to fluctuations of the magnetic field in the trap center. Furthermore, a complete transfer to the untrapped state $|2\rangle$ is insensitive to the rf amplitude as long as the sweep is adiabatic.

Such an output coupler for a two-state system could be realized with alkali atoms by using an rf transition which couples a trapped state in one hyperfine level to an untrapped state in the other hyperfine level. Instead, for experimental simplicity, we realized an output coupler for a three-state (spin 1) system by inducing lower frequency rf transitions within the $F = 1$ ground state hyperfine manifold of sodium. In such a system, the rf radiation couples the magnetically trapped $m_F = -1$ state to the untrapped $m_F = 0$ state, which is in turn coupled to the expelled $m_F = 1$ state; at low magnetic fields, the resonance frequencies for these transitions are the same. Both output coupling schemes discussed above are readily generalized to a

three-state system. A short resonant rf pulse of duration τ prepares the atoms in a superposition state $a_{-1}|m_F=-1\rangle + a_0|m_F=0\rangle + a_1|m_F=1\rangle$ with the coefficients $a_{-1} = \cos^2(\omega_R\tau/2)$, $a_0 = (i/\sqrt{2})\sin\omega_R\tau$ and $a_1 = -\sin^2(\omega_R\tau/2)$. ω_R parametrizes the coupling matrix element which is $\hbar\omega_R/\sqrt{2}$. The coefficients for a non-adiabatic rf sweep are obtained by solving a three-state Landau-Zener model numerically, and are approximated to better than 0.1% by [22]

$$\begin{aligned} |a_{-1}|^2 &= e^{-2\pi\Gamma} \\ |a_0|^2 &= 2e^{-\pi\Gamma}(1-e^{-\pi\Gamma}) \\ |a_1|^2 &= (1-e^{-\pi\Gamma})^2, \end{aligned} \qquad (2)$$

with $\Gamma = \omega_R^2/(2\mathrm{d}\omega_{rf}/\mathrm{d}t)$. These results are also valid for interacting atoms as long as the total wavefunction factorizes into position-dependent and spin-dependent parts.

Since the atoms are trapped in an inhomogeneous magnetic field, the rf resonance frequency varies over the spatial extent of the condensate. However, by using a sufficiently short pulse duration τ or a fast sweep rate $\mathrm{d}\omega_{rf}/\mathrm{d}t$, the inhomogeneous width can be neglected, and the coupling is position independent. Otherwise one would produce spatially dependent superposition states [23].

The rf output coupler was demonstrated for a Bose condensate of sodium atoms, produced in the same way as in our previous work [3]. Briefly, sodium atoms were optically cooled and trapped and then transferred into a magnetic trap, where they were further cooled by rf-induced evaporation [24]. Evaporative cooling was extended well below the transition temperature to obtain a condensate without a discernible normal fraction. Every 30 seconds, a condensate containing 5×10^6 sodium atoms in the $F=1, m_F=-1$ ground state was produced. The condensate was confined in a cloverleaf magnetic trap with the trapping potential determined by the axial curvature of the magnetic field $B'' = 125\,\mathrm{G/cm^2}$, the radial gradient $B' = 150\,\mathrm{G/cm}$ and the bias field B_0, which was set to 1.1 G for the rf pulse output coupler and to about 0.4 G for coupling induced by an rf sweep. The rf magnetic field was linearly polarized and orthogonal to the static magnetic field in the trap center.

Implementation of the output coupler using a resonant rf pulse required a high degree of bias field stability. Shifts in the resonance frequency from drifts of the bias field between cooling cycles had to be much smaller than the inverse duration of the rf pulse. The minimum pulse duration was approximately 5 μs due to limitations of the available rf power. The small bias field B_0 in the center of the trap was achieved by canceling the large magnetic field due to the axial curvature coils with an "anti-bias" field produced by a Helmholtz coil pair. High stability of B_0 was accomplished by operating these coils in series with a single current-stabilized power supply. It should be noted that evaporative cooling removes atoms with an energy of $10\,k_BT$ (which corresponds to 300 kHz at the onset of BEC) and is consequently much less sensitive to bias field drifts.

As discussed above, the rf pulse couples a fraction of initially trapped condensate atoms into the untrapped $F=1, m_F=0,1$ states. Atoms with $m_F=1$ are strong field seekers and are accelerated away from the trap center, while the atoms in the $m_F=0$ state freely expand and eventually experience a weak repulsive potential due to quadratic Zeeman shifts. In addition, both pulses are accelerated downward due to gravity. The time evolution of the $m_F=0$ pulse in the magnetic trap is shown in Fig. 1. The output pulse of atoms in the "repelled" $m_F=1$ state was observed only in the first 3 ms after the rf interaction.

The different propagations of the two output pulses in the magnetic field allowed their separate observation by absorption imaging, either in the $F=1$ level using near-resonant $F=1\rightarrow F'=2$ probe light, or by optically pumping the atoms into the $F=2, m_F=2$ state and using the $F=2\rightarrow F'=3$ cycling transition. The number of atoms was obtained by integrating the absorption signal over the image. The magnetic trap was switched off at least 1 ms before probing to avoid Zeeman shifts. The trapped fraction of atoms was measured after 40 ms of free ballistic expansion between switch-off of the magnetic trap and probing. Due to gravity, the atoms dropped up to 1 cm between release and detection.

Quantitative measurements were performed using resonant rf pulses of variable amplitude at 757 kHz, which is the Larmor frequency at a bias field $B_0 \approx 1.1$ G. The rf was pulsed on for 5 full cycles (6.6 μs). Figure 2 shows Rabi oscillations in the population of the trapped hyperfine state as a function of the rf field amplitude. The oscillations were found to be in excellent agreement with the predicted $\cos^4(\omega_R\tau/2)$ dependence. The observed Rabi frequency (obtained from the theoretical fit in Fig. 2) agreed with the single-particle Rabi frequency $\omega_R = g\mu_B B_{rf}/2$ ($B_{rf}/2$ is the magnetic field amplitude of the rotating wave) to within the accuracy of the rf antenna calibration (estimated to be 20%) [25].

A different variable output coupler for Bose condensed atoms was demonstrated using a non-adiabatic rf-sweep. The bias field was set to a value between 0.3 and 0.4 G, corresponding to a resonance frequency between 200 and 300 kHz. The frequency of the rf radiation was chirped from 0 to 500 kHz at a constant rate within 1 ms. The rf magnetic field amplitude B_{rf} was adjusted between 0 and 16 mG, corresponding to a maximum single-particle Rabi frequency ω_R of $2\pi\times11$ kHz and a Landau-Zener parameter Γ of up to 0.8. Figure 3 shows the fractional populations in the two output pulses versus rf amplitude. The results agree excellently with the solution of the three-state Landau Zener problem [Eq. (2)]. As before, the Rabi frequency obtained from the fit agreed very well

with the one obtained using the antenna calibration.

A third, less controlled method for extracting atoms from a Bose condensate was realized using Majorana flops [26]. These non-adiabatic spin-flips were induced by switching the bias field in the trap center to a small negative value. This created two zero-magnetic field points which were swept through the cloud. In the cases of both the Majorana flops and the rf sweep, the coupling is described by a Landau-Zener crossing at zero or at a finite magnetic field, respectively.

In principle it is possible to continuously couple atoms out of a Bose condensate with resonant rf radiation. The strength of the magnetic trapping field varies by about 10 mG over the spatial extent of the trapped cloud. This variation is mainly due to gravity, which requires a compensating magnetic field gradient of 8 G/cm in the trap center. A controlled cw output coupler therefore requires a very high stability of the magnetic trapping field. It would offer the advantage of coupling out atoms locally, e.g. at the surface of the cloud where the mean-field energy is low.

The spin dynamics of an rf-driven Bose condensate reflects the dynamics of a single atom, as expressed by Eq. (1). The major differences from the classic experiments by Rabi and Ramsey [27] are that 5×10^6 atoms in the same quantum state perform Rabi oscillations synchronously (Fig. 2), and that the inhomogeneous field of a magnetic trap serves as the Stern-Gerlach filter.

We have not demonstrated the coherence of the extracted pulses. However, the rf coupling is non-dissipative and the system undergoes a unitary time evolution. A pure quantum state will thus evolve into another pure quantum state. An rf pulse or sweep applied to a condensate with a definite number of atoms creates an entanglement with respect to trapped and untrapped particle numbers [Eq. (1)] . This is analogous to the situation when a Fock state of light passes through a beam splitter. Indeed, the rf output coupler for a two-state system is the atomic equivalent of an optical beam splitter, e.g. a partially reflective mirror. The three-state case is analogous to a beam splitter which has three inputs and three outputs [28]. A condensate which is initially in a coherent state (i.e. has a well-defined phase) remains in such a state after the rf interaction (with an attenuated field amplitude) while the out-coupled pulse of atoms is also in a coherent state. In this case the total N-body wavefunction factorizes into the trapped condensate and the untrapped pulse.

If the rf coupling scheme is applied to two condensates, observations of the interference between output pulses from each of the condensates can create a definite phase relation between the two trapped condensates through the quantum measurement process. Measurements on subsequent pulses can then be used to verify the initial phase measurement (for a non-interacting condensate) or to observe the phase-diffusion due to the mean field interaction [12,15–20]. For an ideal Bose condensate, repetitive pulses as observed in Fig. 1(d) should be coherent and therefore analogous to the output of a mode-locked laser.

Rf pulses can also be used to manipulate the effective potential of the condensate in two ways. First, when a significant fraction of the atoms is coupled out, the trapped condensate experiences a reduction of the repulsive mean field and should show collective excitations. Similarly, the out-coupled pulse is accelerated both by the repulsion among the extracted atoms, and also by the interaction between the output pulse and the trapped condensate. Second, during resonant rf coupling the effective trapping potential vanishes as the effective magnetic moment of the trapped atoms — that of dressed atoms in an rf field [29] — goes to zero. More generally, by choosing rf pulses with variable detuning the effective magnetic moment can be varied between zero and its maximum value ($\mu_B/2$ in our case). This allows for a sudden switch-off or reduction of the magnetic trapping potential which is faster than the inductivity-limited shut-off time of electromagnets.

In conclusion, we have demonstrated an rf output coupler for a magnetically confined Bose condensate. This scheme was used to generate pulses of coherent atoms, and realizes a beam splitter for matter waves or a variable output coupler for an atom laser.

We are grateful to J. Holley for helpful discussions, and thankfully acknowledge H.-J. Miesner for assistance in the final stages of the experiment. This work was supported by ONR, NSF, and JSEP. D.M.K. would like to acknowledge support from an NSF Graduate Research Fellowship and C.G.T. from a NATO Science Fellowship.

Note added in proof — Since submitting this paper we have observed the coherence of the condensate in an interference experiment [M. R. Andrews et al. (to be published)]. This experiment proved that coherent pulses of atoms can be extracted from a condensate. Therefore a Bose condensate with an output coupler should be regarded as an atom laser.

[1] M. H. Anderson *et al.*, Science **269**, 198 (1995).
[2] K. B. Davis *et al.*, Phys. Rev. Lett. **75**, 3969 (1995).
[3] M.-O. Mewes *et al.*, Phys. Rev. Lett. **77**, 416 (1996).
[4] C. C. Bradley, C. A. Sackett, and R. G. Hulet, preprint.
[5] P. Nozières and D. Pines, *The Theory of Quantum Liquids* (Addison-Wesley, Redwood City, California, 1990), Vol. 2.
[6] H. Wiseman, A. Martins, and D. Walls, Quantum Semicl. Opt. **8**, 737 (1996).
[7] M. Holland *et al.*, Phys. Rev. A **54**, (1996).

[8] R. J. C. Spreeuw, T. Pfau, U. Janicke, and M. Wilkens, Europhys. Lett. 32, 469 (1995).
[9] M. Olshanii, Y. Castin, and J. Dalibard, in *Proceedings of the 12th International Conference of Laser Spectroscopy*, edited by M. Inguscio, M. Allegrini, and A. Sasso (World Scientific, Singapore, 1995), p. 7.
[10] Ch. J. Bordé, Phys. Lett. A 204, 217 (1995).
[11] Y. Castin and R. Dum, to be published.
[12] M. Naraschewski *et al.*, Phys. Rev. A 54, 2185 (1996).
[13] M. Holland and J. Cooper, Phys. Rev. A 53, R1954 (1996).
[14] E. Cornell, J. Res. Natl. Inst. Stand. Technol. 101, 419 (1996).
[15] M. Lewenstein and L. You, Phys. Rev. Lett. 77, 3489 (1996).
[16] T. Wong, M. J. Collett, and D. F. Walls, Phys. Rev. A 54, 3817 (1996).
[17] Y. Castin and J. Dalibard, to be published.
[18] J. I. Cirac, C. W. Gardiner, M. Naraschewski, and P. Zoller, Phys. Rev. A 54, 3714R (1996)..
[19] J. Javanainen and S. M. Yoo, Phys. Rev. Lett. 76, 161 (1996).
[20] H. Wallis, A. Röhrl, M. Naraschewski, and A. Schenzle, to be published.
[21] J. R. Rubbmark, M. M. Kash, M. G. Littman, and D. Kleppner, Phys. Rev. A 23, 3107 (1981).
[22] J. Holley, private communication.
[23] R. J. Ballagh, K. Burnett, and T. F. Scott, poster at the *Workshop on Atom Optics and Interferometry*, Cairns, Australia, 1996.
[24] W. Ketterle and N. J. van Druten, in *Advances in Atomic, Molecular and Optical Physics*, edited by B. Bederson and H. Walther (Academic Press, San Diego, 1996), Vol. 37, p. 181, and references therein.
[25] A model antenna, identical to the one installed in the experiment, was used to calibrate the rf magnetic field. Nonlinearities of the rf amplifier and generation of higher harmonics were accounted for by measuring the power of the rf field at the fundamental frequency.
[26] T. H. Bergeman *et al.*, J. Opt. Soc. Am. B 6, 2249 (1989).
[27] N. F. Ramsey, *Molecular Beams* (Oxford University Press, Oxford, 1955).
[28] D. M. Greenberger, M. A. Horne, and A. Zeilinger, Physics Today, August 1993, p. 22.
[29] C. Cohen-Tannoudji, J. Dupont-Roc, and G. Grynberg, *Atom-Photon Interactions* (Wiley, New York, 1992).

Figure 1. Absorption images of atoms coupled into the untrapped $F = 1, m_F = 0$ state by a short rf pulse. Images were recorded (a) 14 ms, (b) 20 ms and (c) 25 ms after the rf pulse using a vertical probe beam. The trapped condensate fraction appears as a thin line in the center of each image. Figure 1d shows two pulses of $m_F = 0$ atoms coupled out of the same condensate by two consecutive rf pulses spaced 10 ms seconds apart. The image was taken 10 ms after the second rf pulse. It has a noisier background due to lower probe laser power. The width of each image is 3.1 mm.

Figure 2. Rabi oscillations of a Bose condensate. The figure shows the fraction of atoms remaining in the trapped $F = 1, m_F = -1$ state versus the amplitude of the rf pulse. The solid line is the theoretical prediction. The population undergoes Rabi oscillations with the same period as a single particle.

Figure 3. Realization of an rf output coupler using rf sweeps. The figure shows the fractions of condensate atoms coupled into the untrapped $m_F = 0$ and $m_F = 1$ hyperfine states versus the amplitude of the rf radiation expressed in terms of the Landau-Zener parameter Γ of the rf sweep. The solid line is the theoretical prediction [Eq. (2)]. The maximum $m_F = 0$ fraction was set equal to the theoretical value of 50 %, because only relative numbers of $m_F = 0$ atoms were measured.

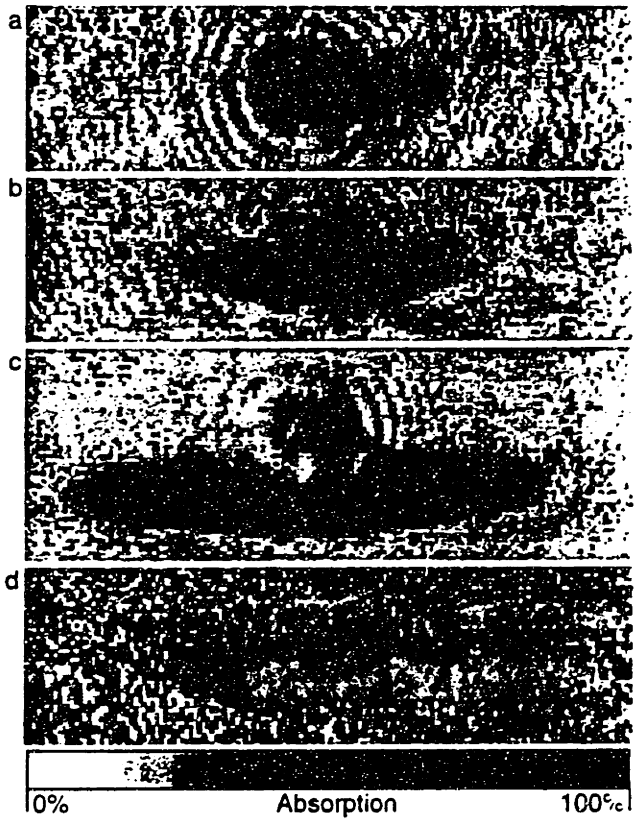

"An output coupler....", Mewes et.al., Fig.1

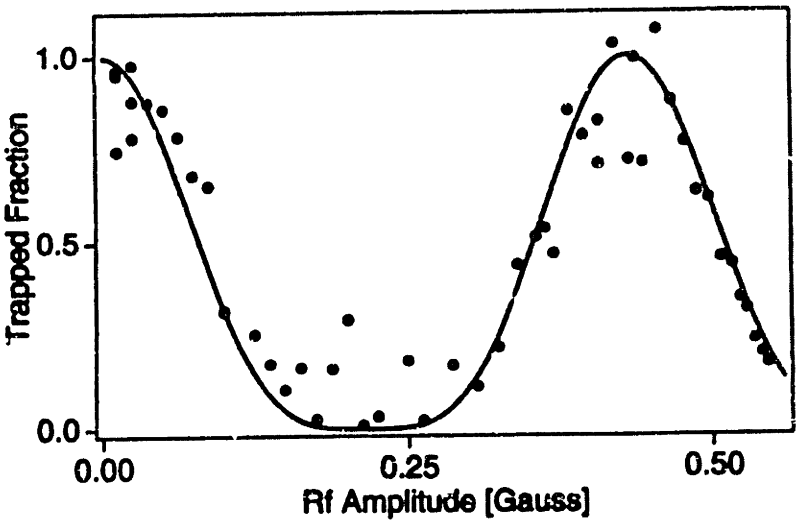
1.0
0.5
0.0
Trapped Fraction
0.00
0.25
0.50
Rf Amplitude [Gauss]

Fig. 2

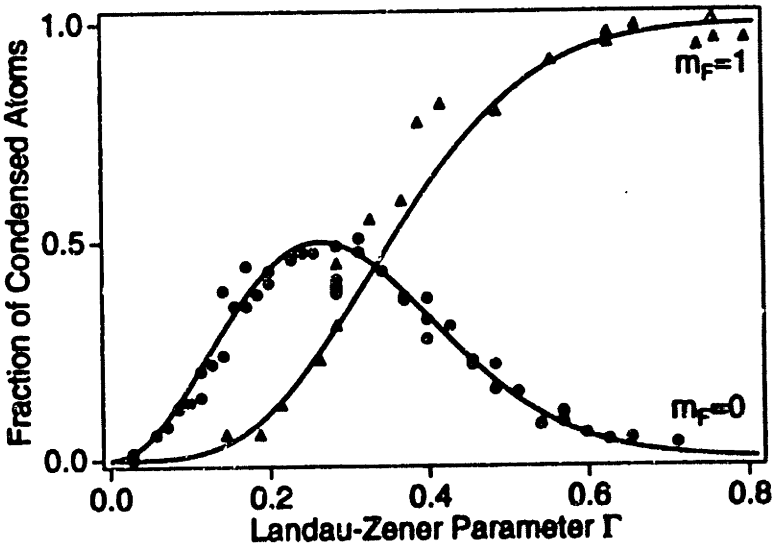
1.0
0.5
0.0
Fraction of Condensed Atoms
m_F=1
m_F=0
0.0
0.2
0.4
0.6
0.8
Landau-Zener Parameter Γ

Fig. 3

ACKNOWLEDGEMENTS

Well, it is finally over and I get to the most important part of this thesis: Thanking everyone who contributed directly or indirectly to this work.

David Pritchard offered me the opportunity to do research in experimental atomic physics at MIT. It was an opportunity I am very thankful for. I learned a lot from his unique intuitive approach to physics. He contributed many many seminal ideas to the experiment and also offered exteremely helpful advice throughout my time at MIT.

I joined Wolfgang Ketterle's group when he was Dave's postdoc and stayed with him when he became an assistant professor at MIT. Wolfgang is an incredible person and a truly amazing physicist. The experiment would not have been possible without his vision, his enormous energy and his brilliant ideas. I learned tremendously from Wolfgang and it is impossible to thank him enough in this limited space.

The experiment is a team effort and I owe many more favours than I can think of to my collaboratos Ken Davis (PhD'95) and Michael Andrews. There is probably noone I spent more nights (in the lab) with during the last 5 years than Ken, Michael and Wolfgang. Many thanks also go to Klassjan van Druten who joined the effort in the pre-BEC phase helped us to wrestle down the experiment. My thesis work would also not have been possible without the efforts of Dan Kurn, Dallin Durffee, Chris Townsend. I also owe many thanks and chocolate chip cookies to Hans-Joachim Miesner. I am grateful to the previous Ntrap generation, Michael Joffe and Alex Martin, who layed down the fundament for this experiment.

MIT is (fortunately) not defined by its architecture but by its people. I had the pleasure to work with, learn from, borrow from and be friends with Michael Bradley,

Michael Chapman, Raissa DeSouza, Joel DeVries, Al-Amin Dhirani, Frank DiFilippo, Ted Ducas, Chris Ekstrom, Joe Habib, Troy Hammond, Jeff Holley, Hong Jiao, David Kokorowski, Alan Lenef, Robert Lutwak, Carmen Miguel, Vasant Natarajan, Fred Palmer, Trey Porto, Simon Rainville, Daniel Ripin, Richard Rubinstein, Joerg Schmiedmayer, Edward Smith, Neil Spellmeyer.

I also would like thank Carol Costa, Peggy Berkovitz, Maxine Samuels, Gerry Power and Pat Solakoff for lots of help and many favors.

Thank you very much.

Later on, when they had all said "Good-bye" and "Thank-you" to Christopher Robin, Pooh and Piglet walked home thoughtfully together in the golden evening, and for a long time they were silent.

"When you wake up in the morning, Pooh," said Piglet at last,
"what's the first thing you say to yourself?"
"What's for breakfast?" said Pooh. "What do you say, Piglet?"
"I say, I wonder what's going to happen exciting to-day?" said Piglet.
Pooh nodded thoughtfully.
"It's the same thing," he said.

A.A. Milne, Winnie the Pooh